# Abstract

XIA, MENG. Cape Fear River Estuary Modeling System. (Under the direction of Dr. LIAN XIE).

The Cape Fear River Estuary (CFRE) region is one of the coastal regions facing frequent threats from tropical cyclones. It is also an important nursery for juvenile fish, crabs, shrimp, and other biological species. Thus, predicting the physical responses of the CFRE system to extreme weather events is important to the protection of life and property and ensuring the economical well beings of local residents. In this study, the Princeton Ocean Model (POM) is used to simulate the storm surge circulation in the CFRE and adjacent Long Bay and Onslow Bay.

The Environmental Fluid Dynamic Code (EFDC), an estuarine and coastal ocean circulation model, is also used to simulate the salinity plume and tracer plume distribution and particle trajectory in the vicinity of the mouth of the Cape Fear River Estuary (CFRE). The effects of astronomical tide, river discharge and wind on the CFRE salinity plume and tracer plume, particle trajectory were investigated. The comparison among the plume structure, particle trajectory, and the passive tracer structure is discussed.

To better simulate the plume structure in Cape Fear River Estuary (CFRE), we also test the sensitivity of the EFDC model to the choice of grid resolution, advection scheme, and external forcing.

# Cape Fear River Estuary Modeling System

By

Meng Xia

A dissertation submitted to the Graduate Faculty of

North Carolina State University

In partial fulfillment of the

Requirements for the degree of

Doctor of Philosophy

**Marine, Earth and Atmospheric Sciences**

Raleigh, NC

Dec, 2006

Approved by:

| | |
|---|---|
| Dr. Leonard J. Pietrafesa | Dr. John M. Morrison |
| Dr. Daniel L. Kamykowski | Dr. Lian Xie<br>(Chair Advisory Committee) |

# DEDICATION

Special thanks to my wife and my parents. Without their love, encouragement and support, I couldn't have completed this dissertation and faced this challenge.

# BIOGRAPHY

Meng Xia was born in Shandong province, People's Republic of China. He attended Ocean University of Qingdao at Qingdao, China, receiving Bachelor of Science degree in Physical Oceanography. He attended First Institute of Oceanography, State Oceanic Administration and got his Master of Science degree in Physical Oceanography. He attended at the Department of Marine, Earth and Atmosphere sciences, North Carolina State University, Raleigh, NC and pursued the Ph.D degree.

## Acknowledgements

I wish to thank Dr. Lian Xie, the chair of the advisory committee, for his guidance, support and encouragement on this research. I appreciate that Dr. Xie provides me a very flexible research environment that is suitable for my research interests and strength. I always have freedom to explore some new ideas with available resources. I also benefit a lot from his methodology in ocean numerical modeling, his many thoughtful ideas that keep my research topic in step with current active research in this area.

I want to express my appreciation to the advisory committee members, Dr. Leonard Pietrafesa, Dr. John Morrison and Dr. Daniel Kamykowski for their support, thoughtful input and advice on this research. They are also very helpful in providing me with various resources for the study. Thanks to all the friends in the Coastal Fluid Dynamics Lab.

# Table of Contents

## List of tables:



## List of figures:

### Chapter2:

## Chapter 3:

## Chapter 4:

Chapter 5:

# Chapter 1. Introduction

## 1. **Scientific Background**

The Cape Fear River, a 322 km river that flows through the heart of the North Carolina (NC) piedmont, has the largest watershed in NC. Originally known as the Waccamaw, the Cape Fear is the largest river basin in NC and the only one that flows directly into the ocean. The Black River joins the Cape Fear 24 km above Wilmington, and the Northeast Cape Fear River enters the system at Wilmington. The freshwater discharge from the Cape Fear River, the Northeast Cape Fear River, and the Black River converges in the Cape Fear Estuary and then flows into Long Bay (Figure 1). The average combined discharge from these rivers is about 221 $m^3$/s (Dame et al., 2000), with a maximum of about 2000 $m^3$ /s.

The head of the CFRE connects to the eastern end of Long Bay on the Atlantic seaboard. Because of the in-welling of coastal waters into the estuary due to the combined effects of the astronomical tides and wind forcing (Pietrafesa and Janowitz, 1988), this region is an extremely important nursery for juvenile fish, crabs, and shrimp (Miller et al., 1984). The Cape Fear River is the only coastal river system in NC where hybrid striped bass are stocked (Patrick and Moser, 2001).

The plume associated with the CFRE system is an interesting phenomenon of the east coast of the United States. Plumes from the CFRE reduce salinity and change other water properties in the coastal waters, such as temperature, nutrients, and phytoplankton. The flowing plumes of fresh and low salinity water carry loads of sediment, nutrients, and

pollutants into the Long Bay and affect the regional water quality and ecosystem (Mallin et al., 2005).

The CFRE also experiences significant cycling of nutrients (Norris and Hackney, 1999) and heavy metals (Shank et al., 2004). Hurricane-induced storm surge circulation could influence sediment and nutrient transport in the river and estuary (Wren and Leonard 2005, Sheremet et al. 2005, Leonard et al. 1995, Nyman et al. 1995). A major storm surge may also impact Dissolved Oxygen which could deleteriously impact living marine resources (Mallin et al., 1999). Hurricane wind induced storm surge and inundation could bring sewage runoff into the river, an environment-damaging impact to the CFRE region. This is especially the case near the mouth of the estuary.

The Cape Fear has faced several threats from tropical and extra-tropical cyclones since 1996. The Cape Fear and adjacent Long Bay seem to have been a magnet for hurricanes. Usually these tropical cyclones invade the region in the late summer and early fall, such as the Fran (Sep, 1996), Bertha (July, 1996), Bonnie (Aug, 1998), and Floyd (Sep, 1999). Hurricane Charley visited the Cape Fear in August, 2004 after several quiet years in the region.

## 2. Purpose of the Study

In this study, the Princeton Ocean Model (POM) will be used to simulate the hurricane-induced storm surge, and the Environmental Fluid Dynamics Code (EFDC) will be used to study salinity and trace plume distribution and the particle trajectories at the CFRE and adjacent coastal region.

Specially, the proposed study will address the following questions:

1) What is the influence of Hurricane track and intensity to the storm surge distribution?
2) What is the effect of Frying Pan Shoals, between Long Bay and Onslow Bay to the storm surge circulation and plume distribution?
3) What is the plume horizontal and vertical structure under different wind forcing, river discharge effect, tidal effect? And what is the possible reason for the transition?
4) What is the best modeling setting to simulate the plume structure? Such as vertical resolution, horizontal resolution, advection scheme?
5) What are the horizontal and vertical structures of passive tracer plumes and the path of particle trajectories under different wind forcing, river discharge effect, tidal effect? What are the possible causes for the differences and similarities?

## 3. Organization of dissertation

A numerical study of storm surge in the Cape Fear River Estuary and adjacent coastal waters are given in chapter 2. Chapter 3 introduces numerical modeling of Cape Fear River Estuary plumes. A sensitivity study of model settings for modeling the Cape Fear River Estuary plumes is investigated in Chapter 4. A numerical study of passive tracer and particle trajectories in the Cape Fear River Estuary are presented in Chapter 5. Finally, Chapter 6 gives the final remarks.

## References

Dame, R., Alber, M., Allen, D., Mallin, M., Montague, C., Lewitus, A., Chalmers, A., Gardner, R., Gilman, C., Kjerfve, B., Pinckney, J., Smith, N. (2000) "Estuaries of the South Atlantic Coast of North America: Their Geographical Signatures" *Estuaries* 23, 793–819.

Leonard, A. L., Hine, C. A., Luther, E. M., Stumpf, P. R., and Wright, E. E. (1995), Sediment transport processes in a west-central Florida open marine marsh tidal creek: The role of tides and extra-tropical storms. *Estuarine, Coastal and Shelf Science*, 41, 225-248.

Mallin, M. A., Posey, M. H, Shank, G. C, Mciver, M. R, Ensign, S. H, and Alphin, T. D. (1999), Hurricane effects on water quality and benthos in the cape fear watershed: Natural and anthropogenic impacts. *Ecological Applications*, 9, 350-362.

Miller, J.M.; Reed, J.P., and Pietrafesa, L.J., (1984), Patterns, mechanisms and approaches to the study of migrations of Estuarine-dependent fish larvae and juveniles. *Mechanisms of migration in: Fishes. McCleave, J.D.; Arnold, G.P.; Dodson,J.J., and Neill, W.H (eds.), New York: Plenum,* 209-225

Nyman, J. A., Crozier, C. R., and DeLaune, R. D. (1995), Roles and patterns of hurricane sedimentation in an Estuarine Marsh. *Estuarine,Coastal and Shelf Science*, 40, 665-679.

Patrick, S. W., and Moser, L. M. (2001), Potential competition between Hybrid Striped Bass (Morone saxatilis X M. americana) and Striped Bass (M. saxatilis) in the Cape Fear River Estuary, North Carolina. *Estuaries,* 24, 425-429.

Pietrafesa, L.J., Janowitz, G.S., (1988) Physical Oceanographic Processes Affecting Larval Transport Around and Through North Carolina Inlets. *American Fisheries Society*, 3, 34-50

Shank, G. C., Skrabal, A.S., Whitehead, F. R., and Kieber, J. R. (2004), Fluxes of strong Cu-complexing ligands from sediments of an organic-rich estuary. *Estuarine, Coastal and Shelf Science*, 60, 349-358.

Sheremet, A., Mehta, J.A., Liu, B., and Stone, W.G. (2005), Wave–sediment interaction on a muddy inner shelf during Hurricane Claudette. *Estuarine, Coastal and Shelf Science*, 63 , 225-233

Wren, P. A., and Leonard, L.A. (2005), Sediment transport on the mid-continental shelf in Onslow Bay, North Carolina during Hurricane Isabel. *Estuarine, Coastal and Shelf Science, 63,43-56*

# Chapter 2. A Numerical Study of Storm Surge in the Cape Fear River Estuary and Adjacent Coast

## Abstract

The Cape Fear River Estuary (CFRE) region is one of the coastal regions facing frequent threats from tropical cyclones. It is also an important nursery for juvenile fish, crabs, shrimp, and other biological species. Thus, predicting the physical responses of the CFRE system to extreme weather events is important to the protection of life and property and ensuring the economical well-beings of local residents. In this study, the Princeton Ocean Model (POM) was used to simulate the storm surge, inundation, and coastal circulation in the CFRE and its adjacent Long Bay using a three-level nesting approach. Hindcasts of the hydrodynamic responses of the CFRE system to historic events were performed for Hurricanes Fran, Floyd, Bertha and Charley. Comparisons were made for the modeling results and the observations.

# 1. Introduction

The Cape Fear River, a 322 km river that flows through the heart of the North Carolina (NC) piedmont, has the largest watershed in NC. Originally known as the Waccamaw, the Cape Fear is the largest river basin in NC and the only one that flows directly into the ocean. The river begins near Greensboro and Winston-Salem as two rivers, the Deep River and the Haw River. These two rivers converge near Moncure to form the Cape Fear River. The Black River joins the Cape Fear 24 km above Wilmington, and the Northeast Cape Fear River enters the system at Wilmington (Figure 1). The Cape Fear River basin covers 23,310 $km^2$ and encompasses streams in 29 of the state's 100 counties.

The mouth of the CFRE connects the eastern end of Long Bay on the Atlantic seaboard. Because of the in-welling of coastal waters into the estuary due to the combined effects of the astronomical tides and wind forcing (Pietrafesa and Janowitz, 1988), this region is an extremely important nursery for juvenile fish, crabs, and shrimp (Miller et al., 1984). The Cape Fear River is the only coastal river system in NC where hybrid striped bass are stocked (Patrick and Moser, 2001). In addition, it is an important natural resource that facilitates industry, transportation, recreation, drinking water, and aesthetic enjoyment.

The CFRE experiences significant cycling of nutrients (Norris and Hackney, 1999) and heavy metals (Shank et al.., 2004). Hurricane-induced storm surge circulation could influence sediment and nutrient transport in the river and estuary (Wren and Leonard 2005,

Sheremet et al. 2005, Leonard et al. 1995, Nyman et al. 1995). A major storm surge may also impact Dissolved Oxygen which could deleteriously impact living marine resources (Mallin et al., 1999). Hurricane wind induced storm surge and land inundation could bring sewage runoff into the river, an environment-damaging impact to the CFRE region. This is especially the case near the mouth of the estuary.

The CFRE has recently experienced the passage of a large number of tropical and extra-tropical cyclones since 1996. Usually these tropical cyclones invaded the region in late summer and early fall, such as Bertha (July, 1996), Fran (September, 1996), Bonnie (August, 1998), Dennis (September, 1999), Floyd (September, 1999), Irene (October, 1999), Charley (August, 2004) and Ophelia (August, 2005). In this study, storm surge and coastal ocean circulation hindcasts are performed for Hurricanes Bertha, Fran, Floyd and Charley since these Hurricanes greatly influenced the CFRE and its adjacent ocean. Their landfall dates and corresponding intensities are listed in Table 1.

Following the earlier model work of Pietrafesa et al. (1997), Peng (2002), Xie et al. (2004) and Peng et al. (2004) in the Croatan-Albemarle-Pamlico Estuary System (CAPES), we will use a three-dimensional storm surge model to simulate hurricane-induced storm surge and land inundation in the CFRE system. In section 2, the storm surge model is briefly described. The method used to compute the hurricane winds is presented in section 3. Main results are presented in section 4, and model validation is performed in section 5, followed by discussions and conclusions in section 6.

## 2. Model configuration of the Cape Fear River Estuary System

The storm surge model in Peng et al. (2004) is applied in this study. The hydrodynamics of the model are based on the Princeton Ocean Model (Mellor, 1996), which is a sigma coordinate model in that the vertical coordinate is scaled on the water column depth. The horizontal grid uses curvilinear orthogonal coordinates and an "Arakawa C" differencing scheme. The model contains an imbedded second moment turbulence closure sub-model to provide vertical mixing coefficients. The horizontal time differencing is explicit, whereas the vertical differencing is implicit. The latter eliminates time constraints for the vertical coordinate and permits the use of fine vertical resolution in the surface and bottom boundary layers. This model has a free surface and a split time step. The external mode portion of the model is two-dimensional and uses a short time step based on the CFL condition and the external gravity wave speed. The internal mode is three-dimensional and uses a long time step based on the CFL condition and the internal wave speed. Complete thermodynamics have been implemented.

The inundation scheme used in the CFRE model is a modified Hubbert and McInnes (1999) scheme which we will refer to as the HM scheme. The HM scheme utilizes the vertically averaged horizontal current as an inundation speed control. This modified scheme was described in Xie et al. (2004) and Peng et al. (2004), hereafter referred to as the PXP scheme. It employs the surface current as the inundation speed parameter. In order to determine if a land grid point is inundated, the PXP procedure compares the water level of a grid cell adjacent to the coastline with the land elevation next to it. If the water level is overtopping

the adjacent land elevation, then another criterion is to be examined. Distances in the horizontal directions, $x$ and $y$, that the water could travel are computed through the time step integral of the surface inundation speed at this grid point. The land grid point will be flooded, or turned into a water point, if the water can travel over the corresponding grid size along either x or y axis or both. Otherwise, the land grid point will remain dry.

The procedure for draining or drying in the PXP scheme also differs from the original HM scheme. In the PXP scheme, draining occurs when the water depth goes below a preset threshold. We also impose a mass balance constraint on the inundation process. An interactive mass rebalancing procedure is implemented in both the flooding and draining processes.

In this study, the storm surge and inundation modeling system is configured to the CFRE and its adjacent shelf and coast ($33.67^{o}$ N-$34.00^{o}$ N, $78.25^{o}$ W-$77.75^{o}$ W) (Figure 2). The horizontal resolution is determined by a 90-m grid size in both the x and y directions, while three sigma levels in the vertical were employed for adequacy and computational efficiency. We used the bathymetry data which was derived from the National Geophysics Data Center (NGDC) Coastal Relief Model Volume 02.

The domain shown in Figure 2 is the inner domain of a three-level nesting system in the study. The outer domain region is set between $32.50^{o}$N-$36.50^{o}$N, $81.00^{o}$W- $75.00^{o}$W; the middle domain is set between $33.17^{o}$N-$34.50^{o}$N, $79.00^{o}$W- $77.17^{o}$W. The middle domain bathymetry data was obtained from the NGDC Coastal Relief Model Volume 02 as well. For

the outer domain, ETOPO2 Global 2-Minute Gridded Elevation Data was used to couple with the NGDC Coastal Relief Model Volume 02. This is because ETOPO2 contains the deep ocean data necessary for the outer domain which are not covered by the NGDC database. The bathymetry and elevation data are shown in Figure 2. A schematic depiction of the nesting scheme is shown in Figure 3.

## 3. Winds and experimental settings

Several hurricanes passed over the CFRE domain since 1996. The tracks are presented in Fig 3.

The hurricane pressure field and surface wind velocity created by the pressure gradient were modeled according to Holland (1980):

$$P = P_c + (P_n - P_c)\exp(-A/r^B) \qquad (1)$$

$$V_c = [AB(P_n - P_c)\exp(-A/r^B)/\rho r^B]^{1/2} \qquad (2)$$

where P is the atmosphere pressure at radius r; $\rho$ is the air density; $P_c$ is the central pressure and $P_n$ is the ambient pressure (in practice, the value of the first anticyclonically curved isobar); both A and B are scaling parameters; $V_c$ is wind profile which results from the hurricane pressure gradient. Those parameters are set to: $\rho = 1.2kg/m^3$, B=1.9, A=$(R_{\max})^B$; $R_{\max}$ is the radius of maximum wind and derived from the Hurricane Research Division (http://www.aoml.noaa.gov/hrd/). $P_C$ and $P_n$ are obtained from the National Hurricane Center (http://www.nhc.noaa.gov).

The surface wind stress is computed through the following bulk formula:

$$\tau = \rho C_d \left|\vec{V}_w\right| \vec{V}_w \qquad (4)$$

where $V_W$ is the wind speed at height of 10m, and $\rho$ is air density. The drag coefficient, $C_d$, is assumed to vary with wind speed:

$$10^3 C_d = \begin{cases} 2.16 & \left|\overrightarrow{V_w}\right| \geq 26 m/s \\ 0.49 + 0.065\left|\overrightarrow{V_w}\right| & 10 m/s \leq \left|\overrightarrow{V_w}\right| < 26 m/s \\ 1.14 & 3 \leq \left|\overrightarrow{V_w}\right| < 10 m/s \\ 0.62 + 1.56/\left|\overrightarrow{V_w}\right| & 1 \leq \left|\overrightarrow{V_w}\right| < 3 m/s \\ 2.18 & \left|\overrightarrow{V_w}\right| < 1 m/s \end{cases} \qquad (5)$$

This $C_d$ formula follows Large and Pond (1981) when the wind speed is less than 26m $s^{-1}$, otherwise, it is assumed as a constant as indicated in Powell et al. (2003).

Detailed information of the tracks and hurricane attributes are important for accurate surface wind stress calculation. The time, location and central pressure of the specific hurricanes are shown in tables 2-5. For example, the computation time for Hurricane Fran (1996) is from 09/05/15Z to 09/06/09Z based on the track, time, location, and pressure as shown in Table 2 and in Figure 3. The wind velocity distribution at different times is illustrated in Figures 4. Similarly, the track, time, location and pressure information of hurricane Bertha (1996), Floyd (1999), Charley (2004) are listed in Table 3, 4, 5 respectively. The corresponding wind distributions are illustrated in Figure 5, 6, 7.

# 4. Results

## 4.1 Hurricane Fran (1996)

Hurricane Fran struck NC as a category three hurricane, and it swept across NC leaving a swath of destruction throughout most of the state. Its track moved directly over the city of Wilmington and Cape Fear Estuary, traveling north when it approached the CFRE and then a little northwestward after that (Figure 3). Its best track position and pressure are given in Table 2 and Figure 4.

From September 5 to September 6 in 1996, Hurricane Fran passed this region within 10 hours at a translation speed of 10 km/h. The simulated storm surge and inundation from 09/05/2100Z to 09/06/0300Z are shown every two hours in Figures 8 a-d. At 09/05/21Z, the hurricane eye located at 32.90N, 77.90W as shown by the surface wind field (Figure 4a). The major storm surge stood at over 2 m to the east of NC, and an approximate area of 0.97 $km^2$ was inundated in the northeastern part of the domain (Fig 8). In the CFRE, the storm surge was lower than mean sea level while the river estuary bank did not vary much. Two hours later, the hurricane eye moved close to the CFRE with the center at 33.40N, 78.1W. The storm surge was more than 3 m at the east part of NC coast, and the northeastern part of land continued to be inundated. In the Cape Fear Estuary, the storm surge was more than 1 meter and the northeast river estuary bank began to be inundated. At 09/06/01Z, the hurricane eye was at 33.9N, 78.0W. The storm surge was still high in the CFRE with nearly 1 m, while the storm surge level was about 1.5 m and began to retreat along the southeastern coast of NC and Onslow Bay. A 2.27 $km^2$ region encompassing both the northeastern coast part and river

estuary bank were still inundated. At 09/06/03Z, the hurricane eye passed this region with the center at 34.5N, 78.1W. The storm surge along the southeastern part of the NC coast and Onslow Bay continued to decrease, and flooding in both the northeastern coast part and river estuary bank began to decrease.

A range of 2.44 - 3.66 meter surge was estimated on the NC coast by the National Hurricane Center (NHC) (1996a, preliminary report on Hurricane Fran), which is consistent with our results (Figure 8b). Overall, as the storm moved northward towards the Cape Fear region, high surge levels occurred along the eastern coast of the NC including Carolina Beach and Onslow Bay, and medium surge levels occurred at the river estuary bank of the CFRE. This category three hurricane induced a peak surge as high as three meters, and the high storm surge level occurred in the Onslow Bay whereas little response occurred in the Long Bay due to its track path. So the storm surge is strongly dependent on the intensity of forcing and the path of the hurricane.

**4.2 Hurricane Bertha (1996)**

Unlike Hurricane Fran, Hurricane Bertha was a category two hurricane and its damage was much less. The best track of the Hurricane Bertha was also different from that of Hurricane Fran though their translation speeds were very similar. Hurricane Bertha traveled northward and then northeastward when it passed this region (Figure 3). The simulated storm surge and inundation from 07/12/1700Z to 07/12/2300Z are shown at two hour intervals in Figures 9a-d. At 07/12/1700Z, the hurricane eye was at 33.3N, 78.0W and the wind distribution is shown in Figure 5a. The storm surge stood at nearly 2 m at the Onslow Bay and eastern part

of NC, while it had little effect in Long Bay and the CFRE. An approximate area of $0.92\,km^2$ of the northeast part of land was inundated due to the high storm surge in this region. Two hours later, the hurricane eye was at 33.8N, 77.8W, and the storm surge level was about 1 m at the Onslow Bay. $0.82\,km^2$ of the outer section of land in the northeast continued to be inundated. At 07/12/21Z, the hurricane eye was at 34.3N, 77.7W, and the storm surge level began to subside in this region since the hurricane center moved to the north part of NC. The inundation of the outer portion of the northeastern part of land began to decrease. At 07/12/23Z, the hurricane eye was at 34.9N, 77.6W, which is far away from this region. The storm surge in the southeastern coast of NC was lessened and the inundation area continued to decrease.

In all four depicted phases, the storm surge level in the CFRE and Long Bay was low and few areas were inundated. As the hurricane moved northward to the Cape Fear region, high surge levels occurred along the eastern section of the NC coastline (Figure 9a), which is very similar to the scenario of Hurricane Fran (Figure 8a, 8b), but the storm surge level is not as high as that caused by Hurricane Fran due to the difference in hurricane intensity. As shown in Figure 9a, the storm surge in the southeastern part of NC exceeded 1.8 m. A 1.52 meter surge was estimated on the NC coast from the mouth of the Cape Fear to Cape Lookout according to the NHC (1996b, Preliminary report on hurricane Bertha), which is consistent with our results.

**4.3 Hurricane Floyd (1999)**

Hurricane Floyd is another major disaster to NC after Hurricane Fran. It took a straight

course when it approached and passed the Cape Fear region (Figure 3). As the hurricane moved northeastward towards the Cape Fear region, high surge levels occurred along the eastern sector of the NC coastline, and medium surge levels occurred at the northern part of CFRE. Storm surges in the southeastern part of NC and Onslow Bay reached 3 meters, which is consistent to that reported by the NHC which indicated storm surge heights of 2.74 to 3.05 meter along the NC coast (Preliminary Report hurricane Floyd, 1999).

The simulated storm surge and inundation from 09/16/0500Z to 09/16/1100Z are shown with two hour intervals in Figures 10 a-d. At 09/16/05Z, the hurricane eye was at 33.3N, 78.1W and the wind distribution is illustrated in Figure 6a. The storm surge level stood at more than 3 m in the eastern coast of NC with approximate $0.79\,km^2$ regions in the northeast part of land being inundated. In the Cape Fear estuary, the sea surface elevation remained below sea level. No distinct perturbation occurred in the river estuary bank. Two hours later, the hurricane eye was at 34.0N, 77.9W, and the storm surge level was about 1 m in the eastern part of NC with the northeast part of land remaining in inundation. In the Cape Fear Estuary, the storm surge stood at more than 0.5 meter, and the river estuary bank part began to be inundated. A total area of $0.86\,km^2$ of the land was inundated. At 09/16/09Z, the hurricane eye was at 34.5N, 77.6W, and the storm surge stood lower than mean sea level in the southeastern part of NC. But the storm surge level was higher in the Cape Fear Estuary, which reached 1.2m, and $0.13\,km^2$ of the part at the river estuary bank was inundated. At 09/16/11Z, the hurricane eye was at 35.2N, 77.1W. The storm surge started to drop at the Onslow Bay and the CFRE. The flooding area in both the northeastern part and the river

estuary bank of CFRE continued to retreat.

### 4.4 Hurricane Charley (2004)

Hurricane Charley visited the CFRE in 2004. Unlike the above three hurricanes, its track is to the left of the CFRE and it traveled northeastward towards the southern NC/SC coast (Figure 3). The simulated storm surge and inundation from 08/14/1400Z to 08/14/1700Z are shown in Figures 11a-d. At 08/14/14Z, the hurricane eye was at 32.9N, 79.23W and the storm surge was over 1 m along the south-facing coast of NC and in the southern part of the CFRE as well (Figure 10). However, the eastern-facing coastline of NC had little change in water level. At 08/14/15Z, the hurricane eye located at 33.20N, 79.00W (Figure 6). The storm surge level remained higher than 1 m in the entrance of the Cape Fear Estuary and along the southern portion of the NC coast with $0.19\,km^2$ land being inundated. The eastern coast part of NC still had little change in water level. At 08/14/16Z, the hurricane eye was at 33.73N, 78.63W, and the storm surge level stood lower than sea level in the southern part of NC and the Cape Fear Estuary. At 08/14/17Z, the hurricane eye moved to 34.26N, 78.30W, and the influence of Hurricane Charley tapered off in our domain. Overall, little perturbation occurred in the Onslow Bay because Hurricane Charley's track is located to the left of the CFRE. Comparing the storm surge response of Hurricane Charley to the above three hurricanes, we can see that the track location is crucial to the storm surge in the CFRE although the hurricane intensity plays an important role to the storm surge level in the whole model domain.

## 5. Model Verification

From the historic water level data archived in the NOAA-CO-OPS (co-ops.nos.noaa.gov) website, we obtained the times series of verified water level data for our model region for the chosen hurricane cases discussed in Section 4. Five to six gauge stations were available for each hurricane sea level history. These data were used to verify the model results. In each case, the time series astronomical tide was added to the wind induced storm surge water levels. Then the subsequent model storm tide was compared with the measured water level with special interest on the maximum water levels. The comparisons of modeled and observed maximum water levels for Hurricanes Bertha, Fran, Floyd and Charley are respectively shown in Figs. 12, 13, 14 and 15. Overall, the model results are very close to the observations.

Moreover, we did several additional experiments with Hurricanes Bertha, Fran, Floyd and Charley. Simulation with a larger track window was performed for each hurricane, so that more complete hurricane history can be reflected in the new experiments. We compared new model output to the originals, and found that the differences can be safely ignored. The comparisons between modeled and observed maximum water levels are shown in Figure 16.

## 6. Discussion and Conclusions

In this study, the integrated storm surge and inundation model (Peng et al., 2004; Xie et al.., 2004) was applied to the CFRE system and its adjacent coast region. The storm surge and inundation patterns induced by Hurricanes Bertha, Charley, Floyd and Fran were studied.

From the verifications, it is evident that the model shows a good skill in simulating the hurricane-induced storm surge in the region. From Figures 8-11, the study indicates that the responses of the storm surge inside the CFRE and the adjacent coast are much different to these four hurricanes. Hurricane Charley generated high storm surge level in the Long Bay with almost no pronounced response in the Onslow Bay, while Hurricane Floyd, Fran and Bertha generated high storm surge in the Onslow Bay but caused little effect in the Long Bay. The maximum surge level is also different for these four different hurricanes. The maximum storm surge level was more than 3 m during Hurricane Fran, 3 m during Hurricane Floyd, more than 2 m during Hurricane Bertha, and about 1.5 m during Hurricane Charley. Within the CFRE, there was little storm surge response to Hurricane Bertha while Hurricane Fran, Charley and Floyd caused significant responses. Under the influence of Hurricane Charley, there was strong response even at Long Bay and the entrance of the CFRE. For Hurricane Fran at the CFRE, the storm surge level was driven by the local wind forcing, while the storm surge induced by Hurricane Charley most likely was propagated as free gravity wave from Long Bay. It is noticeable that Frying Pan Shoals, between Long Bay and Onslow Bay, can affect water exchange between the two water bodies. As a result, the storm surge level is much different on the right and left side of Frying Pan Shoals. For example, severe storm surge occurred at the Long Bay while a minor surge existed in the Onslow Bay during the passage of Hurricane Charley. An opposite storm surge distribution pattern was also found in Long Bay and Onslow Bay during the passage of Hurricanes Fran, Floyd, Bertha.

In summary, we obtained the following results:

1) Hurricane-induced storm surge in the CFRE is very sensitive to hurricane tracks. When a hurricane's track passes to the west of the CFRE as in the case of Hurricane Charley, there is a greater likelihood of water being pushed into the entrance of Cape Fear Estuary to bring severe storm surge in the CFRE. When the hurricane track passes above or to the east of the CFRE as in Hurricanes Fran and Floyd, the chance is little of water being pushed towards and into the entrance of the CFRE. The storm surge will be generated locally in the Onslow Bay.
2) The inundation is very sensitive to bathymetry and land elevation besides hurricane intensity and tracks. For examples, the northeastern part of the Cape Fear is more easily inundated since it is the low-lying land. In addition, the inundation area has a direct relationship with the category of the hurricane and the track orientation. Hurricane Fran inundation was more severe than those of Hurricanes Floyd and Bertha, while the inundation area induced by Hurricane Charley was the smallest among the four hurricanes.
3) Apparently, the maximum storm surge level in the CFRE and the adjacent ocean is very consistent with the hurricane intensity. The maximum storm surge level was highest for Hurricane Fran, then Hurricane Floyd and Bertha, and lowest for Hurricane Charley, which are corresponded very well to their respective intensities.
4) The bottom topography plays an important role in the movement of storm-induced currents. It may cause dramatic difference in storm surge level between the right and left side of Frying Pan Shoals. The storm surge level in the Long Bay is much higher than that in the Onslow Bay during the passage of Hurricane Charley, while the distribution of surge reverses during the passage of Hurricanes Fran, Floyd, and Bertha.

5) Our integrated storm and inundation model proves to be robust in simulating storm surge and inundation in the CFRE and could be employed to real-time forecasting storm-induced currents and water levels in real time.

## Acknowledgements

This study was supported by the Coastal Ocean Research and Monitoring Program (CORMP) which was funded by NOAA under grand award #NA16RP2675 through a subcontract from University of North Carolina at Wilmington. All modeling activities are carried out in the Coastal Fluid Dynamics Lab of North Carolina State University.

## References


Holland, G.J. (1980), An analytic model of the wind and pressure profiles in hurricanes. *Mon. Weather Rev.*, 108, 1212-1218.

Hubbert, G.D., McInnes, K.L., (1999) A Storm Surge Inundation Model for Coastal Planning and Impact Studies. *Journal of Coastal Research* . 15(1), 168-185.

Large, W. G. and Pond, S. (1981) Open ocean momentum fluxes in moderate to strong winds. *J.Phys. Oceanogr*., 11, 324-336.

Leonard, A. L., Hine, C. A., Luther, E. M., Stumpf, P. R., and Wright, E. E. (1995), Sediment transport processes in a west-central Florida open marine marsh tidal creek: The role of tides and extra-tropical storms. *Estuarine, Coastal and Shelf Science*, 41, 225-248.

Mallin, M. A., Posey, M. H, Shank, G. C, Mciver, M. R, Ensign, S. H, and Alphin, T. D. (1999), Hurricane effects on water quality and benthos in the cape fear watershed: Natural and anthropogenic impacts. *Ecological Applications*, 9, 350-362.

Mellor, G. L. (1996), User's guide for a three dimensional primitive equation, numerical ocean model. *Princeton University, NJ*.

Miller, J.M.; Reed, J.P., and Pietrafesa, L.J., (1984), Patterns, mechanisms and approaches to the study of migrations of Estuarine-dependent fish larvae and juveniles. *Mechanisms of migration in: Fishes. McCleave, J.D.; Arnold, G.P.; Dodson,J.J., and Neill, W.H (eds.), New York: Plenum,* 209-225

National Hurricane Center, (1996a), Preliminary Report Hurricane Bertha, (available at ftp://ftp.nhc.noaa.gov/pub/storm_archives/atlantic/prelimat/atl1996/Bertha/).

National Hurricane Center, (1996b), Preliminary Report Hurricane Fran, (available at ftp://ftp.nhc.noaa.gov/pub/storm_archives/atlantic/prelimat/atl1996/fran/).

National Hurricane Center, (1999). Preliminary Report Hurricane Floyd, (available at http://www.nhc.noaa.gov/1999floyd_text.html).

Norris, R. A., and Hackney, T. C. (1999), Silica content of a Mesohaline tidal marsh in North Carolina. *Estuarine, Coastal and Shelf Science*, 49, 597-605.

Nyman, J. A., Crozier, C. R., and DeLaune, R. D. (1995), Roles and patterns of hurricane sedimentation in an Estuarine Marsh. *Estuarine,Coastal and Shelf Science*, 40, 665-679.

Patrick, S. W., and Moser, L. M. (2001), Potential competition between Hybrid Striped Bass (Morone saxatilis X M. americana) and Striped Bass (M. saxatilis) in the Cape Fear River Estuary, North Carolina. *Estuaries,* 24, 425-429.

Peng, M. (2002), A numerical modeling study of the hydrodynamicsof the Croatan-Albemarle-Pamlico Estuary System, North Carolina, http://www.lib.ncsu.edu/etd/public/etd165492721023850/etd.pdf

Peng, M., Xie, L., and Pietrafesa, L.J. (2004), A numerical study of storm surge and inundation in the Croatan-Albemarle-Pamilico Estuary System. *Estuarine, Coastal and Shelf Science,* 59, 121-137.

Pietrafesa, L.J., Janowitz, G.S., (1988) Physical Oceanographic Processes Affecting Larval Transport Around and Through North Carolina Inlets. *American Fisheries Society*, 3, 34-50

Pietrafesa, L.J., Xie, L., Morrison, J., Janowitz, G.S., Pelissier, J., Keeter, K., Neuherz, R.A.,(1997) Numerical modelling and computer visualization of the storm surge in and around the Croatan-Albemarle-Pamlico Estuary system produced by Hurricane Emily of August 1993. *Mausam* , 48, 567-578.

Powell, M.D., Vivkery, P. J., Reinhold, T. A. (2003), Reduced drag coefficient for high wind speeds in tropical cyclones. *Nature*. 422, 278-283.

Shank, G. C., Skrabal, A.S., Whitehead, F. R., and Kieber, J. R. (2004), Fluxes of strong Cu-complexing ligands from sediments of an organic-rich estuary. *Estuarine, Coastal and Shelf Science*, 60, 349-358.

Sheremet, A., Mehta, J.A., Liu, B., and Stone, W.G. (2005), Wave–sediment interaction on a muddy inner shelf during Hurricane Claudette. *Estuarine, Coastal and Shelf Science*, 63 , 225-233

Wren, P. A., and Leonard, L.A. (2005), Sediment transport on the mid-continental shelf in Onslow Bay, North Carolina during Hurricane Isabel. *Estuarine, Coastal and Shelf Science, 63,43-56*

Xie, L., Pietrafesa, L.J., and Peng, M. (2004), Incorporation of a mass-conserving inundation scheme into a three-dimensional storm surge model. *J. Coastal Research*, 20, 1209-1223

## The list of the table captions



## The list of the figure captions

Figure 11 Simulation of storm surge (m) and inundation at 08/14/1400Z, 08/14/1500Z, 08/14/1600Z, 08/14/1700Z when Hurricane Charley brushed the Cape Fear region in 2004.

Figure 12. The comparison of model data and water level observation in Hurricane Bertha (From left to Right: Yaupon Beach, NC, Wilmington, NC, Lenoxville Point, NC, Morehead City Harbor, NC, Beaufort, NC, Duck Pier, NC)

Figure 13. The comparison of model data and water level observation in Hurricane Fran (From left to Right: Springmaid Pier, SC, Yaupon Beach, NC, Wilmington, NC, Beaufort (Taylor Creek ), NC, Morehead City Harbor, NC.)

Figure 14. The comparison of model data and water level observation in Hurricane Floyd (From left to Right: Army Depot, SC, Wilmington, NC, Beaufort, NC, Cape Hatteras Fishing Pier, NC, Duck Pier , NC. )

Figure 15. The comparison of model data and water level observation in Hurricane Charley (From left to Right: Springmaid Pier, SC, Sunset Beach, NC, Wilmington, NC, Wrightsville Beach, NC, Beaufort, NC.)

Figure 16. The comparison of modeled result and the observed water level.

Table 1. Dates and corresponding intensities of the Hurricanes

| Date of Impact | Name | Saffir-Simpson scale |
|---|---|---|
| 07-13-96 | Bertha | 2 |
| 09-06-96 | Fran | 3 |
| 09-16-99 | Floyd | 2 |
| 08-15-04 | Charley | 1 |

Table 2. The time, location and pressure of hurricane Fran (1996)

| Time | Latitude | Longitude | Pressure(mb) |
|---|---|---|---|
| 09/05/15Z | 31.5 | -77.4 | 954 |
| 09/05/17Z | 32.0 | -77.6 | 954 |
| 09/05/19Z | 32.5 | -77.9 | 953 |
| 09/05/21Z | 32.9 | -77.9 | 953 |
| 09/05/23Z | 33.4 | -78.1 | 954 |
| 09/06/01Z | 33.9 | -78.0 | 956 |
| 09/06/03Z | 34.5 | -78.1 | 965 |
| 09/06/05Z | 34.9 | -78.5 | 970 |
| 09/06/07Z | 35.6 | -78.7 | 970 |
| 09/06/09Z | 36.1 | -78.9 | 980 |

Table 3. The time, location and pressure of Hurricane Bertha (1996)

| Time | Latitude | Longitude | Pressure (mb) |
|---|---|---|---|
| 07/12/09Z | 31.6 | -78.7 | 985 |
| 07/12/12Z | 32.3 | -78.5 | 977 |
| 07/12/15Z | 32.8 | -78.4 | 974 |
| 07/12/17Z | 33.3 | -78.0 | 974 |
| 07/12/19Z | 33.8 | -77.8 | 974 |
| 07/12/21Z | 34.3 | -77.7 | 979 |
| 07/12/23Z | 34.9 | -77.6 | 979 |
| 07/13/01Z | 35.3 | -77.5 | 985 |
| 07/13/03Z | 35.8 | -77.4 | 987 |
| 07/13/05Z | 36.1 | -77.2 | 990 |

Table 4. The time, location and pressure of Hurricane Floyd (1999)

| Time | Latitude | Longitude | Pressure(mb) |
|---|---|---|---|
| 09/15/21Z | 31.3 | -79.0 | 949 |
| 09/15/23Z | 32.1 | -78.7 | 949 |
| 09/16/01Z | 32.4 | -78.6 | 950 |
| 09/16/03Z | 32.9 | -78.3 | 952 |
| 09/16/05Z | 33.3 | -78.1 | 952 |
| 09/16/07Z | 34.0 | -77.9 | 955 |
| 09/16/09Z | 34.5 | -77.6 | 956 |
| 09/16/11Z | 35.2 | -77.1 | 960 |
| 09/16/13Z | 36.0 | -76.6 | 962 |

Table 5. The time, location and pressure of Hurricane Charley (2004)

| Time | Latitude | Longitude | Pressure(mb) |
|---|---|---|---|
| 08/14/06Z | 30.1 | -80.8 | 993 |
| 08/14/09Z | 31.2 | -80.5 | 994 |
| 08/14/12Z | 32.3 | -79.7 | 993 |
| 08/14/15Z | 33.2 | -79 | 990 |
| 08/14/18Z | 34.8 | -77.9 | 995 |
| 08/14/21Z | 36 | -77 | 1000 |
| 08/15/00Z | 36.9 | -75.9 | 1008 |

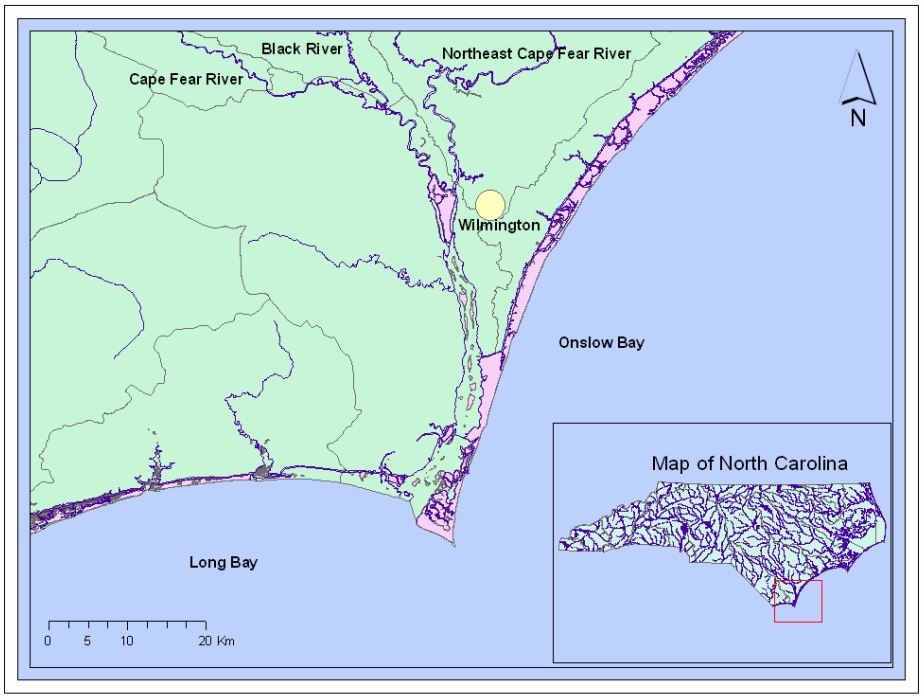


Fig 1 The location of Cape Fear River Estuary and adjacent coastal area

Figure 1. The location of Cape Fear River Estuary and adjacent coastal area

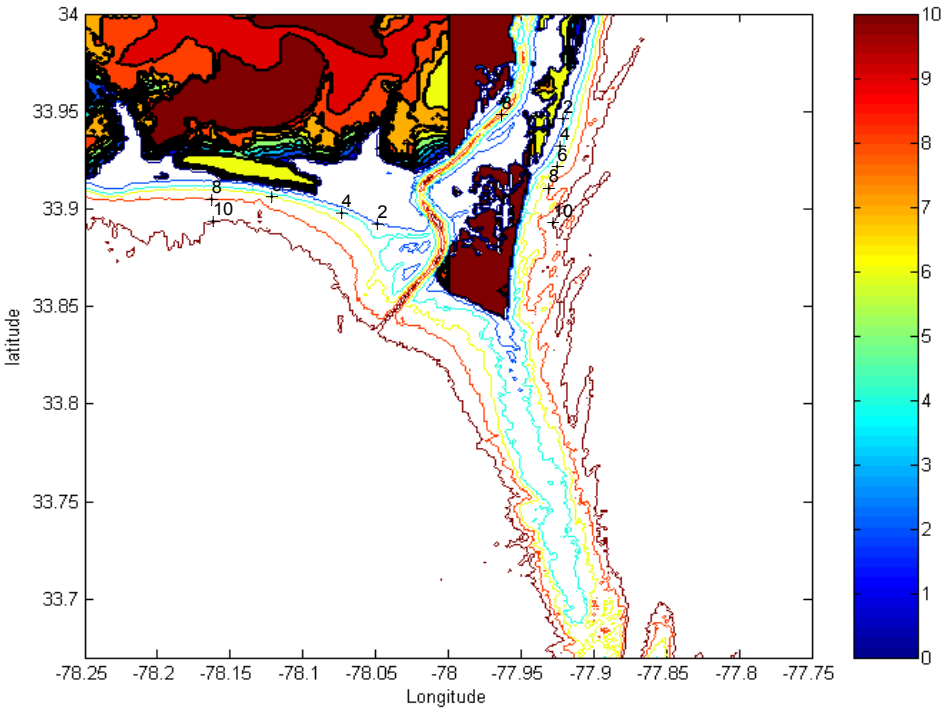


Figure 2. The land relief and bathymetry of the Cape Fear Estuary System (In meters)

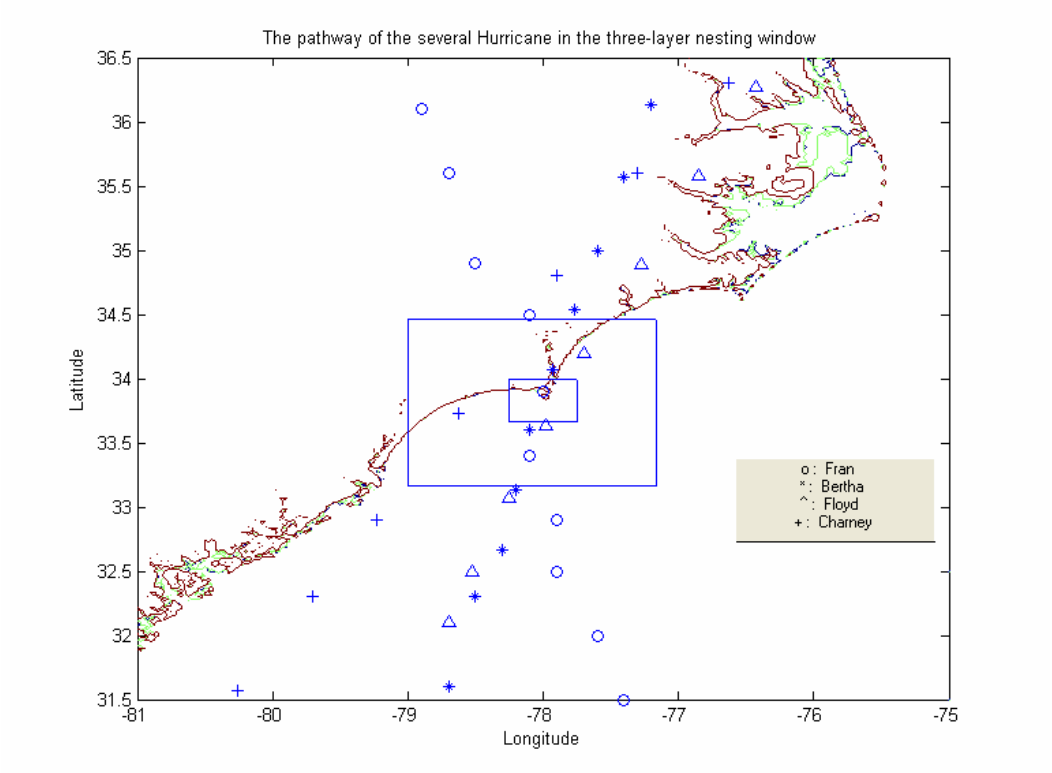


Figure 3. The tracks of four hurricanes which passed by the CFRE region

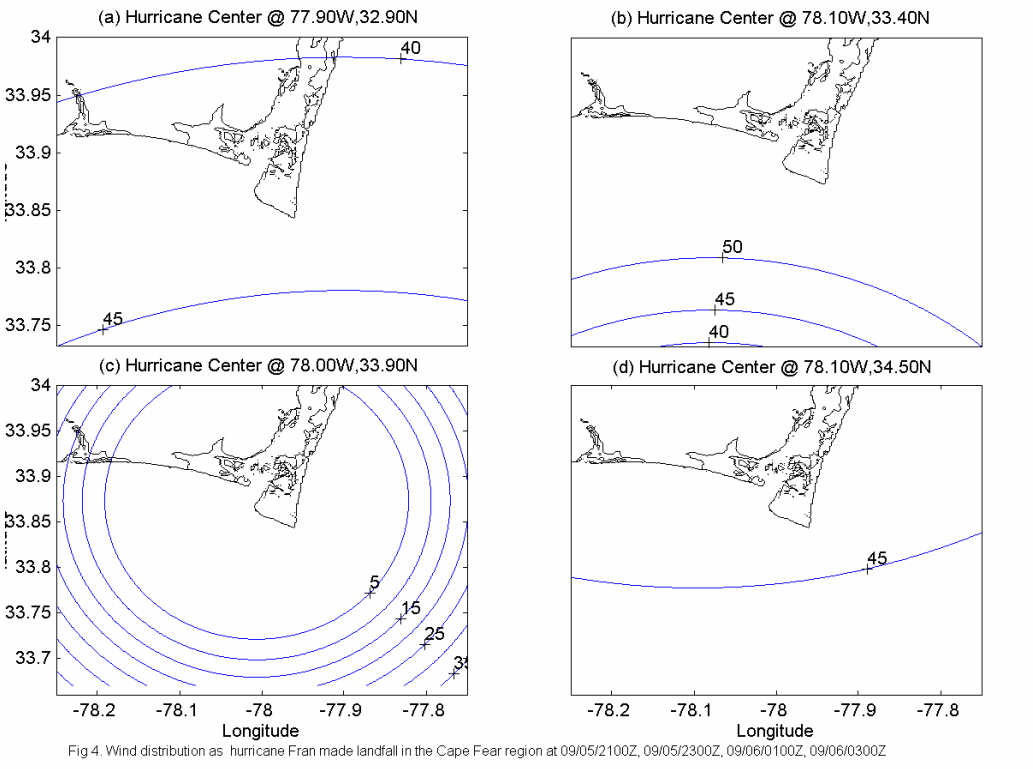


Figure 4. Wind distribution at 09/05/2100Z, 09/05/2300Z, 09/06/0100Z, 09/06/0300Z as Hurricane Fran made landfall in the Cape Fear region.

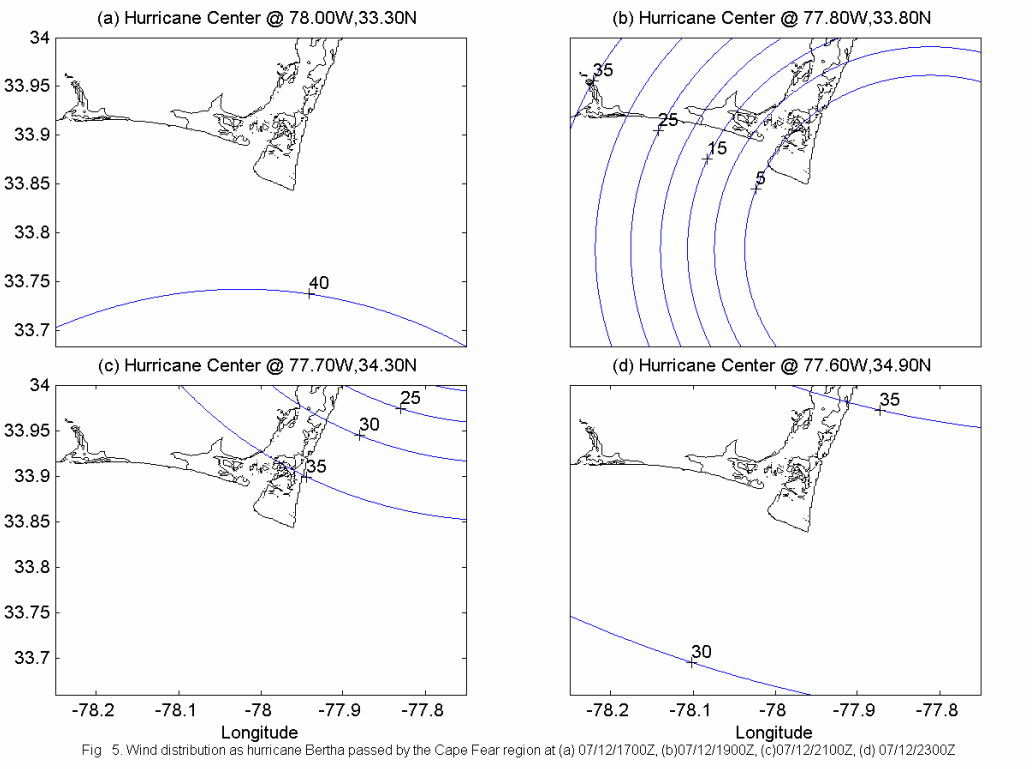


Fig 5. Wind distribution as hurricane Bertha passed by the Cape Fear region at (a) 07/12/1700Z, (b)07/12/1900Z, (c)07/12/2100Z, (d) 07/12/2300Z

Figure 5. Wind Distribution at 07/12/1700Z, 07/12/1900Z, 07/12/2100Z, 07/12/2300Z as Hurricane Bertha passed by the Cape Fear region.

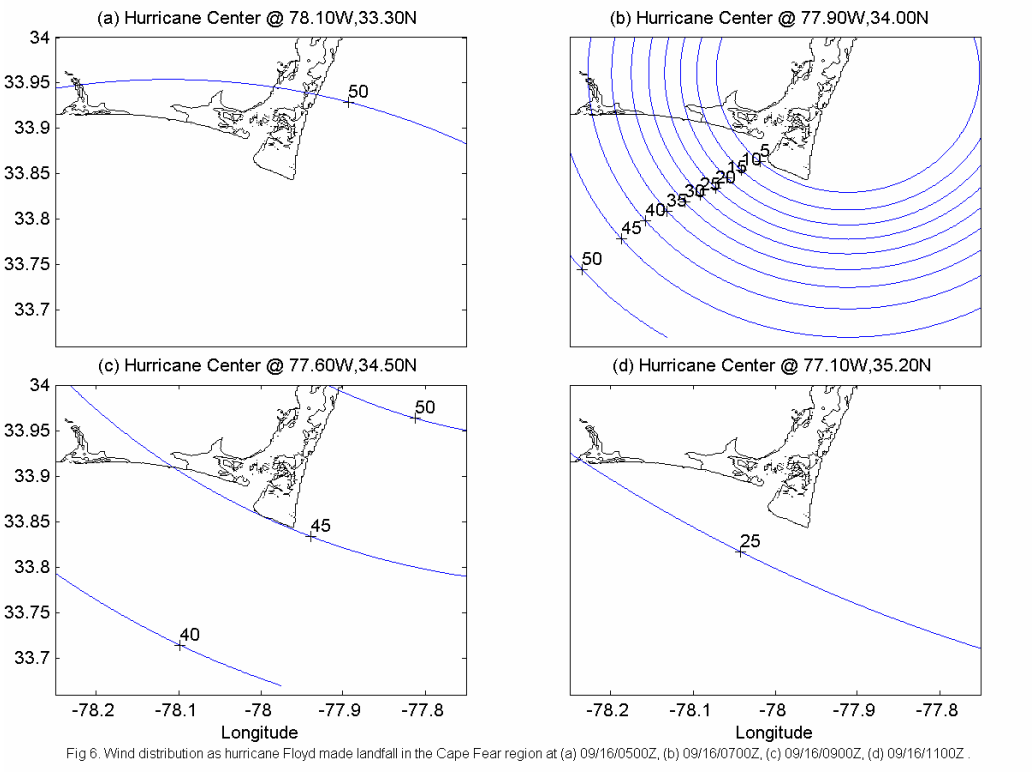


Figure 6. Wind distribution at 09/16/0500Z, 09/16/0700Z, 09/16/0900Z, 09/16/1100Z as Hurricane Floyd passed by the Cape Fear region.

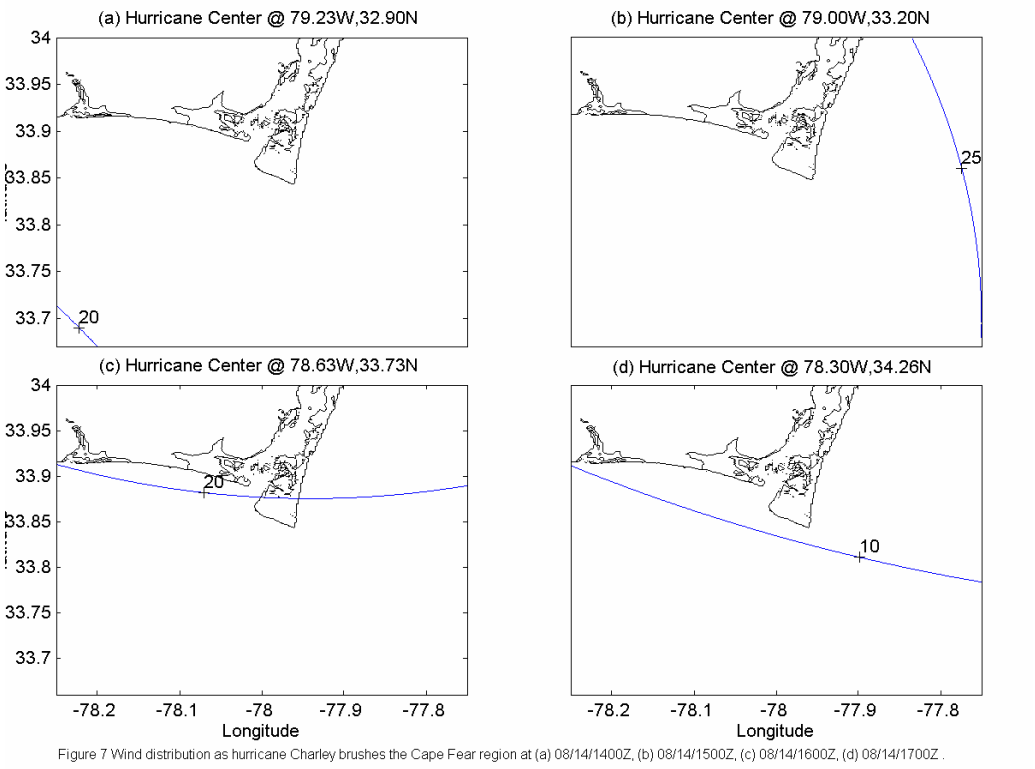


Figure 7 Wind distribution as hurricane Charley brushes the Cape Fear region at (a) 08/14/1400Z, (b) 08/14/1500Z, (c) 08/14/1600Z, (d) 08/14/1700Z .

Figure 7. Wind distributions at 08/14/1400Z, 08/14/1500Z, 08/14/1600Z, 08/14/1700Z as Hurricane Charley brushes the Cape Fear region.

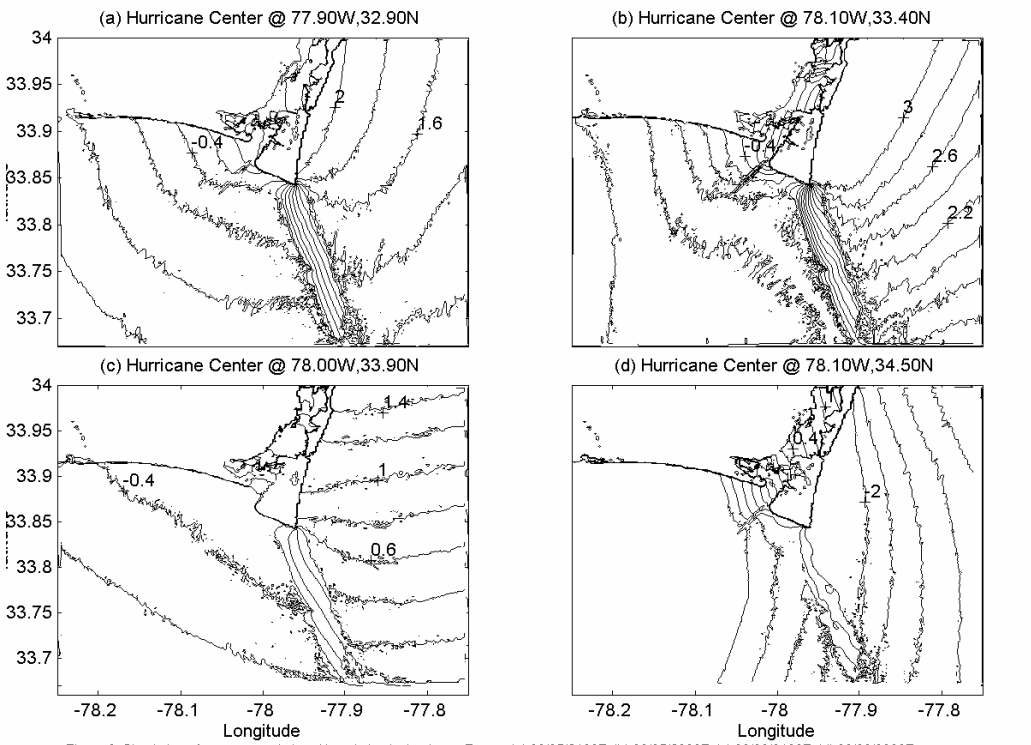


Figure 8. Simulation of storm surge (m) and inundation at 09/05/2100Z, 09/05/2300Z, 09/06/0100Z, 09/06/0300Z when Hurricane Fran crossed the Cape Fear region in 1996.

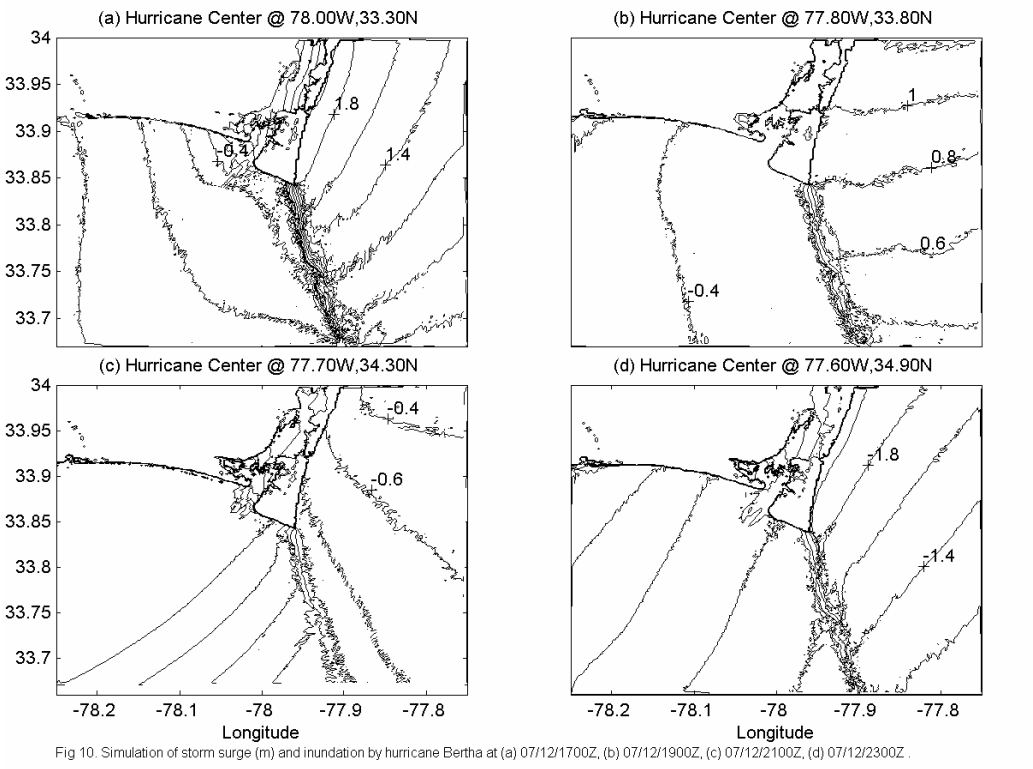

Fig 10. Simulation of storm surge (m) and inundation by hurricane Bertha at (a) 07/12/1700Z, (b) 07/12/1900Z, (c) 07/12/2100Z, (d) 07/12/2300Z .

Figure 9. Simulation of storm surge (m) and inundation at 07/12/1700Z, 07/12/1900Z, 07/12/2100Z, 07/12/2300Z when Hurricane Bertha brushed the Cape Fear region.

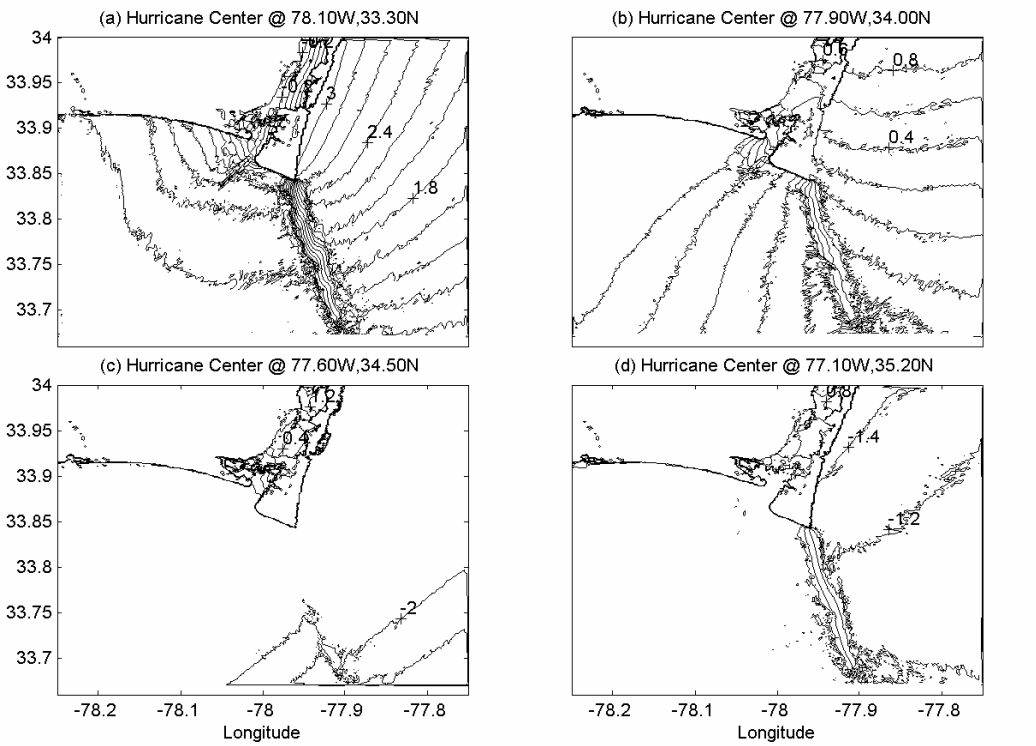


Figure 10. Simulation of storm surge (m) and inundation by hurricane Floyd at (a) 09/16/0500Z, (b) 09/16/0700Z, (c) 09/16/0900Z, (d) 09/16/1100Z .

Figure 10. Simulation of storm surge (m) and inundation at 09/16/0500Z, 09/16/0700Z, 09/16/0900Z, 09/16/1100Z when Hurricane Floyd passed by the CFRE.

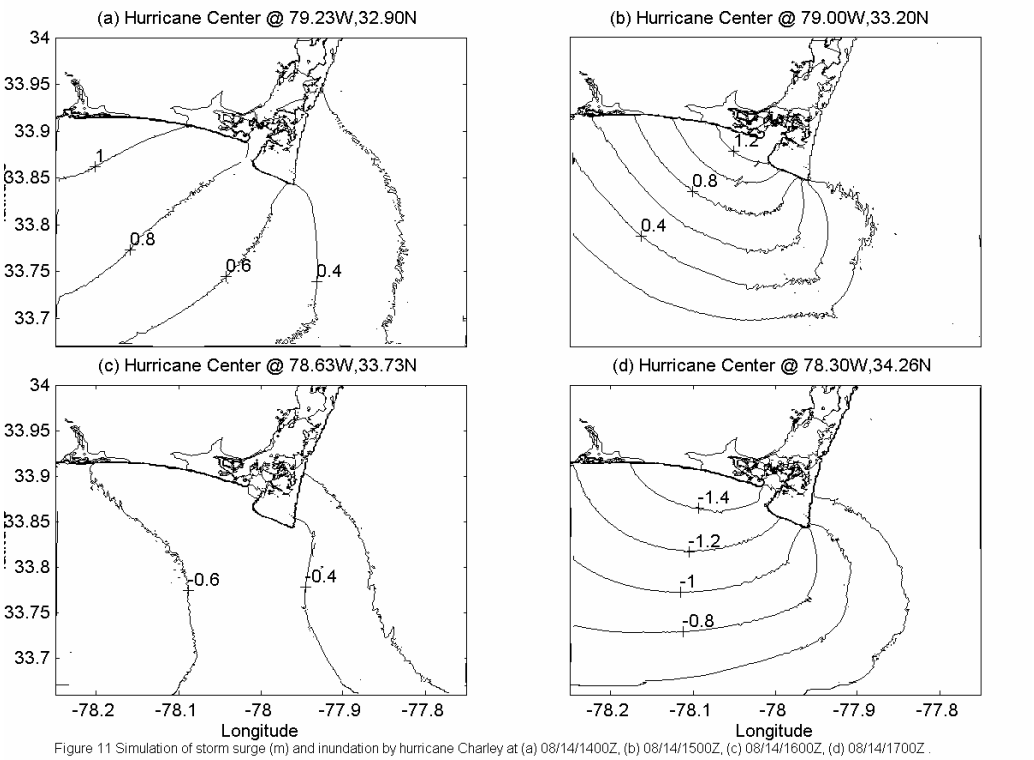

Figure 11 Simulation of storm surge (m) and inundation by hurricane Charley at (a) 08/14/1400Z, (b) 08/14/1500Z, (c) 08/14/1600Z, (d) 08/14/1700Z .

Figure 11. Simulation of storm surge (m) and inundation at 08/14/1400Z, 08/14/1500Z, 08/14/1600Z, 08/14/1700Z when Hurricane Charley brushed the Cape Fear region in 2004.

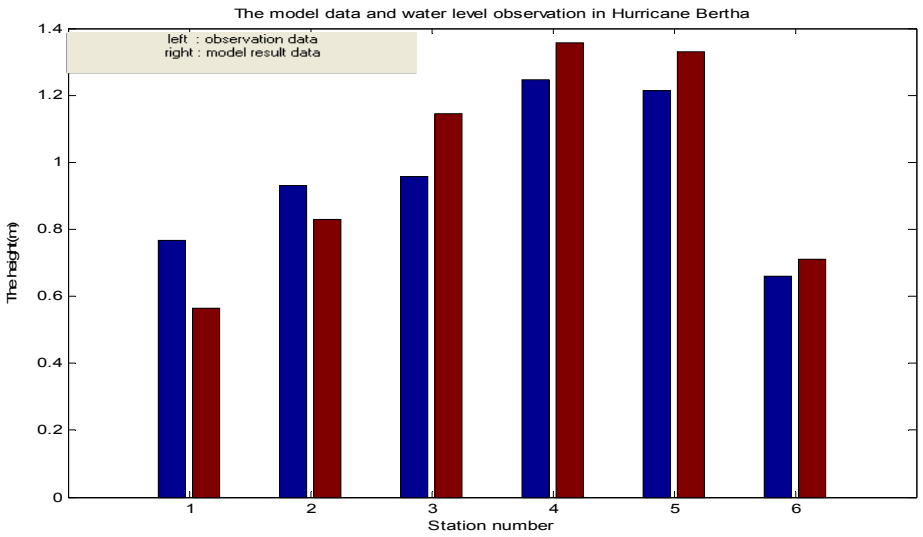


Figure 12. The comparison of model data and water level observation in Hurricane Bertha (From left to Right: Yaupon Beach, NC, Wilmington, NC, Lenoxville Point, NC, Morehead City Harbor, NC, Beaufort, NC, Duck Pier, NC)

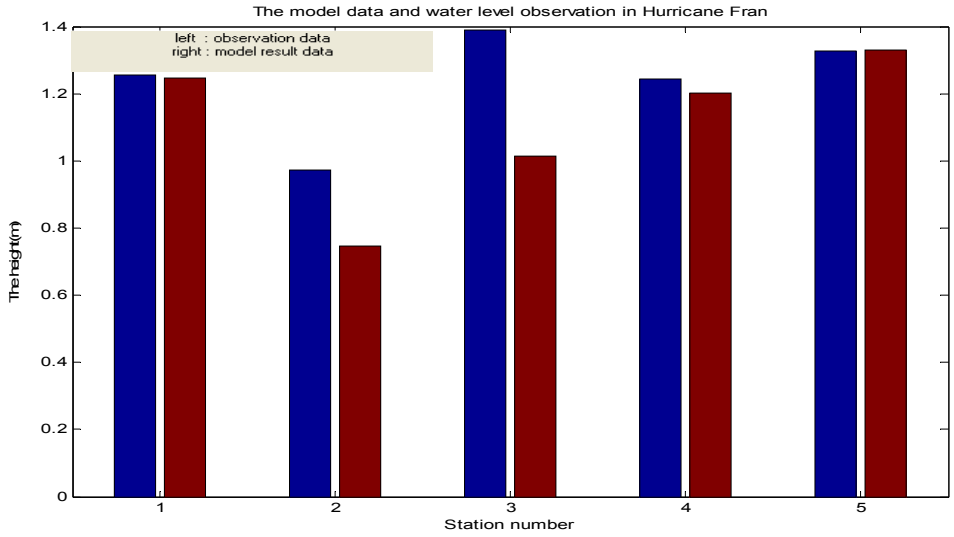


Figure 13. The comparison of model data and water level observation in Hurricane Fran (From left to Right: Springmaid Pier, SC, Yaupon Beach, NC, Wilmington, NC, Beaufort (Taylor Creek ), NC, Morehead City Harbor, NC.)

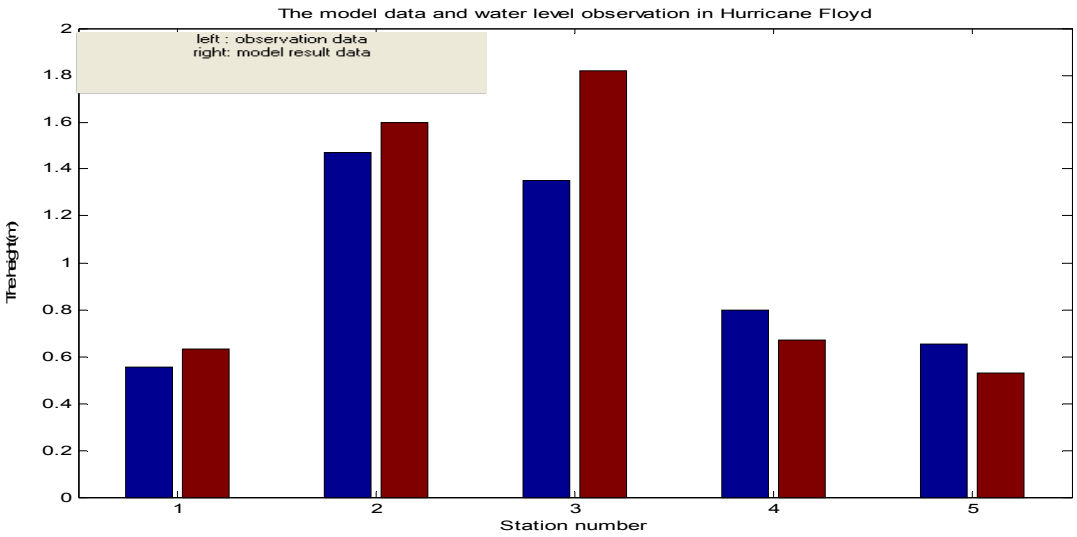


Figure 14. The comparison of model data and water level observation in Hurricane Floyd (From left to Right: Army Depot, SC, Wilmington, NC, Beaufort, NC, Cape Hatteras Fishing Pier, NC, Duck Pier , NC. )

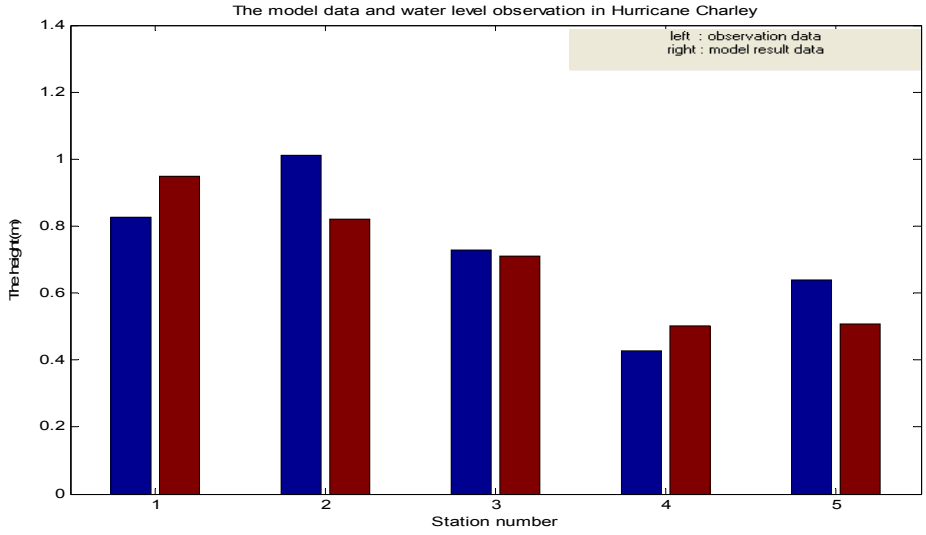


Figure 15. The comparison of model data and water level observation in Hurricane Charley (From left to Right: Springmaid Pier, SC, Sunset Beach, NC, Wilmington, NC, Wrightsville Beach, NC, Beaufort, NC.)

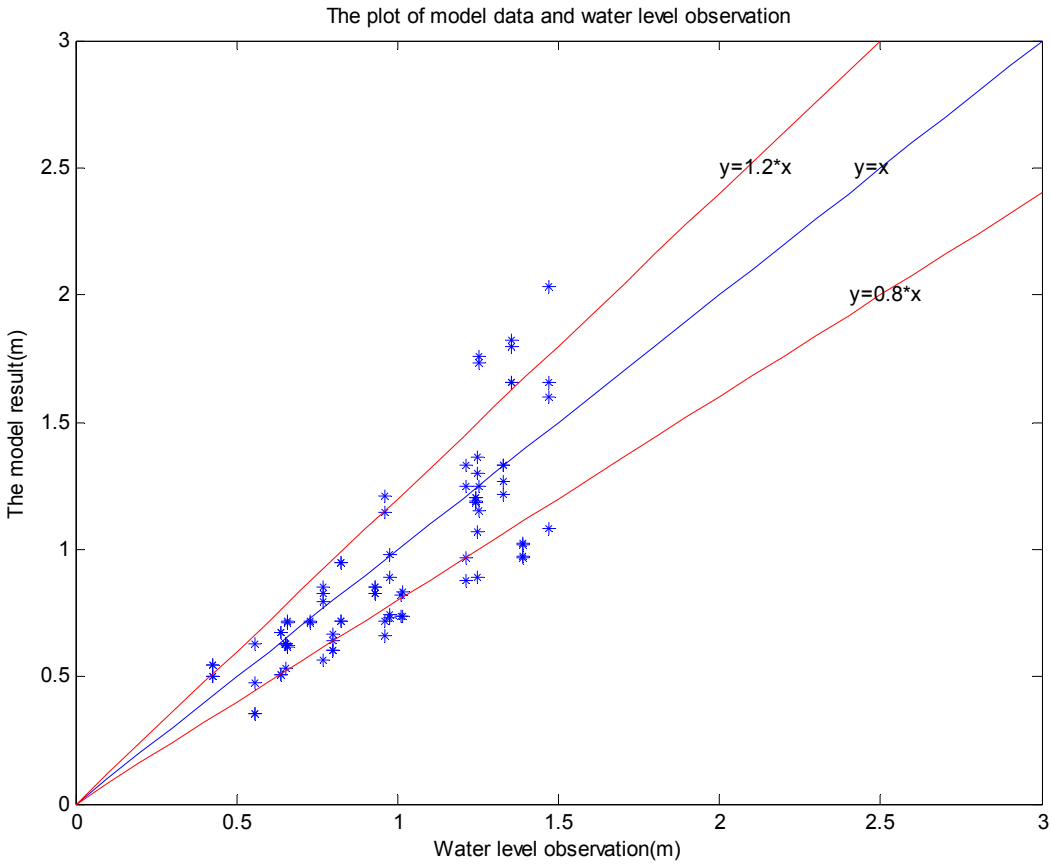


Figure 16. The comparison of modeled result and the observed water level.

# Chapter 3: Modeling of the Cape Fear River Estuary Plume


## Abstract

In this study, the Environmental Fluid Dynamic Code (EFDC), an estuarine and coastal ocean circulation model, is used to simulate the distribution of the salinity plume in the vicinity of the mouth of the Cape Fear River Estuary (CFRE). The individual and coupled effects of the astronomical tides, river discharge and atmospheric winds on the spatial and temporal distributions of coastal water levels and the salinity plume were investigated. These modeled effects were then compared with water level observations made by the National Oceanic and Atmospheric Administration, and salinity surveys conducted by the Coastal Ocean Research and Monitoring Program (CORMP). Model results and observations of salinity distributions and coastal water level show good agreement. The simulations indicate that strong winds tend to reduce the surface plume size and distort the bulge shape near the estuary mouth due to enhanced wind induced-surface mixing. Under normal discharge conditions, tides and light winds, the southward outwelling plume veers west. However relatively moderate winds can mechanically reverse the direction of flow of the plume. Under conditions of weak to moderate winds the water column does not mix vertically to the bottom, unlike the strong wind case in which the plume becomes vertically well mixed. Under conditions of high river discharge the plume increases in size and reaches the bottom. Vertical mixing induced by strong spring tides also results in the plume reaching the bottom.



Key Words: Cape Fear, EFDC, plume, coastal ocean.

# 1. Introduction

The freshwater discharge from the Cape Fear River, the Northeast Cape Fear River, and the Black River converges in the Cape Fear Estuary and then flows into Long Bay as an outwelling salinity plume (Figure 1). The average combined discharge from these rivers is about 221 $m^3$/s (Dame et al., 2000), with a maximum of about 2000 $m^3$ /s. The relatively fresh plume of the CFRE reduces salinity and modifies other water properties such as temperature, nutrients, and phytoplankton in the adjacent coastal ocean, thereby affecting the water quality and sediment structure of the total local ecosystem (Mallin et al., 2005).

Generally, river-derived fresh water discharging into an adjacent continental shelf forms a trapped river plume that propagates to its right in the Northern Hemisphere in a narrow region along the coast due to the effect of the Earth's rotation (Zhang et al, 1987). However using satellite imagery, field observations and models, additional factors such as the tides, winds, strength of vertical stratification and bottom topography have been found by previous investigations to influence the orientation and structure of river plumes in general.

Chao and Boicourt showed that vertical mixing induces much stronger seaward transport at the mouth of Chesapeake Bay. Fong and Geyer (2002) found that fresh water discharges from Chesapeake and Delaware bays create a predominantly freshwater signature toward the right and downstream of the bay mouths. Zhang et al (1987), Hickey at el (1997), and Fong and Geyer (2002) found that upwelling-favorable winds tend to move the plume water offshore while downwelling favorable winds reinforce the natural outwelling mode and further pin the plume to the coastline. Light winds were found to have minor effects on

plume orientation, while moderate to strong winds were found to be capable of fully reversing the plume and changing its structure (Zhang et al, 1987; Kourafalou et al., 1996a). The astronomical tides greatly influence the plume structure, especially the vertical salinity distribution as discussed by Cheng and Casulli (2004). Tidal currents also contribute significantly to the total kinetic energy in the shelf and near-shore region (Kourafalou et al., 1996b).

Over the past two decades there have been a series of analytical and numerical studies that have attempted to simulate the plume formation and subsequent time a space history. Chao and Boicourt (1986) and Chao (1988) used a three-dimensional, primitive-equation model to simulate the onset of plumes. Zhang et al. (1987) used a non-tidal theoretical model to simulate the various orientations of outwelled plumes. Garvine (1987) used a layered model to simulate an estuary plume by inclusion of the Coriolis force. Garvine (1999, 2001) used a three-dimensional numerical model ECOM3d and conducted numerous experiments to denote the distribution of the plume on an idealized continental shelf. O'Donnell (1990) modeled the formation of the river plume by using a mathematical model. Kourafalou et al. (1996a, b) modeled the Savannah River plume. Sheng (2001) examined the nonlinear dynamics of a buoyancy-driven coastal current and estuarine plume using a z-level ocean model. Berdeal et al. (2002) used ECOM3d to simulate the high river discharge plume in the Columbia River. Cheng and Casulli (2004) and Baptista et al. (2005) used the unstructured grid model to simulate the dynamical processes of plumes in general.

As discussed above there is an extensive and robust literature on plume modeling. However, there are significant limitations in all of these prior studies. First, ideal geometry

and physical settings were used. Second, due to the lack of observational data in the plume region, the results of most of those studies could only be validated using limited observations. For example, salinity observations are in general lacking and thus could not be used for model validation. Additionally, there is a lack of a detailed description of the vertical plume structure under the influence of various physical environmental conditions.

In this study, the Environmental Fluid Dynamic Code (EFDC) is used to simulate the CFRE plume and investigate the sensitivity of plume to wind, river discharge and tidal effects. Xia et al. (2006) used EFDC to simulate the CFRE plume, but only the surface structure of the plume was discussed. The domain is enlarged and the wind-induced currents could be generated in the plume modeling. Furthermore, the effects of the astronomical tides were not considered. In this study, the prior study of Xia et al is extended in three aspects: 1) both surface and vertical plume structures are considered; 2) a higher resolution domain is used in the plume region to resolve the details of the three dimensional plume near the mouth of the estuary; 3) the effects of wind, river discharge and tides are considered separately and collectively. In section 2, the EFDC model is briefly described. The calibration of the model is presented in section 3. Ideal plume simulation experiments and results are presented in section 4, and main conclusions are summarized in section 5.

## 2. Model description and configuration

### 2.1 A brief description of the EFDC model

The numerical model used in this study is based on a general purpose three-dimensional hydrodynamic model, EFDC (Hamrick, 1992). The physics of the EFDC model and many

aspects of the computational scheme resemble the widely used Blumberg-Mellor model (Blumberg and Mellor, 1987). It has been widely used for estuarine and coastal modeling (Ji et al., 2001, Shen and Haas, 2004; Park et al., 2005, Yang and Hamrick, 2005).

The following are the main reasons that we selected the EFDC model in this study. First, the embedded turbulence closure sub-model (Mellor and Yamada, 1982; Galperin et al., 1988) for parameterizing vertical turbulence mixing was included in the model. Second, the use of sigma coordinates (Blumberg and Mellor, 1987) in the model is well suited to study the near surface structure of plumes. Third, the model includes the anti-diffusion upwind advection scheme which is suitable for the plume study over the upwind scheme and the central difference scheme (Berdeal et al., 2002). Furthermore, EFDC uses orthogonal curvilinear or Cartesian horizontal coordinates in the grid generation which allows the grid size to be variable in order to fit the coastlines of the river and the estuary. Another important reason for selecting the EFDC model is that it includes sediment and water quality simulation sub-models which will be used for future CFRE plume studies, using the EFDC hydrodynamic backbone.

In the simulations of the CFRE plume, eleven sigma layers were utilized in the vertical dimension. As Berdeal et al. (2002) pointed out, sufficient vertical resolution is important for plume modeling. Since fresh water plumes are confined to near surface waters of the upper coastal ocean, “finer” levels were used near the free surface, while more “coarse” vertical levels were used closer to the bottom in the model. An orthogonal curvilinear grid was used in the model simulation with higher resolution in the river proper, estuary, and river mouth to

resolve the complex coastline. There are a total of 1895 grid cells in the relatively complex domain (Figure 2a). The grid size varies from 100 meters to 10 km within the model domain. Since horizontal resolution is critical for plume simulations (Fong, 1998), higher resolution grids were generated near the mouth of CFRE and the plume region. Some detailed resaon about modeling setting will be discussed at Chapter 4. The model also includes an efficient mode-splitting technique. The time step is set to 60 seconds to comply with the Courant-Friedrich-Levy (CFL) criterion. The bathymetry is derived from the National Geophysical Data Center (NGDC) Coastal Relief Model Volume 02 (Figure 2b).

**2.2 River discharge settings**

The Cape Fear River Watershed in North Carolina consists of the Cape Fear, Black and Northeast Cape Fear rivers. For retrospective simulations, sources for field data used in the modeling study were obtained from United States Geological Survey (USGS) stream flow gages in the rivers. Based on these data, the daily averaged Cape Fear River Discharge is 158 $m^3/s$ and the maximum historical river discharge is 1618 $m^3/s$. For the Black River, the daily averaged river discharge and the historical maximum discharge are 23 $m^3/s$ and 773 $m^3/s$ respectively. The corresponding discharges from the Northeast Cape Fear River are 20 $m^3/s$ and 847 $m^3/s$ respectively. These observed data are the bases for setting river discharges for sensitivity studies.

**2.3 Tides**

Three semi-diurnal constituents (M2, S2, N2), and two diurnal constituents (K1, O1) were used to simulate the tides in the model. The open boundary conditions were specified in

keeping with the harmonic constants of the five major tidal constituents using tide datum (http://www.marine.unc.edu/C_CATS/tides/tides.htm) (Table 1).

Table 1: Illustrative tidal constituents at the open boundary and in the model domain

| Name | Period | Open Boundary | | Open Boundary | | Sunset Beach Pier | | Wilmington Gauge | |
|---|---|---|---|---|---|---|---|---|---|
| | | Amplitude | | Phase | | | | | |
| | Second | Max. | Min. | Max. | Min. | Amplitude | Phase | Amplitude | Phase |
| M2 | 44714.16 | 0.75 | 0.51 | 348.98 | 352.53 | 0.72 | 355.90 | 0.63 | 63.10 |
| S2 | 43200.00 | 0.13 | 0.09 | 10.41 | 5.96 | 0.12 | 13.10 | 0.08 | 97.70 |
| N2 | 45570.05 | 0.17 | 0.11 | 334.83 | 339.52 | 0.17 | 339.00 | 0.13 | 51.00 |
| K1 | 86164.09 | 0.12 | 0.09 | 183.74 | 180.66 | 0.09 | 188.90 | 0.08 | 229.80 |
| O1 | 92949.62 | 0.09 | 0.07 | 196.51 | 193.82 | 0.07 | 196.10 | 0.06 | 233.50 |

Note: Amplitudes are in Meters; Phases are in degrees, referenced to UTC (GMT)

The data from Sunset Beach Pier and the Wilmington Gauge were obtained from the National Oceanic and Atmospheric Administration (NOAA). The Sunset Beach Pier site was deployed as part of the NOAA sponsored Carolinas Coastal Ocean Observations & Prediction Program (Caro-COOPS).

## 2.4 Wind forcing

The model domain is confined to the continental shelf area since the CFRE plume does not extend beyond the shelfbreak. The wind data used in the simulation are from the Wilmington International Airport and the Brunswick County Airport stations (figure 2c). Model sensitivity experiments used surface wind stress calculated from the well known relationship

$$\left(\tau_{xz}, \tau_{yz}\right) = \left(\tau_{sx}, \tau_{sy}\right) = c_s \sqrt{U_W^2 + V_W^2}\left(U_W, V_W\right) \qquad (1)$$

with $U_W$ and $V_W$ being the x and y components of the wind velocity with the drag

coefficient $c_s$ based on (Wu, 1982)

$$c_s = 0.001\frac{\rho_a}{\rho_w}\left(0.8 + 0.065\sqrt{U_w^2 + V_w^2}\right) \qquad (2)$$

with $\rho_a$, $\rho_w$ denoting air and water densities respectively.

### 2.5 Salinity and Temperature Fields

The salinity and temperature fields in the CFRE undergo considerable seasonal variability, with lower values in the winter and higher values in the summer. The initial salinity and temperature of the river and estuary were set in keeping with values measured in the Lower Cape Fear River Program, while continental shelf water was initialized using data from CORMP's shipboard monitoring survey. At the open boundary, the salinity was set as a constant (36.5 PSU) while daily changes of sea temperature was based on the observations collected as part of the CORMP sampling program. A five-day spin-up was used in all experiments to allow for thermodynamic adjustment in the model.

## 3. The simulation of the March 22, 2005 case

On March 22, 2005, a shipboard survey was conducted to collect salinity data at designated CFRE stations (Figure 2c). During that period, river discharge was near average. The plume model simulation of this case was used for testing model sensitivity. Xia et al (2006) employed the EFDC to verify simulated water levels under conditions of no river discharge and no wind. The simulated tides and the constructed tides show good agreement in the CFRE and adjacent coastal ocean.

With the five tidal constituents as well as the river discharge and wind effects considered, the model was used to simulate water level and salinity trends. Time-series data for the surface elevation were obtained by using tide gauges at the two stations from the NOAA (www.co-ops.noaa.gov), Wilmington Gauge and (a Caro-COOPS station) Sunset Beach Pier (figure 2c). The comparison of simulated water level and observation data was plotted in Figures 3a and 3b. From this comparison, the simulated and observed water levels show good agreement. Correlation coefficients are 0.918 for the Sunset Pier and 0.911 for the Wilmington gages with an average absolute error of 0.171m for Sunset Pier and 0.168m for Wilmington Gauge.

In the survey of the March 22, 2005 cruise, the salinity values were collected for six cruise stations, which cover most of the plume region (Figure 2c). The model-calculated salinity was compared with measured data at the six stations (Figure 4). The line represents the simulated salinity value near each station, while the point value represents the observational data. The model simulation appears to provide a reasonable reproduction of the observed salinity in the CFRE plume region.

## 4. Sensitivity Experiments

### 4.1 CFRE plume induced by normal river discharge

The base case simulation was a plume simulated under the influence of river discharge only. As shown in Figure 5, in the absence of other physical factors, such as wind and tidal effects, the plume shows a bulge structure off the mouth of the CFRE and a narrow coastal

current, which propagates towards the west downstream along the North Carolina east-west aligned south coast. This bulge structure is consistent with the discussion of Chao and Boicourt (1986), Zhang et al (1987) and Pietrafesa et al (1988).

As shown in Figure 6, the vertical salinity distribution shows a strong stratification due to fresh water discharge. The depth of the plume changes with the bathymetry. The salinity gradient varies greatly in the plume region while its changes are smaller outside the plume region. Under the average fresh water discharge effect, low salinity water is only limited to a portion of the surface water. The vertical plume distribution is constricted to the upper 2 or 3 meters at the mouth of CFRE and coastal ocean.

### 4.2 Response to normal river discharge and 5m/s wind speed under different wind directions

Winds are omni-present in the CFRE region (Pietrafesa et al, 1976), so it is important to include wind effects in plume modeling. We first consider how wind directions influence the plume structure during upwelling (westerly or eastward winds) and downwelling (easterly or westward winds) events. Under all simulations, the each river discharge is set to its daily average value and the wind speed is set to 5m/s. Easterly downwelling favorable winds will push the plume along the coast to the west of the mouth of the CFRE, and the plume hugs the southern coast (Figure 7a). Under a southwesterly upwelling favorable wind, the plume turns to the left towards east and this upwelling-favorable wind keeps the plume away from the coast. The southwesterly wind driven plume could breech Frying Pan Shoals and enter Onslow Bay (Figure 7b) as discussed previously by Singer et al (1980). So we see that the

surface plume structure is much different under the opposing cases of downwelling vs. upwelling winds. By comparing the plume structure with and without wind effects (Figure 7 and Figure 5), we find that the surface CFRE plume size is reduced and the plume bulge is distorted due to surface mixing under wind conditions.

We next consider how different wind directions influence the vertical structure of the plume, and how the wind cases compare to the no-wind case, as shown in Figures 6 and 8. The surface salinity value is higher, while deep water salinity is reduced due to the effect of wind-induced vertical mixing. The stratification is a little weaker and the depth of the vertical plume is deeper compared to the situation without winds. The plume depth reaches 4 meters under southwesterly upwelling favorable wind, which is deeper than those without wind effects. Moreover, the vertical plume structure varies under different wind directions, although the change is not as dramatic as that of the surface plume structure. Vertical mixing is strong throughout the entire channel under the case of southwesterly winds compared to the easterly wind case, in which mixing is stronger in the left part of the channel (Figure 8). Southwesterly winds also resulted in a deeper plume than those under other wind directions.

The bottom structure of salinity at the mouth of CFRE is nearly the same under the various wind conditions, and was marginally influenced by weak or moderate winds. However, there is a critical depth beyond which mixing induced by winds of specific magnitude cannot penetrate. As Hetland (2005) pointed out, wind forcing does not affect bottom salinity when the plume has reached its critical depth, and wind induced turbulent mixing is suppressed after this point. As shown in Figure 8, this critical salinity depth is determined by the various

values of wind stress. Overall, the plumes do not make bottom contact in the deepest water for the 5m/s wind speed. This phenomenon is also consistent with the discussion of Berdeal et al (2002), i.e., moderate wind forcing will strengthen the surface salinity mixing while it has little influence on the salinity near the bottom.

### 4.3 Response to different wind speeds under southwesterly winds

The southwesterly wind direction is approximately parallel to the major axis of the estuary and blows offshore. It also dominates this region in the spring (Pietrafesa et al., 1986). We therefore select southwesterly wind direction to study the sensitivity of the CFRE plume structure to wind forcing.

As shown in Figures 7b and 9, the plume size was reduced as the wind speed increased from 5m/s to 20m/s under southwesterly winds due to enhanced surface mixing associated with increased wind speeds. As shown in Figures 8b and 10, the vertical plume salinity distribution is more uniform as the wind speed and the subsequent vertical mixing increase. The stratification remains weak. The surface salinity value increases as the wind speed increased from 5m/s to 20m/s under southwesterly winds. This is consistent with the discussion of Berdeal et al (2002). The plume becomes deeper with decreasing stratification as wind stress increases due to increased vertical mixing.

The bottom salinity value decreases slightly as wind speed increases. The critical salinity depth becomes deeper with increasing wind forcing. The bottom salinity was apparently influenced by the 20 m/s wind speed. At the same time, the plume's length is much smaller

with the increasing wind speed while the depth of the plume increases slightly as shown in Figure 9. This is consistent with the condition that salt is conserved.

### 4.4 Sensitivity to river discharge under the influence of a southwesterly wind

Since southwesterly winds are very common in the CFRE and adjacent ocean (Pietrafesa et al., 1986), we run the simulation of varying discharge with a 5m/s southerly wind to study the sensitivity of the CFRE plume. As the river discharge increasing from zero to flood conditions, the size of plume is dramatically increased. There is nearly no plume formation under the no river discharge condition (Figure 11a). The plume remains small under average discharge conditions while the plume size increases dramatically under relatively high discharge or flood conditions (Figures 11b and 7b).

With the increasing river discharge, the stratification is dramatically increased in the deep water, while the vertical mixing is also increased in the shallow water due to high surface water velocity (Figure 12 and 8b). The vertical plume scale is increasing with increased river discharge. Even under the flooding condition, high stratification still exists in the deep bottom water. So the surface vertical mixing induced by the river discharge is not as strong as that of wind-induced mixing. Also the high river discharge could induce the bottom-advected plumes in the shallow water, which was discussed by Yankovsky and Chapman (1997). Additionally, higher eddy diffusivity will be induced by the increased discharge (Whitney and Garvine, 2006). Unlike the wind induced plume, mixing could deepen the plume depth while shortening the plume length. The strong river discharge will deepen the plume depth and increase the plume length.

### 4.5 Sensitivity to tidal effect under the influence of wind and river discharge

#### 4.5.1 Sensitivity to tidal effect under the normal river discharge and the influence of no wind

The surface salinity distributions were much different during high tide and low tide phases (Figures 13a and 13b). A dramatic difference of the salinity distribution exists at the mouth of the CFRE, and the alongshelf movements are much weaker compared to the non-tidal simulation. At the same time, the surface plume structure is still weaker under low tide conditions compared to the non-tidal conditions (Figures 13a, Figure 5). The salinity is more than 30 PSU with the tidal mixing along the coast while the surface salinity could reach less than 20 PSU without the tidal effect. So the strong tidal mixing plus the tidal current weakens the stratification and decreases the surface salinity value.

From the vertical plume structures, we see that the stratification is weak under flood tide and low tide (Figure 14). The plume depth is much deeper compared to the non-tidal effect case. Low salinity water could even contact the bottom. Under flood tide phases, there is strong bottom contact. The flooding tide event is strong enough to influence the vertical plume structure, decrease the stratification, and increase the vertical mixing. Under the ebb condition, the plume also has some degree of bottom contact and the stratification is weak. Garvine (2001) and Whitney and Garvine (2006) studied tidally-average vertical salinity distributions in both observations and modeling and found that plumes could reach the bottom using the tidally-averaged field so the modeling results presented here are consistent with their findings.

Compared to the non-tidal simulation, the surface salinity is lower during the ebb tide and tidal mixing plays a crucial role in the vertical plume structure. The non-tidal simulation shows that the plume makes bottom contact only under flood conditions. Berdeal et al. (2002) mentioned that the plumes do not make bottom contact for the relatively weak wind stress in their simulation since they did not include tidal effects in the model.

### 4.5.2 Sensitivity to tidal effect under the normal river discharge and the influence of a southwesterly wind

Compared to the non-tidal effect, the upshelf and downshelf coastal circulation are weak (Figure 15). There is no plume formation in either the upshelf or downshelf direction. As in the previous discussions of tidally-driven plumes under no wind effect, the plume size is much smaller during low tide conditions (Figure 7b) and is even smaller during high tide conditions.

From Figure 16, the distribution of the plume is very similar to that of the no wind scenario. Compared to weak or moderate wind effects, tidal mixing plays a crucial role in determining the plume structure.

## 4.6 The plume distribution plot under the wind direction, wind speed and river discharge

Overall, we run 144 experiments for the sensitivities of the plume modeling that include eight different wind directions, 5 different wind speeds from 0m/s to 20m/s, and 4 different

runoffs settings from no river discharge to flood conditions. Under the eight different winds directions, we draw the plot for the possible plume structure from the modeling results. We define the plume as six types: the type 1 with the plume being along the south coast as the plume distribution of Figure 5(a); the type 2 with the plume being apart a little bit from the south coast as the plume distribution of Figure 7(a); the type 3 as the plume distribution of Figure 17(a); the type 4 with the plume moving to the south of the CFRE as the distribution of Figure 17(b); the type 5 with the plume passing the frying pan shoal and arriving at Onslow Bay as the distribution of Figure 7(b); the type 6 in which the plume can't move out of the Long Bay and the ocean water even could reverse to the estuary part as the figure 9. Based on the above definition, we draw the possible plume plots in the Figure 18.

From the Figure 18(a), we could see the southwest wind induced plume mostly like within the Type 5 and Type 6. The plume will move the south and even could reach Onslow Bay under the most condition but the plume won't reach the Long Bay when the wind forcing is strong and river runoff is weak. The west wind induced plume is very close the southwest wind induced plume while the west wind induced plume could turn to the Type 4 with the high runoff and weak wind forcing.

The plume distribution was plotted by Figure 18(b) under the northeast and north wind. We could see the north and northeast wind induced plume mostly like within the Type 1, Type 2 and Type 3. The majority of northeast wind induced plume are within the Type 2 while it move to the Type 1 under strong wind forcing and weak runoff. The north wind induced plume are mostly defined by Type 3 plume but it turn to type 2 with very high runoff like flood condition and weak wind speed.

It is very easy to define the plume distribution under the southeast, east and south wind forcing because these wind induced plume are located either Type 1 or Type 6 (figure 18(c)). Overall, these wind induced plume could turn to the Type 6 with high wind forcing and low river discharge.

For the northwest wind induced plume distribution, it ranged from Type 3, Type 4 to Type 5, Type6. It changed according to the changing of wind speed and river runoff (figure 18(d)).

## 5. Summary and conclusions

In this study, the three-dimensional EFDC model is configured for the CFRE region to simulate the salinity plume structure. The main conclusions are summarized below.

1) When average river discharge is imposed without wind effects, the CFRE plume is generally confined to the south-facing coastal shore line in upper Long Bay and extends in the west direction to form a long narrow trapped structure. For the vertical distribution, low salinity water is only limited to the upper 2 or 3 meters at the mouth of CFRE and coastal ocean.
2) As the river discharge increased from zero to flood conditions, the size of surface plume dramatically increased. The high river discharge induced plume could reach shallow water bottoms but not deep water bottoms, and high stratification still exists in the deep bottom water.

3) The plume's surface structure is significantly different depending on wind directions when the effect of wind is added. Even a moderate wind could fully reverse the buoyancy-driven plume structure in the CFRE under average river discharge conditions. During average river discharge condition, southwesterly upwelling favorable winds all cause the CFRE plume to depart from the coast to the south of CFRE. In contrast, under easterly downwelling favorable winds, the CFRE plume trapped along the coast under periods of normal river discharge. The surface plume structure is much different under the opposing cases of downwelling vs. upwelling winds. Moreover, the surface plume size was significantly reduced with the increasing wind forcing. Under the strong wind forcing, there is nearly no plume formation at the mouth of CFRE.
4) Under moderate or weak wind forcing and moderate fresh water discharge, the plume is unlikely to make contact with the bottom given the limitation of the critical salinity depth. There is a very strong stratification in these cases, and the different wind direction could lead to slightly different vertical plume structures. Under strong wind forcing condition, the stratification is weaker and could cause the vertical salinity distribution uniform. The plume also could reach the bottom at the mouth of CFRE.
5) Astronomical tides are an important factor in influencing the plume's horizontal structure. The plume is extended well offshore in Long Bay during the ebb tide whereas the plume reverses into the estuary during the flood tide (Figures 13a and 13b). Even the moderate wind effects was included, the plume still show strong difference during the flood tide and ebb tide (Figures 15a and 15b). Therefore, tidal currents play a key role in influencing the plume's structure in addition to the vertical tidal mixing effect.

6) Under the effect of tidal mixing, the plume could make bottom contact for most cases, while it seldom makes bottom contact without the tidal effect in the simulation. When compared to the weak or moderate wind effect, tidal mixing plays a crucial role in determining the vertical plume structure.

7) Frying Pan Shoals, between Long Bay and Onslow Bay, can affect the plume structure by inhibiting a plume from spreading from Long Bay to Onslow Bay. Under flood conditions, the plume region was mostly confined to the Long Bay region (Figure 11b). This is consistent with the discussion of Mallin et al. (2005), which showed that the water mass in Onslow Bay differs greatly from that in Long Bay since very little freshwater enters Onslow Bay from the south. From Figure 7b, we still can see that some of the plume could breech the Shoals and reach Onslow Bay. This is consistent with the observations of Singer et al (1980) which shows that under conditions of strong westerly to southwesterly winds, CFRE plume waters can breach the shoals and have been detected in southern Onslow Bay.

## Acknowledgements

This study was supported by the Coastal Ocean Research and Monitoring Program (CORMP) which was funded by NOAA under grand award #NA16RP2675 through a subcontract from University of North Carolina at Wilmington. All modeling activities are carried out in the Coastal Fluid Dynamics Lab of North Carolina State University. We thank for Dr. John Hamrick for providing the source code for the simulations. The authors appreciate the detailed editorial suggestions made by three anonymous reviewers.

## References

Baptista, A.M., Zhang, Y.L., Chawla, A., Zulauf, M., Seaton, C., Myers III, E.P., Kindle J., Wilkin, M., Burla, M., Turner, P.J. (2005). "A cross-scale model for 3D baroclinic circulation in estuary–plume–shelf systems: II. Application to the Columbia River." *Continental Shelf Research,* 25, 935–972.

Berdeal, I.G., Hicky, B.M., and Kawase, M. (2002). "River-forced estuarine plume." *J. Phys. Oceanogr.*, 18, 72-88.

Blumberg, A.F., and Mellor, G.L. (1987). "A description of a three-dimensional coastal ocean circulation model, in Three-Dimensional Coastal Ocean Models." *Editor:* N.S. Heaps*, Am. Geophys. Union*, 1-16.

Chao, S.Y., and Boicourt, W. C., (1986). "Onset of estuarine plumes." *J. Phys. Oceanogr.,* 16, 2137-2149.

Chao, S.Y. (1988). "River-forced estuarine plume." *J. Phys. Oceanogr.,* 18, 72-88.

Cheng, R.T., and Casulli, V. (2004). "Modeling a Three-dimensional River Plume over Continental Shelf Using a 3D Unstructured Grid Model" *Proceedings of the Eighth International Conference on Estuarine and Coastal Modeling*, Editors: Malcolm L. Spaulding, 1027-1043.

Dame, R., Alber, M., Allen, D., Mallin, M., Montague, C., Lewitus, A., Chalmers, A.,

Gardner, R., Gilman, C., Kjerfve, B., Pinckney, J., Smith, N. (2000) "Estuaries of the South Atlantic Coast of North America: Their Geographical Signatures" *Estuaries* 23, 793–819.

Fong, D.A (1998). Dynamics of freshwater plumes: observations and numerical modeling of the wind-forced response and alongshore freshwater transport*, Ph.D. thesis, MIT/WHOI Joint Program in Oceanogr.,* Woods Hole, MA.

Fong, D.A., and Geyer, W.R., (2001). "Response of a river plume during an upwelling favorable wind event." *J. Geophys. Res.,* 106, 1067–1084.

Fong, D.A., and Geyer, W.R. (2002). "The alongshore transport of freshwater in a surface-trapped river plume." *J. Phys. Oceanogr.*, 32, 957-972.

Galperin, B., Kantha, L.H., Hassid,S., and Rosati, A. (1988). "A quasi-equilibrium turbulent energy model for geophysical flows." *J. Atmos. Sci.,* 45, 55-62.

Garvine, R.W. (1987). "Estuary plumes and fronts in shelf waters: A layer model" *J. Phys. Oceanogr.,* 17, 1877-1896.

Garvine, R.W. (1999). "Penetration of buoyant coastal discharge onto the continental shelf: A numerical model experiment." *J. Phys. Oceanogr.,* 29, 1892-1909.

Garvine, R.W. (2001). "The impact of model configuration in studies of buoyant coastal

discharge." *J. Marine Research.*, 59, 193-225.

Hamrick, J.M. (1992). "A Three-Dimensional Environmental Fluid Dynamics Computer Code: Theoretical and Computational Aspects" *Special Report,* 317. *The College of William and Mary, Virginia Institute of Marine Science,* Williamsburg, Virginia. 63 PP.

Hetland, D.R. (2005) "Relating river plume structure to vertical mixing" *J. Phys. Oceanogr ,* 35, 1667-1688.

Hickey, B.M., Pietrafesa, L.J., Jay D.A., and Boicourt, W.C. (1998). "The Columbia River plume study: Substantial variability in the velocity and salinity field." *J. Geophys. Res.,* 103, 10339-10368.

Ji, Z., Morton, M.R., Hamrick, J.M. (2001). "Wetting and Drying Simulation of Estuarine Processes Estuarine." *Coastal and Shelf Science,* 53(5), 683-700.

Kourafalou, V.H., Oey, L., Wang, J., and Lee,T.N. (1996a). "The fate of river discharge on the continental shelf, 1, Modeling the river plume and inner shelf coastal current." *J. Geophys. Res.,* 101, 3415–3434.

Kourafalou, V.H., Lee, T.N., Oey, L., and Wang, J. (1996b). "The fate of river discharge on the continental shelf, 2, Transport of coastal low-salinity waters under realistic wind and tidal forcing." *J. Geophys. Res.*, 101, 3435– 3456.

Mallin, M.A., Cahoon, L.B., and Durako, M.J. (2005). "Contrasting food-web support bases for adjoining river-influenced and non-river influenced continental shelf ecosystems Estuarine." *Coastal and Shelf Science,* 62, 55–62.

Mellor, G.L., and Yamada T. (1982). "Formation of a turbulent closure model for geophysical fluid problems." *Rev. Geophys. Space Phys.,* 20, 851-875.

O'Donnell, J. (1990). "The formation and fate of a river plume: A numerical model.*" J. Phys. Oceanogr*., 20, 551-569.

Park, K., Jung, H., Kim, H., and Ahn, S. (2005). "Three-dimensional hydrodynamic-eutrophication model(HEM-3D):application to Kwang-Yang Bay, Korea." *Marine Environmental Research,* 60, 171– 193.

Pietrafesa, L.J., Janowitz, G.S., Chao, T.Y., Weisberg, R.H., Askari, F., and Noble, E. (1986). "The physical oceanography of the Pamlico Sound." *UNC Sea Grant Publication UNC-WP-86-5*, Raleigh, N.C. 125PP.

Pietrafesa, L.J., Janowitz, G.S. (1988) "Physical Oceanographic Processes Affecting Larval Transport Around and Through North Carolina Inlets." *American Fisheries Society*, 3, 34-50.

Shen, J., Haas, L. (2004). "Calculating age and residence time in the tidal York River using

three-dimensional model experiments." *Estuarine, Coastal and Shelf Science,* 61, 449-461.

Sheng, J., (2001). "Dynamics of a buoyancy-driven coastal jet: The Gaspe Current.", *J. Phys. Oceanogr*., 31, 3146-3163.

Singer, J., Atkinson, L.,Pietrafesa, L.J., (1980). "Summertime advection of low salinity sruface water into Onslow bay" *Estuarine and Coastal Marine Science,* II, 73-82.

Whitney, M.M and Garvine, R.W., (2006). "Simulating the delaware bay buoyant outflow: comparison with observations" *J. Phys. Oceanogr,* 36, 3-21

Wu, J., (1982). "Wind-Stress Coefficients Over Sea Surface from Breeze to Hurricane." *J. Geophys. Res.,* 87, 9704-9706.

Xia, M., Xie, L., Pitrefesa, L.J., (2006). "Cape Fear River Estuary Plume Modeling: Model Configuration and Sensitivity Experiments" *Proceedings of the Eighth International Conference on Estuarine and Coastal Modeling*, Editors: Malcolm L. Spaulding, 66-84.

Xie, L., Pietrafesa, L.J. (1999). "System wide modeling of wind and density driven circulation in the Croatan-Albemarle Pamlico estuary system. Part I: Model configuration and testing." *J. Coastal Research,* 15, 1163-1177.

Xing, J.X., Davies, A.M., (1999). "The effect of wind direction and mixing upon the

spreading of a buoyant plume in a non-tidal regime." *Continental Shelf Research,* 19, 1437-1483.

Yang, Z., Hamrick, J.M. (2005). "Optimal control of salinity boundary condition in a tidal model using a variational inverse method." *Estuarine Coastal and Shelf Science*, 62, 13-24.

Yankovsky, A.E., Chapman, D.C., 1997. "A simple theory for the fate of buoyant coastal discharges." *J. Phys. Oceanogr.*, 27, 1386-1401.

Zhang, Q.H, Janowitz, G.S., Pietrafesa, L.J. (1987). "The interaction of estuarine and shelf waters: A model and applications" *J. Phys. Oceanogr.,* 17, 455-469.

## List of Figures

Figure 16. Plume structure with southwest wind forcing and normal discharge: (a) Response to low water level condition (b) Response to normal condition after low tide (c) Response to high water level condition (d) Response to normal condition after high tide

Figure 17. Surface salinity fields forced by 5m/s winds and normal discharge
(a) Response to northerly winds (b) Response to northwesterly winds

Figure 18. The plume type under the different physical settings

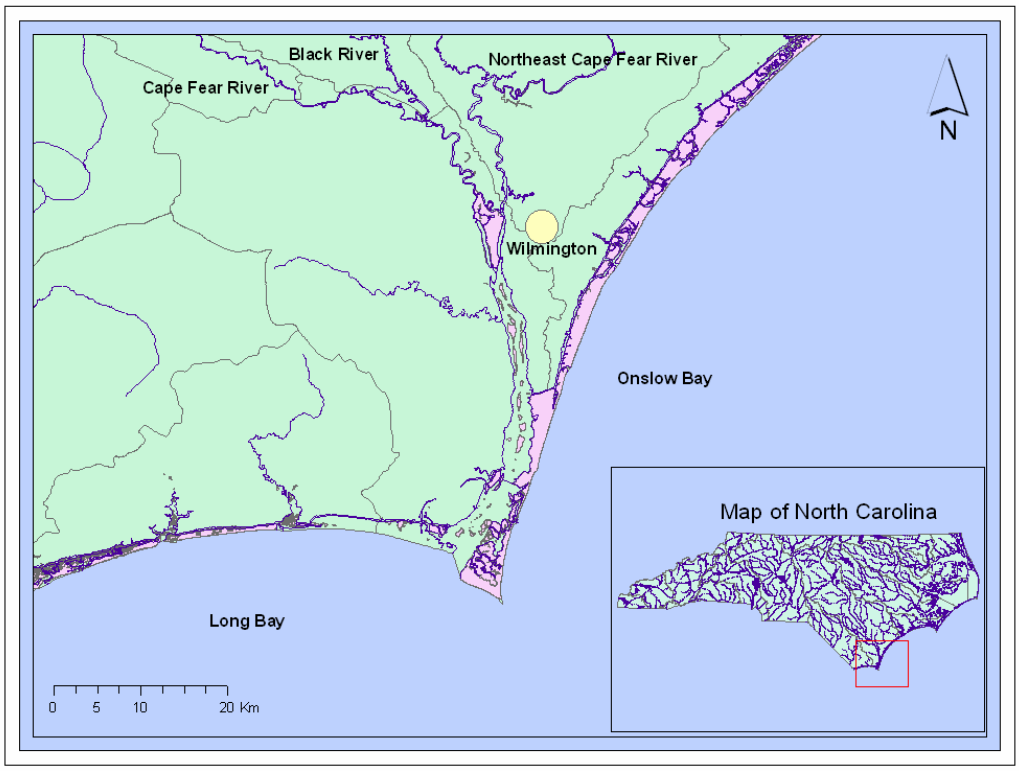


Figure 1. The location of the Cape Fear River Estuary

(a) The grid of the model domain (b) The bathymetry of the model domain

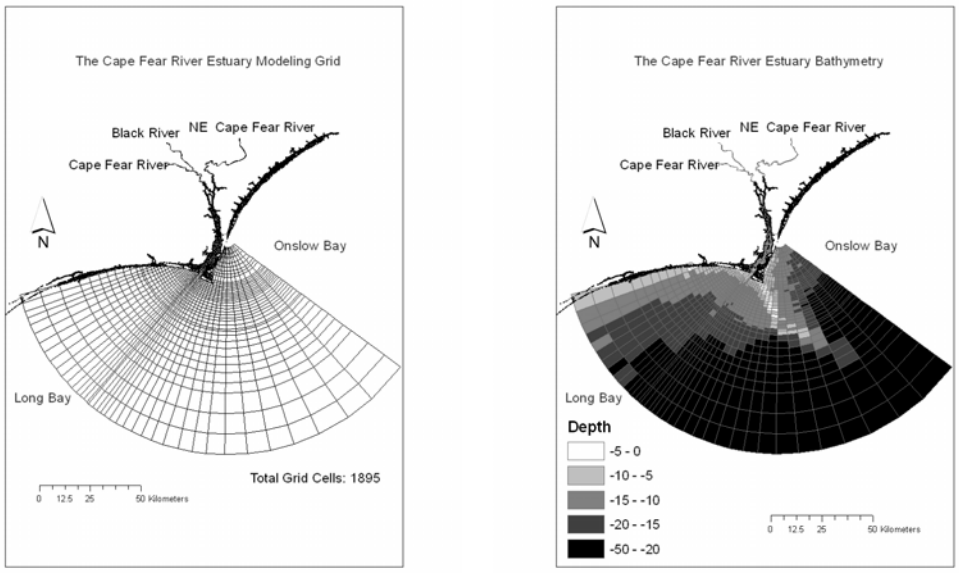


(c) The Sample Location

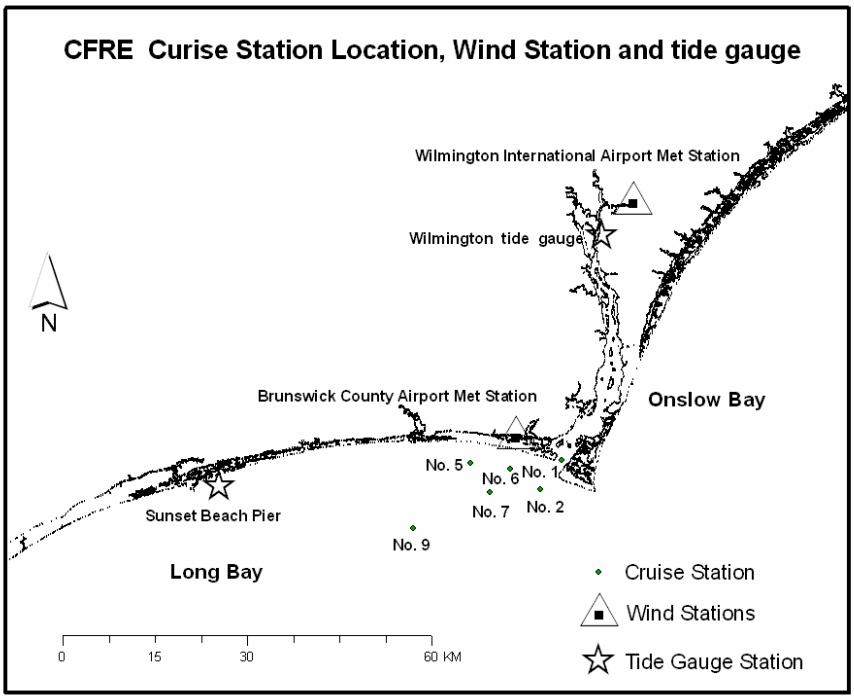


Figure 2. The grids and bathymetry in the CFRE modeling domain. Dots indicate the locations of cruise stations during the CORMP field survey.

(a) Comparison at Wilmington Gauge

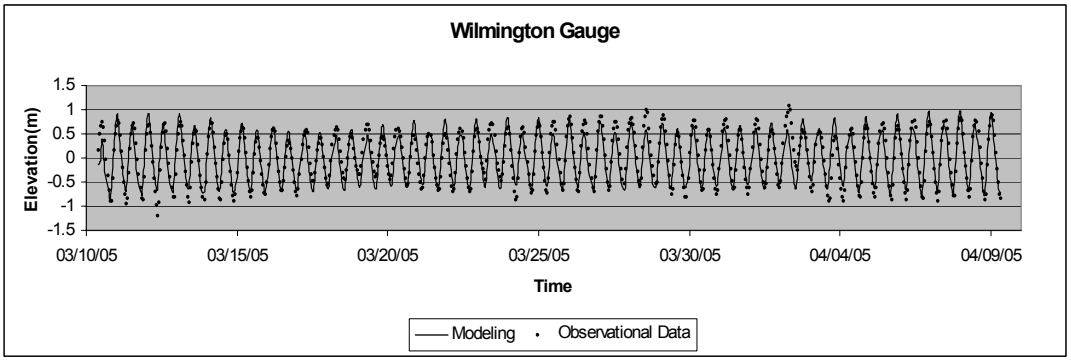


(b) Comparison at Sunset Beach Pier

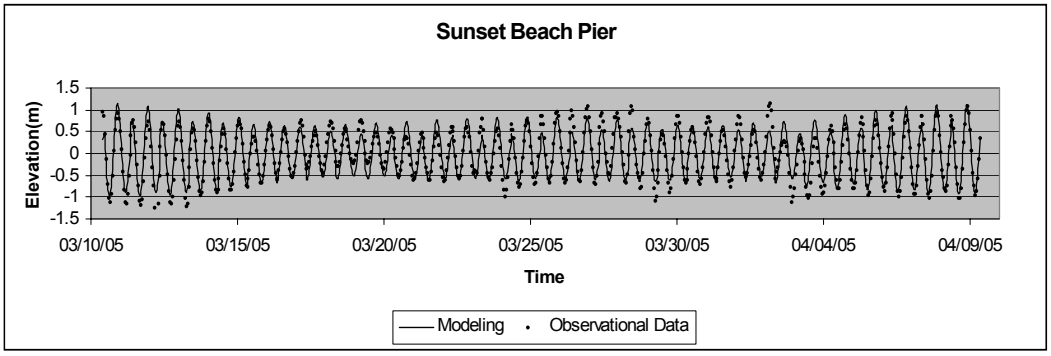


Figure 3. Comparison between model simulated and observed water level (The model was forced by wind, tides and river discharge).

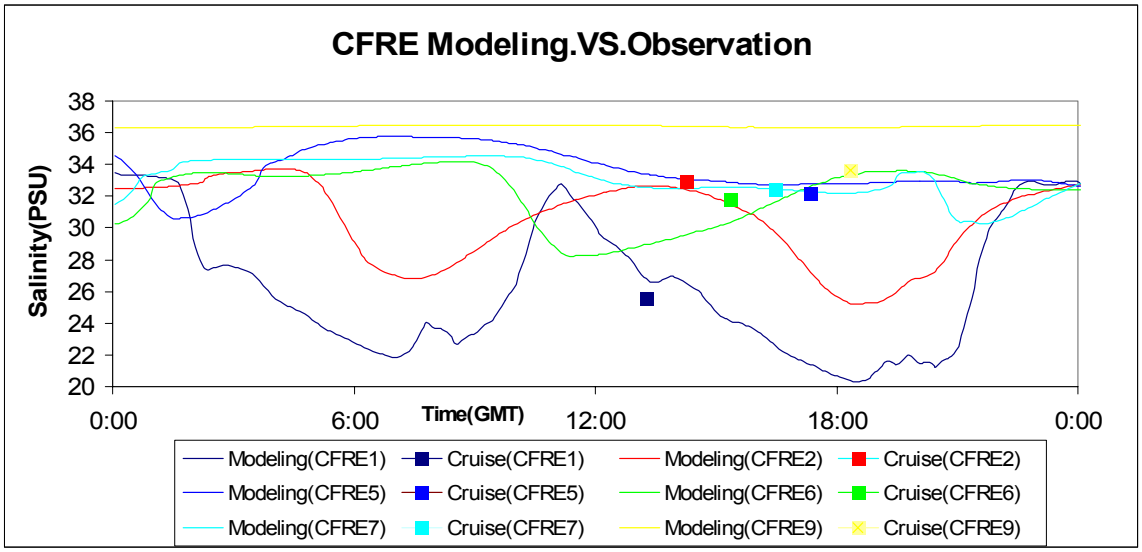


Figure 4. Comparison between the simulated and observed salinity

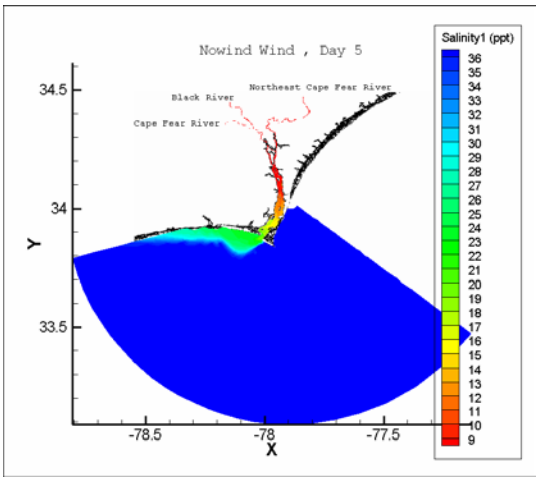


Figure 5. The Sea surface salinity fields forced by normal river discharge after 5 day simulation

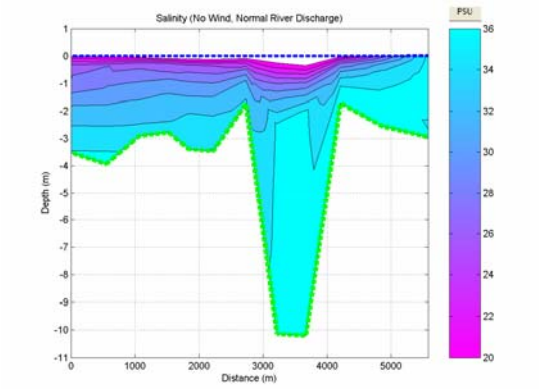


Figure 6. The vertical salinity fields forced by normal river discharge after 5 day simulation

(a) Response to easterly winds

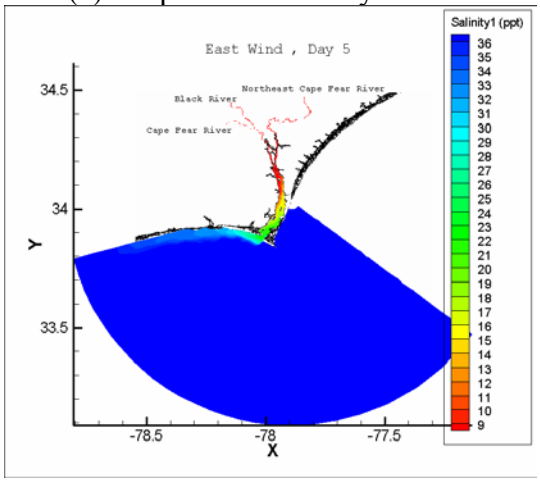


(b) Response to southwesterly winds

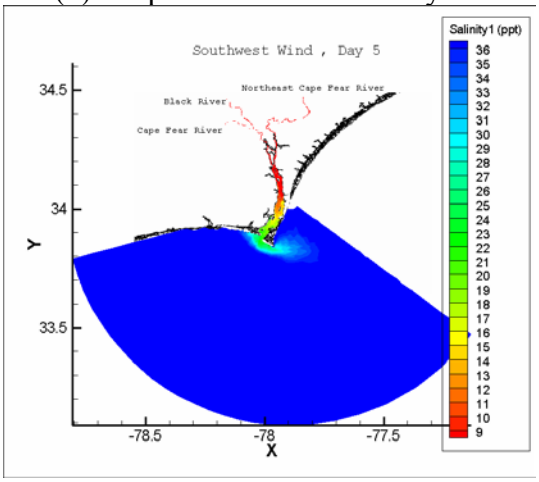


Figure 7. Surface salinity fields forced by 5m/s winds and normal discharge

(a) Response to the easterly wind

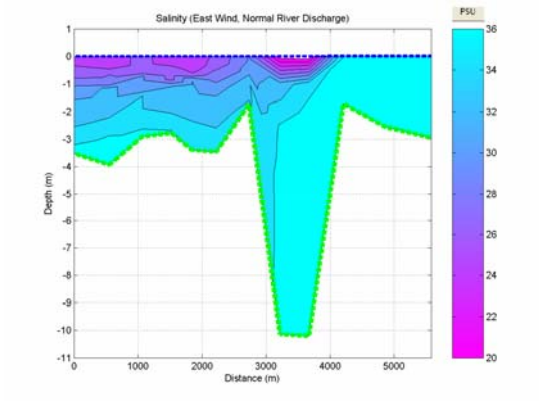


(b) Response to southwesterly wind

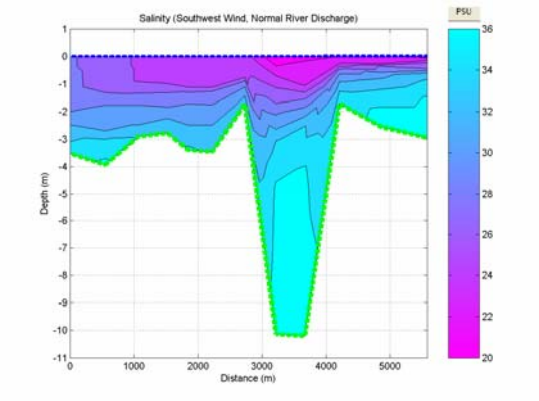


Figure 8. Vertical salinity fields forced by 5 m/s winds and normal discharge

Response to 20 m/s wind speed

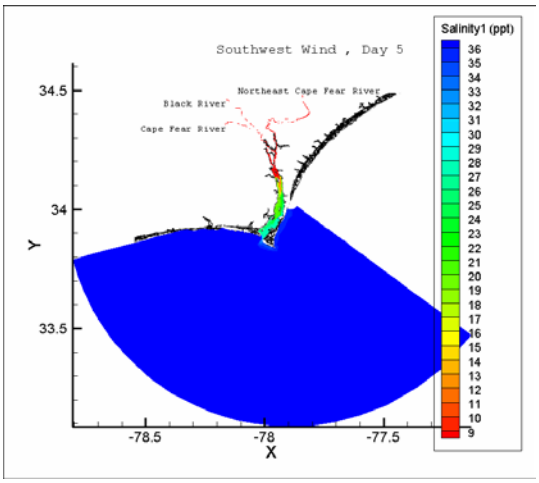


Figure 9. Plume structure under southwesterly winds and normal river discharge

(a) Response to 20 m/s wind speed

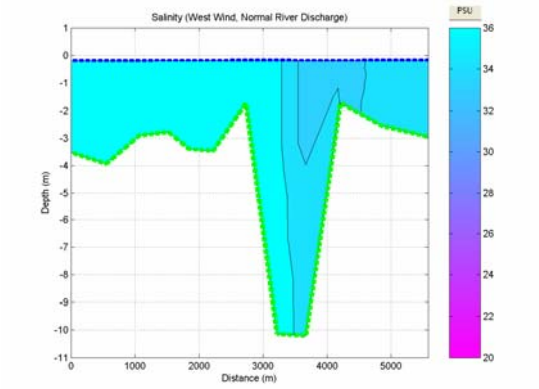


Figure 10. Plume structure under southwesterly winds and normal river discharge

(a) Response to no river discharge (b) Response to flood conditions

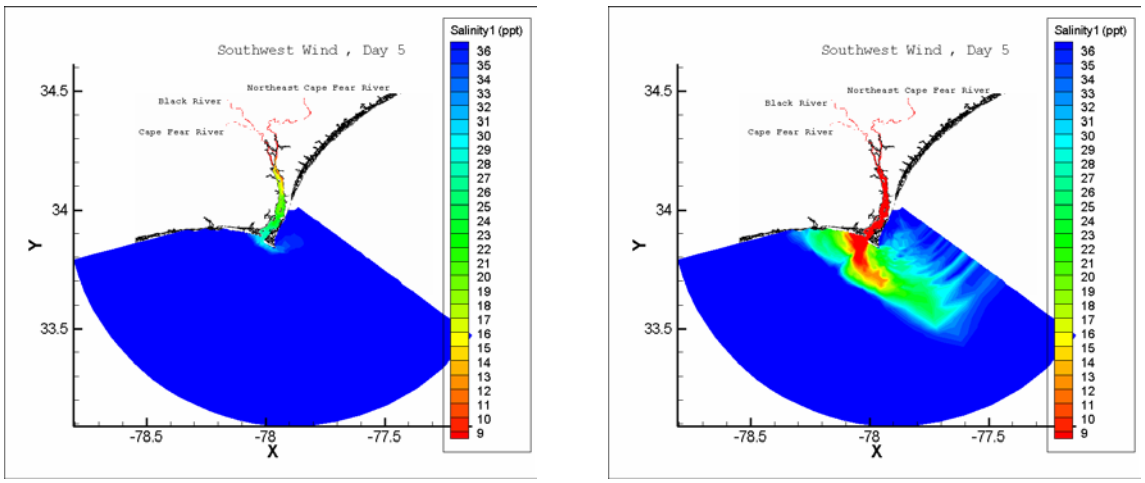


Figure 11. Plume structure with southwesterly winds of 5m/s

(a) Response to no river discharge (b) Response to the flood condition

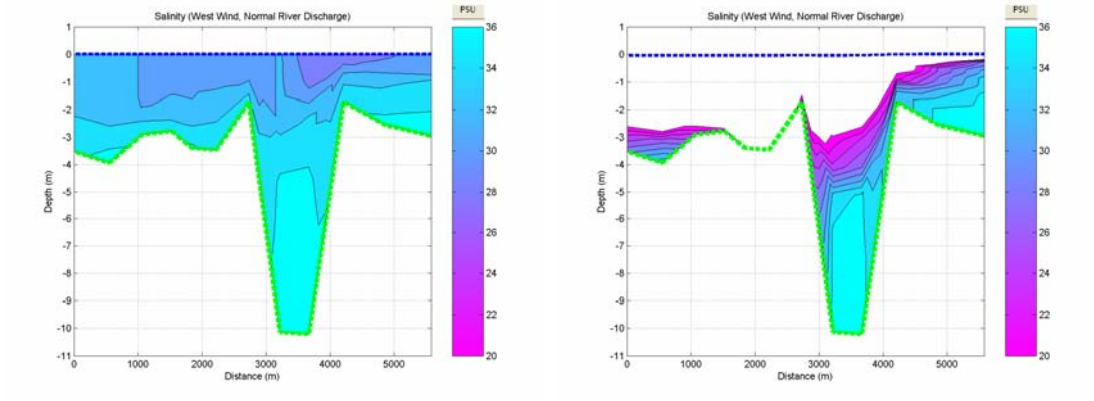


Figure 12. Plume structure with southwesterly winds of 5m/s

(a) Response to low water level condition (b) Response to high water level condition

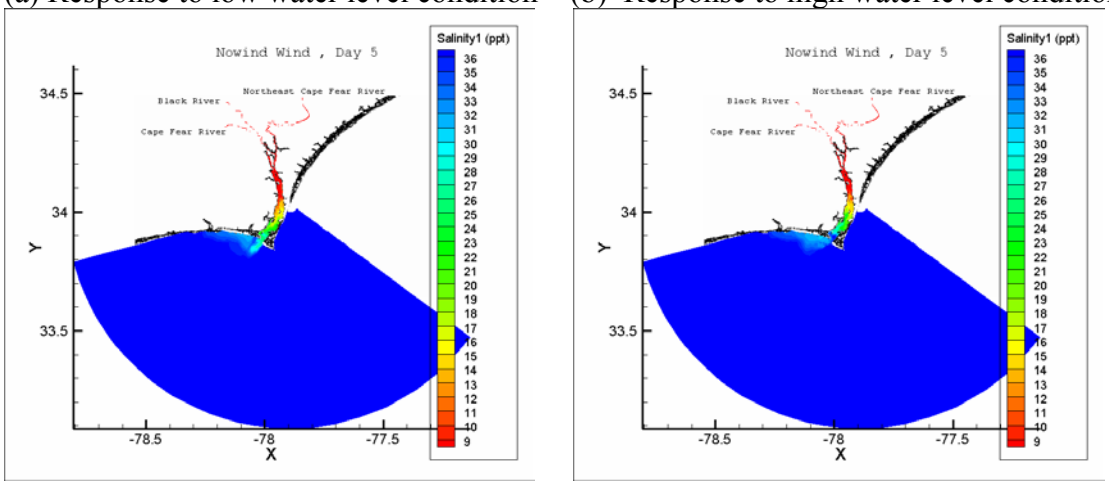


Figure 13. Plume structure with no wind forcing and normal discharge

(a) Response to low water level condition

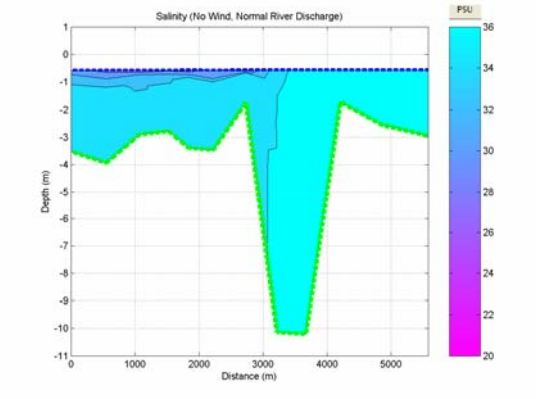


(b) Response to normal condition after low tide

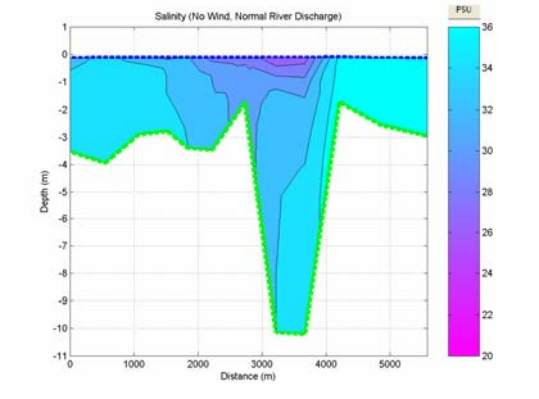


(c) Response to high water level condition

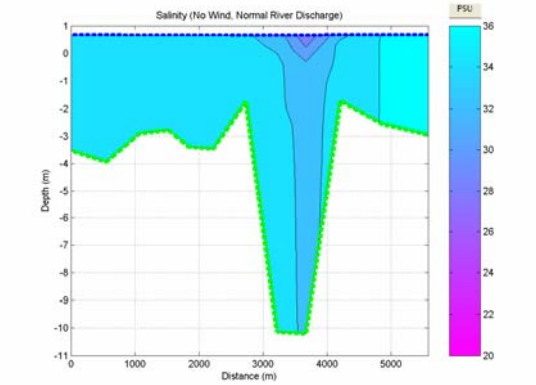


(d) Response to normal condition after the high tide

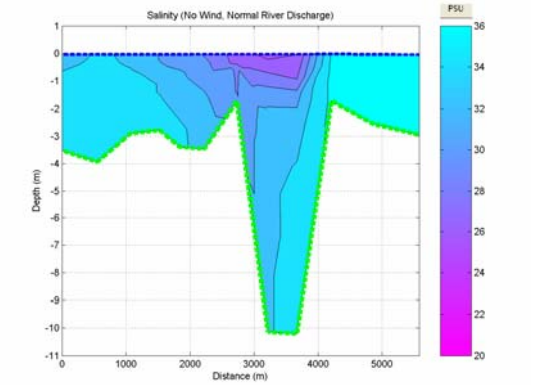


Figure 14. Plume structure with no wind forcing and normal discharge

(a) Response to low water level condition

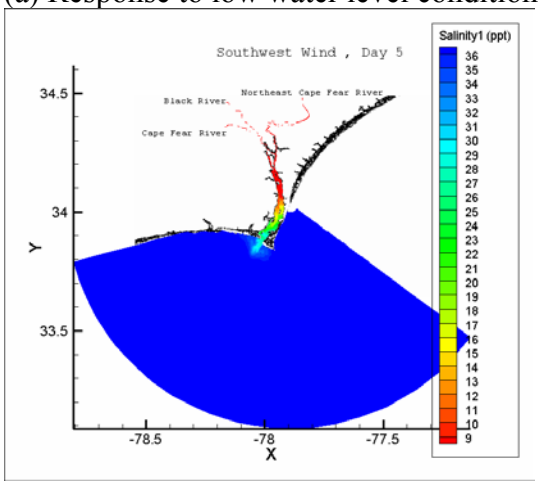


(b) Response to high water level condition

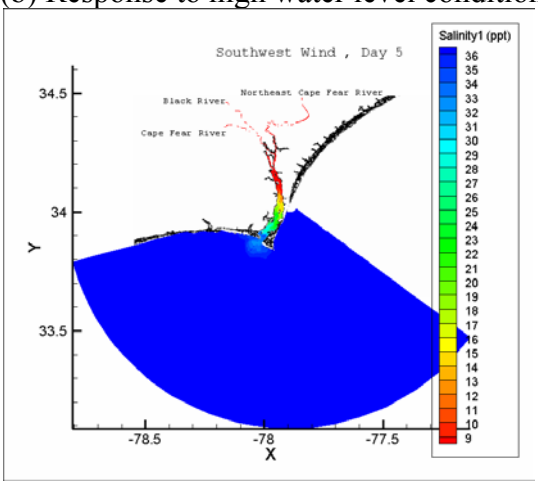


Figure 15. Plume structure with southwest wind forcing and normal discharge

(a) Response to low water level condition

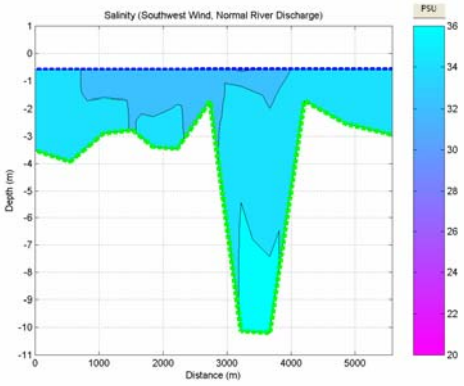


(b) Response to normal condition after low tide

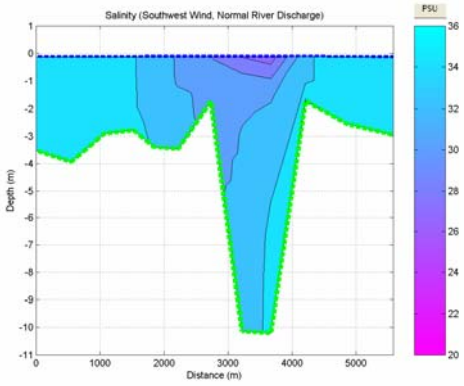


(c) Response to high water level condition

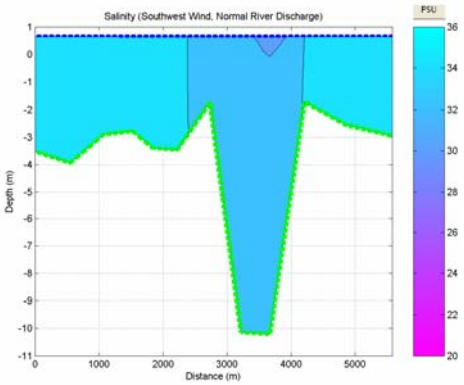


(d) Response to normal condition after high tide

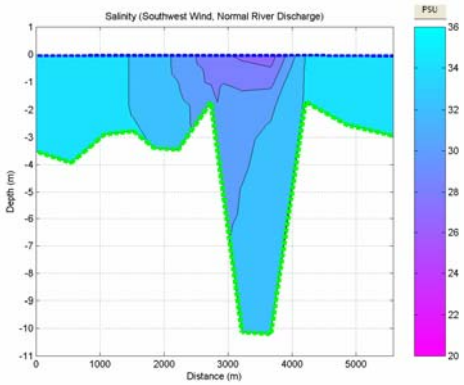


Figure 16. Plume structure with southwest wind forcing and normal discharge

(a) Response to northerly winds (b) Response to northwesterly winds

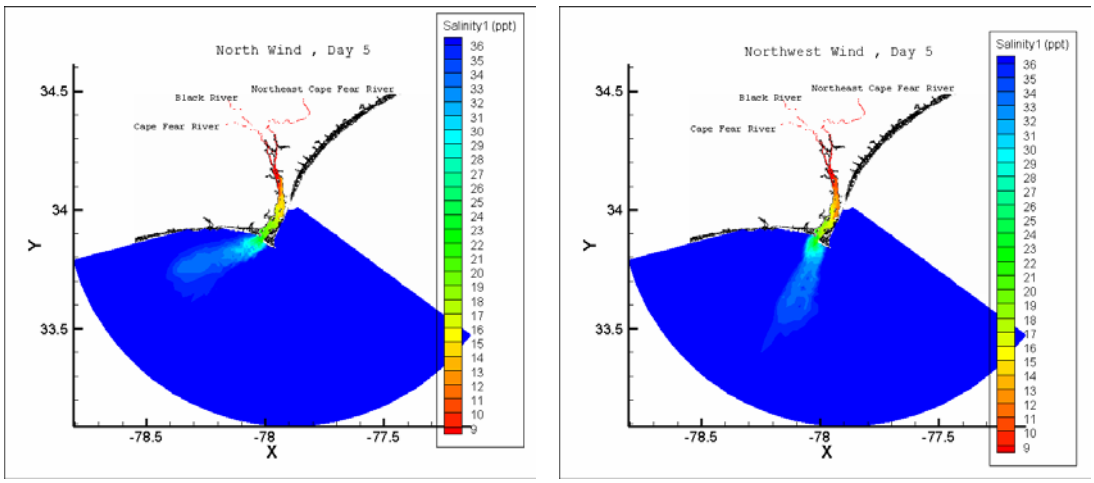


Figure 17. Surface salinity fields forced by 5m/s winds and normal discharge

(a) The plume type under the Southwest and West wind (b) The plume type under the Northeast and North wind

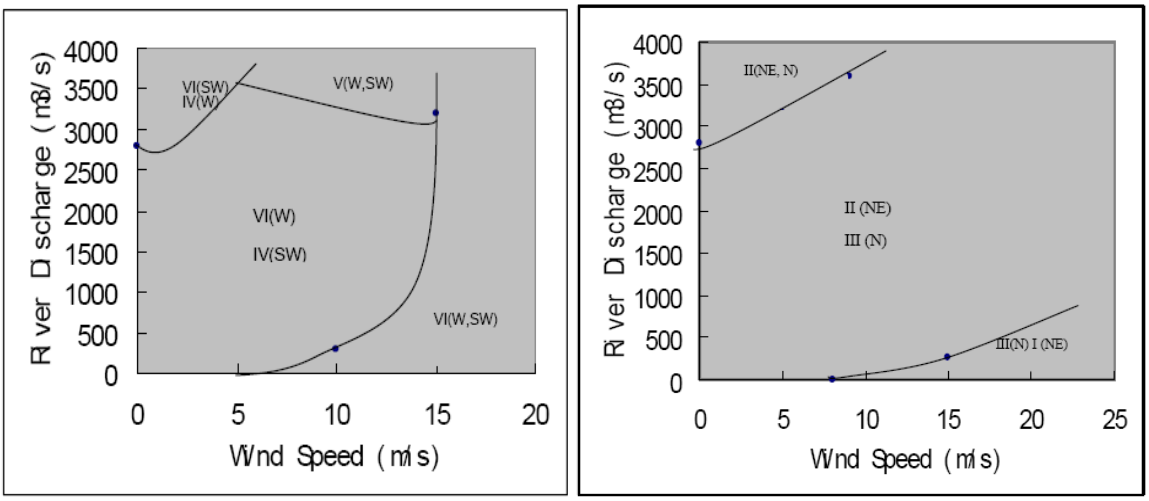


(c) The plume type under the Southeast, East and South wind (b) The plume type under the Northwest wind

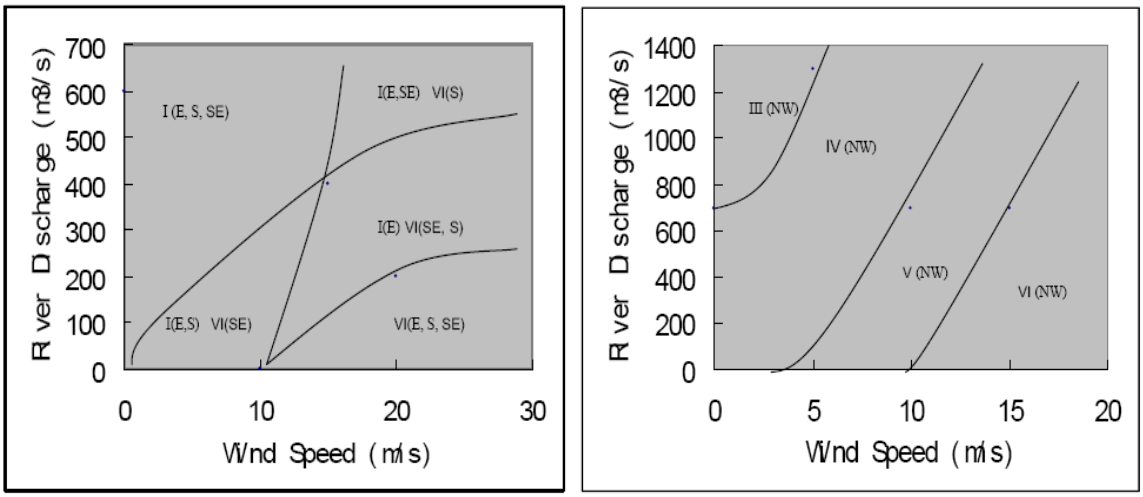


Figure 18. The plume type under the different physical settings

# Chapter 4. Modeling Cape Fear River Estuary Plumes: A Sensitivity Study to Model Settings

## Abstract

In this study, the Environmental Fluid Dynamic Code (EFDC) is used to simulate the salinity plume distribution in the mouth of the Cape Fear River Estuary (CFRE). To better simulate the plume structure in Cape Fear River Estuary (CFRE), we test the sensitivities of the EFDC model to the choice of grid resolution, advection scheme, and external forcing. The sensitive to the vertical grid resolution is studied. Advection schemes tested are central difference, upwind, and the Smolar-2 schemes. These advection schemes were tested in both no-wind runs and wind runs. Also the presence of the wind was simulated to test its influence to the plume simulation. The implication of these idealized tests for realistic simulations, as well as ramifications on previous studies of idealized plume models, is discussed.

## 1. Introduction

River-derived fresh water discharging into an adjacent continental shelf forms a trapped river plume that propagates in a narrow region along the coast. Previous satellite images and field observations provide evidence of the presence of river estuary plumes (Hicky et al., 1998; Xie and Pietrafesa, 1999; Berdeal et al., 2002; Fong and Geyer, 2002).

The plume associated with the CFRE system is an interesting phenomenon on the east coast of the United States. The freshwater discharges from the Cape Fear River, the Northeast Cape Fear River, and the Black River converge in the Cape Fear Estuary and then flow into Long Bay (Figure 1). The average combined discharge from these rivers is about 221 $m^3/s$ (Dame et al., 2000), with a maximum of about 2000 $m^3/s$, which is larger than that of the Tar River, Neuse River and York River. Plumes from the CFRE reduce salinity and change other water properties, such as temperature, nutrient, and phytoplankton, in the coastal water. The flowing plumes of fresh and low salinity water carry loads of sediment, nutrients, and pollutants onto the Long Bay that could affect the regional water quality and ecosystem (Mallin et al., 2005).

There is a series of analytical and numerical studies that simulate the plume formation process. Under ideal geometry, Chao and Boicourt (1986) and Chao (1988) used a three-dimensional, primitive-equation model to simulate the onset of plumes. Zhang et al. (1987) used a theoretical model to simulate the possible trend of plumes. Garvine (1987) used a layer model to simulate the estuary plume by inclusion of the Coriolis force. Garvine (1999,

2001) also used a three-dimensional numerical model ECOM3d and conducted 66 experiments to depict the distribution of the plume on an idealized continental shelf. O'Donnell (1990) also used a mathematical model to describe the formation of a dilution of the river plume. Kourafalou et al. (1996a, b) configured a model to the continental shelf and then applied it to the plume simulation of South Atlantic Bight. Berdeal et al. (2002) also used ECOM3d to simulate the high river discharge plume in the Columbia River. Cheng and Casulli (2004) and Baptista et al. (2005) used an unstructured grid model to simulate the dynamical processes of plumes. Xia et al (2006) used a three-dimensional model to simulate the surface plume structure in the CFRE.

In addition to the geographically determined factors, such as the influence of earth rotation (Coriolis force) and the influence of the coastline or shelf slope for the CFRE, a number of oceanographic and meteorological variables affect the dynamics and structure of CFRE plumes. Further, the grid size and advection scheme are also important factors for the numerical simulation of plumes.

Although there were extensive plume modeling studies in the past, which provided a solid foundation for understanding river estuarine plumes, some limitations exist in most of the past plume modeling studies. They usually give less discussion on numerical setting for the plume modeling before simulating the plume. It is better to discuss how numerical calculations of river plume dynamics are sensitive to the advection scheme, grid resolution, and wind forcing used before performing the numeric simulation of the plume. The different settings are much different to the plume modeling result.

In this study, the Environmental Fluid Dynamic Code (EFDC) is used to simulate the CFRE plume and investigate its sensitivity to model settings. In section 2, the EFDC model is briefly described. Model Settings are presented in section 3, and results are discussed in section 4. The discussions are summarized in section 5.

## 2. Model description

The numerical model is based on a general purpose three-dimensional hydrodynamic model, EFDC (Hamrick, 1992). The physics of the EFDC model and many aspects of the computational scheme resemble the widely used Blumberg-Mellor model (Blumberg and Mellor, 1987). There are a total of 1895 grids in the relatively complex domain in grid 1 (Figure 2a), and 2174 grids in grid 2 (Figure 2b). The grid size varies from 100 meters to 10 km within the model domain.

The time step is 60 seconds which is in compliance with the Courant-Friedrich-Levy (CFL) criterion. The bathymetry is derived from the National Geophysical Data Center (NGDC) Coastal Relief Model Volume 02.

## 3. Model Settings

The initial salinity and temperature of the river and estuary were set up according to their respective values measured by the Lower Cape Fear River Program, while the continental shelf water was initially set up using recent, several year values obtained from the shipboard surveys conducted as part of the Coastal Ocean Research and Monitoring Program

(CORMP). At the open boundary, the salinity was set as a constant (36.5 PSU) while the daily changes of the sea temperature was based on the observations collected as part of the CORMP routine sampling program. At least a five-day spin-up was used in all experiments to allow for thermodynamic adjustment in the model.

## 4. Results

### 4.1 Sensitivity to the advection scheme under no wind effect

EFDC allows us to use three advection schemes, including Central, Upwind, and Smolar-2. Each advection scheme has its advantages and disadvantages. The Central difference advection scheme was widely used in various simulations and has second order accuracy with no numerical diffusion. The Upwind advection scheme has no dispersion and is positive definite, while it could introduce strong numerical diffusion because of the first-order truncation. Smolar_2 advection scheme makes exactly two corrective sweeps for numerical diffusion to the upwind advection scheme.

Berdeal et al (2002) pointed out that, the hydrodynamic stability of the modeled plume is extremely sensitive to the advection scheme and the simulated plume structures depend on the advection scheme. As the base case and a start point of the simulation, we simulated the plume structure with different advection schemes only under the influence of the river discharge and eleven vertical layers. The base case running with the three different advection schemes lead to markedly different results (Figures 3, 4, 5). As shown in Figure 5a, the plume shows an anticyclonic bulge structure off the mouth of the CFRE and a narrow coastal

current which propagates downstream along the southern coast of the North Carolina under the Smolar-2 advection scheme. Comparing the simulation using the central difference advection scheme to that with the Smolar-2 advection scheme, the results are very similar near the surface, but dramatically different at the bottom. The central difference advection scheme clearly gives an erroneous salinity value, which exceeds 40 PSU (Figure 4b), especially in the deep channel. Fennel and Mutzke (1997) showed that the central difference advection scheme could create negative salinities in regions of strong contrast of sea and fresh-water near the river mouth. In the upwind scheme simulation, the mouth of CFRE does not show a narrow coastal current which propagates downstream along the south of the North Carolina coast (Figure 3a). This phenomenon is not consistent with the observations and previous modeling studies. This is consistent with the findings of Hyatt and Signell (1999), that the upwind advection scheme can not properly simulate the plume under the no wind forcing conditions.

In summary, the simulation results indicate that the central difference and the upwind advection schemes are not suited for the simulation of plumes. Thus, we select Smolar-2 scheme as the advection scheme in EFDC model to simulate the plume in CFRE.

### 4.2 Sensitivity to the advection scheme under wind forcing condition

Southwesterly (SW) wind is very common in the CFRE and adjacent ocean (Pietrafesa et al., 1986) during the summer season. We run the simulation with southwest wind to study the sensitivity of the CFRE plume to advection scheme settings. This set of modeling

experiments examine further if there is some significant difference in the plume modeling for different advection schemes.

Under the central advection scheme, the surface salinity field is very noisy, whereas the bottom salinity values are unrealistically large (Figure 7). This phenomenon is very similar to that of the no wind simulation (Figure 5). So the central advection scheme should not be used for plume simulation either with or without the wind forcing. Although the central difference simulation produces noisy surface salinity field, its structure is very close to the structure of the simulation under the Smolar-2 as shown by a comparison between Figure 7a and Figure 8a. From Figures 6a and 8a, we also find that the simulations under the upwind and smolar-2 advection scheme remain substantially different in the presence of wind forcing. The upwind advection scheme can not simulate the plume well even under wind forcing conditions compared to the central difference and Smolar-2 advection scheme.

Based on the above simulation, we would recommend that the Smolar-2 is very suitable to the plume modeling in the EFDC model.

### 4.3 Sensitivity to Vertical Resolution

The vertical resolution is another important factor that influences the plume structure. In order to investigate the effect of vertical resolution on the CFRE plume, sensitivity simulations are carried out using 4, 6, 11 vertical layers with an equal thickness surface layer

for all simulations. This process allows us to directly compare the model runs with different vertical layers. For all simulations, the Smolar-2 advection scheme is used. We find that the surface plume structure is very similar under all simulations, but the weak upshelf intrusion continues to decrease with the increasing vertical resolution (Figure 9a, 10a, 11a). Although Garvine (1999) mentioned that upshelf movement of a portion of the buoyant water is not simply an artifact and can be commonly found, our modeling results showed the magnitude could be significantly reduced by increasing vertical resolution. As Berdeal et al (2002) suggested, adequate vertical resolution of the surface-trapped plume was important to the stability of the result under the Somlar_2 advection scheme simulation. At the same time, we could find that all three structures are very similar and the surface plume structure is mostly controlled by the relative thickness of the vertical resolution.

In addition, simulations under the 10, 11 and 12 layers are carried out to check the relative importance of the thin surface layer. The surface layer was divided into two equal layers under the 12 layer simulation from the 11 layer simulation while we merge two surface layer of the 11 layer simulation to create the 10 layer simulation. From the comparison of Figure 11a and Figure 12a, we can find that the surface-trapped plume is much smaller under the 10 layer simulation than that of the 11 layer simulation and there is a strong upshelf intrusion trend (Figure 12a). This is consistent with the result of Garvine (2001) that maintaining a very shallow depth at the coast could prevent the formation of upshelf intrusion. We find that there are some differences for surface structure under the 10 layer simulation and 11 layer simulation, and similarly under the simulation of 11 layers and 12 layers (Figure 11a and Figure 13a). Therefore, the relative thickness of surface layer is very important to capture the

surface trapped plume, we could see that the 5% of thickness could clearly simulate the surface trapped plume in CFRE since this region is shallow.

Unlike surface plume structure, our results showed that the bottom structure is very similar among all simulations.

**4.4 Sensitivity to Horizontal Resolution:**

As mentioned in the introduction, horizontal grid is another important factor influencing the plumes. Under the two different modeling grids, sensitivity simulations of the CFRE plume are carried out to examine the influence of the two grids on plume structure. The initial setting and vertical setting are the same in both cases. Figure 14a shows the simulated by using gird 2, while the Figure 14b is simulated by grid 1. Both the length and the bulge structure have dramatic differences between these two simulations. The length of plume in the grid-2 simulation is about 20 KM longer than that of grid-1. The grid-2 simulation has a strong up shelf intrusion trend while the grid-1 only has subtle up shelf intrusion.

There is no meander in the bulge region, so the horizontal resolution is high enough to erase the wave-like meander. This is consistent with the findings of Fong (1998) that horizontal resolution can influence the plume results and generate wave-like meander around the bulge. The horizontal resolution is never-the-less very important to the plume simulation. The main difference at the south coast of NC in our modeling domain where grid 2 has a grid size of a couple hundred meters whereas grid-1 a resolution of a couple thousand meters.

The upshelf intrusion is also very sensitive to the model grid settings. In the Figure 14a, the upshelf intrusion is very prominent by using grid 1 which has a low horizontal grid resolution in this region, while there is only subtle upshelf intrusion under the high horizontal resolution in grid 2 (Figure 14b). In the down-shelf Kelvin wave propagation, grid-2 has a little higher horizontal grid resolution than that of the grid 1, so we could see that the length of coastal trapped plume has some differences.

## 5. Discussion and conclusion

The experiments in this chapter discuss the effect of horizontal and vertical resolutions, advection scheme commonly used in river plume modeling. We find that the model configuration is very critical to the modeling results. Main results are summarized below.

1) Advection schemes can have a significant effect either with or without wind forcing. Central differencing scheme should not be used in plume modeling since it produces unrealistic results. Upwind scheme can not simulate the plume structure well even under the wind forcing condition. Higher order advection schemes such as the Smolar-2 scheme can produce realistic plumes. As Berdeal et al ( 2002 ) pointed out that the Smolar_2 advection scheme could simulate the plume well under adequate vertical resolution.

2) Vertical resolution is important to the upshelf intrusion. With the same surface thickness, the surface upshelf intrusion could be eliminated by increasing the number of layers. The surface plume structure is also controlled by the surface thickness. An sufficiently thin surface layer is required to capture the surface plume structure.

3) Horizontal grid is very important for the plume modeling. Hyatt and Signell (1999) did not find the importance of the horizontal grid resolution. One possible reason is that their grid is not fine enough. When the grid size is reduced to about a couple hundred meters, upshelf intrusion will be significantly reduced. Furthermore, the structure and the size of the plume are also very sensitive to the grids used.

4) Reasonable vertical and horizontal resolutions and advection scheme should be carefully considered to eliminate model instability.

## References

Baptista, A.M., Zhang, Y.L., Chawla, A., Zulauf, M., Seaton, C., Myers III, E.P., Kindle J., Wilkin, M., Burla, M., Turner, P.J. (2005). "A cross-scale model for 3D baroclinic circulation in estuary–plume–shelf systems: II. Application to the Columbia River." *Continental Shelf Research,* 25, 935–972.

Berdeal, I.G., Hicky, B.M., and Kawase, M. (2002). "River-forced estuarine plume." *J. Phys. Oceanogr.*, 18, 72-88.

Blumberg, A.F., and Mellor, G.L. (1987). "A description of a three-dimensional coastal ocean circulation model, in Three-Dimensional Coastal Ocean Models." *Editor:* N.S. Heaps, *Am. Geophys. Union,* 1-16.

Chao, S.Y., and Boicourt, W. C., (1986). “Onset of estuarine plumes.” *J. Phys. Oceanogr.*, 16, 2137-2149.

Chao, S.Y. (1988). “River-forced estuarine plume.” *J. Phys. Oceanogr.*, 18, 72-88.

Cheng, R.T., and Casulli, V. (2004). “Modeling a Three-dimensional River Plume over Continental Shelf Using a 3D Unstructured Grid Model” *Proceedings of the Eighth International Conference on Estuarine and Coastal Modeling*, Editors: Malcolm L. Spaulding, 1027-1043.

Dame, R., Alber, M., Allen, D., Mallin, M., Montague, C., Lewitus, A., Chalmers, A., Gardner, R., Gilman, C., Kjerfve, B., Pinckney, J., Smith, N. (2000) “Estuaries of the South Atlantic Coast of North America: Their Geographical Signatures” *Estuaries* 23 793–819.

Fennel, W and Mutzke, A., 1997, The initial evolution of a buoyant plume Journal of Marine Systems *12*, p. 53-68.

Fong, D.A (1998). Dynamics of freshwater plumes: observations and numerical modeling of the wind-forced response and alongshore freshwater transport, *Ph.D. thesis, MIT/WHOI Joint Program in Oceanogr.*, Woods Hole, MA.

Fong, D.A., and Geyer, W.R. (2002). “The alongshore transport of freshwater in a surface-trapped river plume.” *J. Phys. Oceanogr.*, 32, 957-972.

Garvine, R.W. (1987). “Estuary plumes and fronts in shelf waters: A layer model” *J. Phys. Oceanogr,* 17, 1877-1896.

Garvine, R.W. (1999). “Penetration of buoyant coastal discharge onto the continental shelf: A numerical model experiment.” *J. Phys. Oceanogr.*, 29, 1892-1909.

Garvine, R.W. (2001). “The impact of model configuration in studies of buoyant coastal discharge.” *J. Marine Research*, 59, 193-225.

Hamrick, J.M. (1992). “A Three-Dimensional Environmental Fluid Dynamics Computer Code: Theoretical and Computational Aspects” *Special Report*, 317.*The College of William and Mary, Virginia Institute of Marine Science,* Williamsburg, Virginia. 63 PP.

Hickey, B.M., Pietrafesa, L.J., Jay D.A., and Boicourt, W.C. (1998). “The Columbia River plume study: Substantial variability in the velocity and salinity field.” *J. Geophys. Res.*, 103, 10339-10368.

Hyatt, J. and Signell, R.P., (2000), “Modeling surface trapped river plumes: A sensitivity study.” *in* Estuarine and Coastal Modeling, 6th Int. Conf., ASCE, New Orleans, LA, November 3-5, 1999. Editors: Malcolm L. Spaulding and Alan F. Blumberg.

Kourafalou, V.H., Oey, L., Wang, J., and Lee,T.N. (1996a). “The fate of river discharge on the continental shelf, 1, Modeling the river plume and inner shelf coastal current.” *J. Geophys. Res.*, 101, 3415–3434.

Kourafalou, V.H., Lee, T.N., Oey, L., and Wang, J. (1996b). “The fate of river discharge on the continental shelf, 2, Transport of coastal low-salinity waters under realistic wind and tidal forcing.” *J. Geophys. Res.*, 101, 3435– 3456.

Mallin, M.A., Cahoon, L.B., and Durako, M.J. (2005). “Contrasting food-web support bases for adjoining river-influenced and non-river influenced continental shelf ecosystems Estuarine.” *Coastal and Shelf Science*, 62, 55–62.

O’Donnell, J. (1990). “The formation and fate of a river plume: A numerical model.” *J. Phys. Oceanogr*. 20, 551-569.

Pietrafesa, L.J., Janowitz, G.S., Chao, T.Y., Weisberg, R.H., Askari, F., and Noble, E. (1986). “The physical oceanography of the Pamlico Sound.” *UNC Sea Grant Publication UNC-WP-86-5*, Raleigh, N.C. 125PP.

Xia, M., Xie, L., Pietrafesa, L.J. (2006). “Cape Fear River Estuary Plume Modeling: Model Configuration and Sensitivity Experiments.” *Proceedings of the Ninth International Conference on Estuarine and Coastal Modeling*, Editors: Malcolm L. Spaulding, 88-104.

Xie, L., Pietrafesa, L.J. (1999). “System wide modeling of wind and density driven circulation in the Croatan-Albemarle Pamlico estuary system. Part I: Model configuration and testing.” *J. Coastal Research*, 15, 1163-1177.

List of figures:

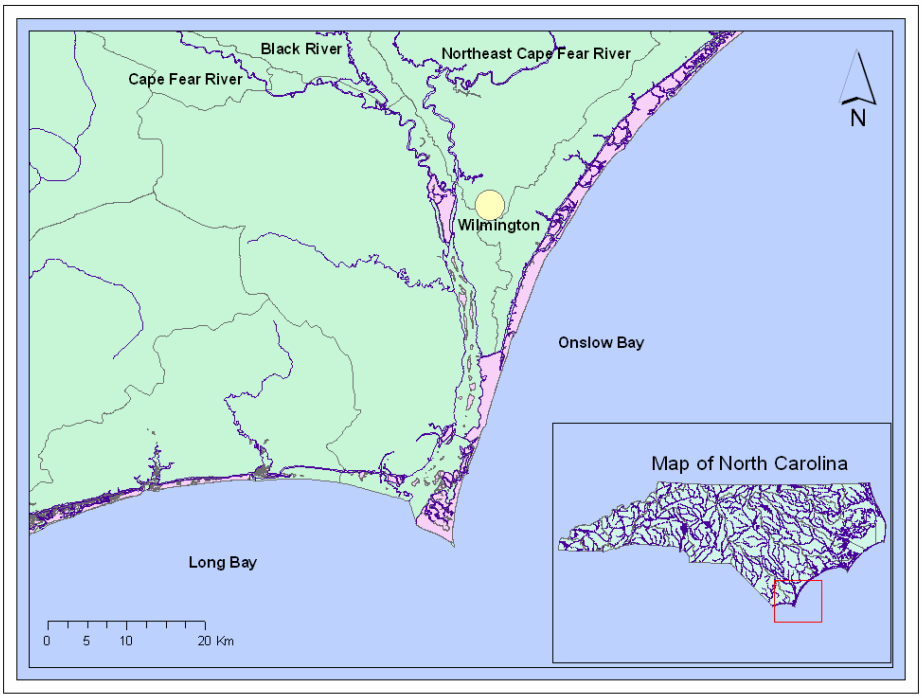


Fig 1 The location of Cape Fear River Estuary and adjacent coastal area

Figure 1. The location of Cape Fear River Estuary and adjacent coastal area

(a) Grid 1 of the model domain (b) Grid 2 of the model domain

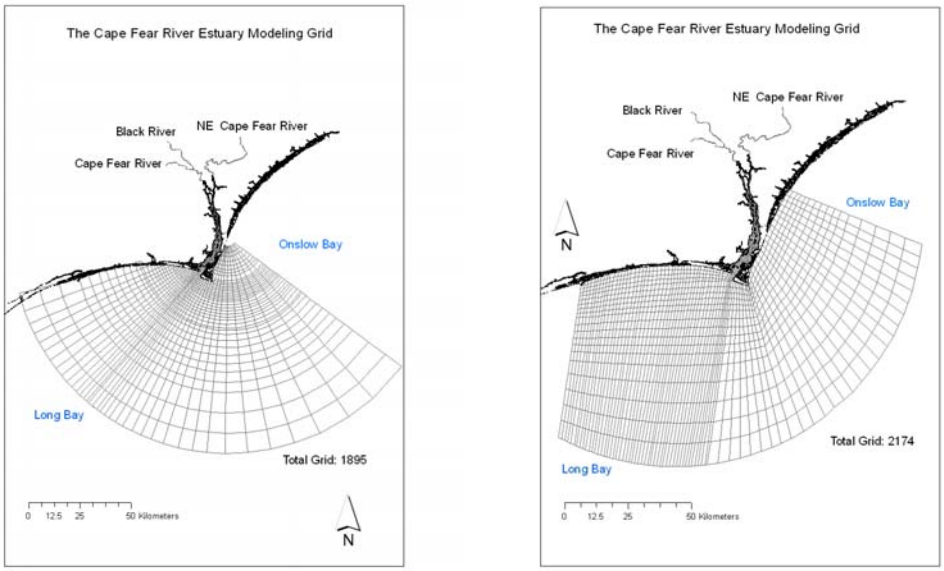


Figure 2. The grids of the CFRE modeling

(a) Surface plume structure (b) Bottom plume structure

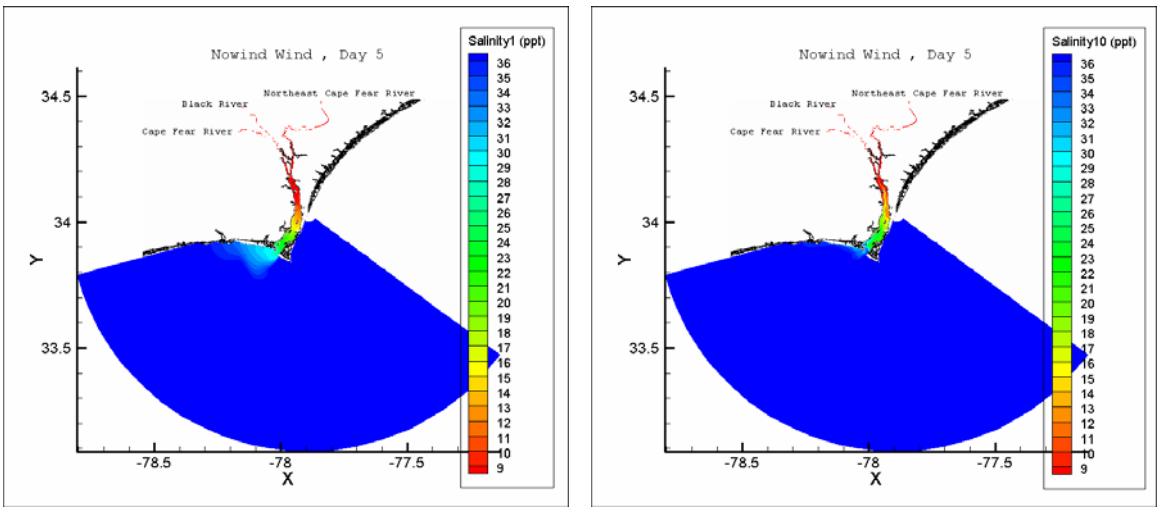


Figure 3. Simulation under the normal river discharge and upwind advection scheme

(a) Surface plume structure (b) Bottom plume structure

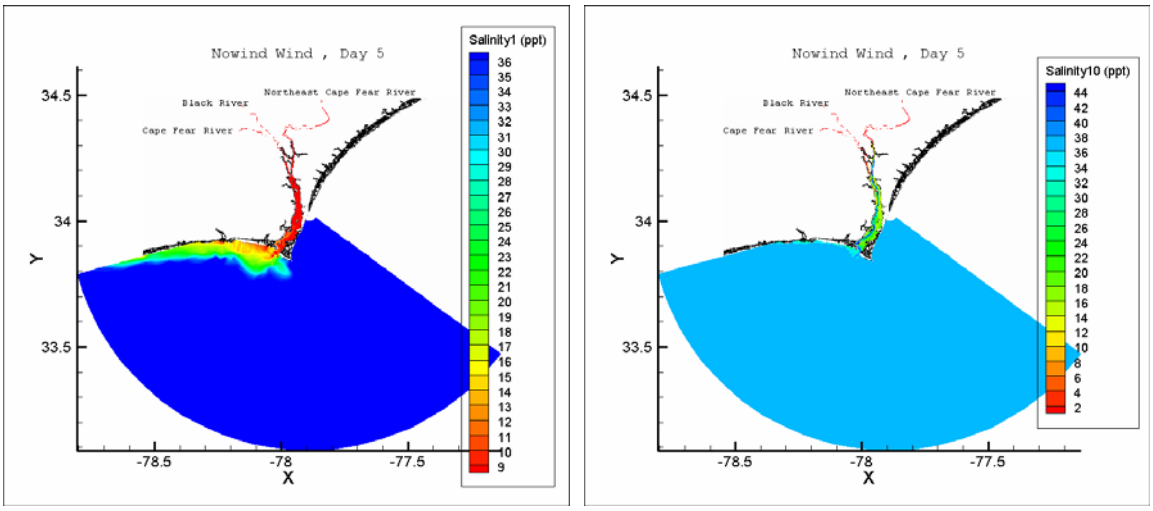


Figure 4. Simulation under the normal river discharge and central difference advection scheme

(a) Surface plume structure (b) Bottom plume structure

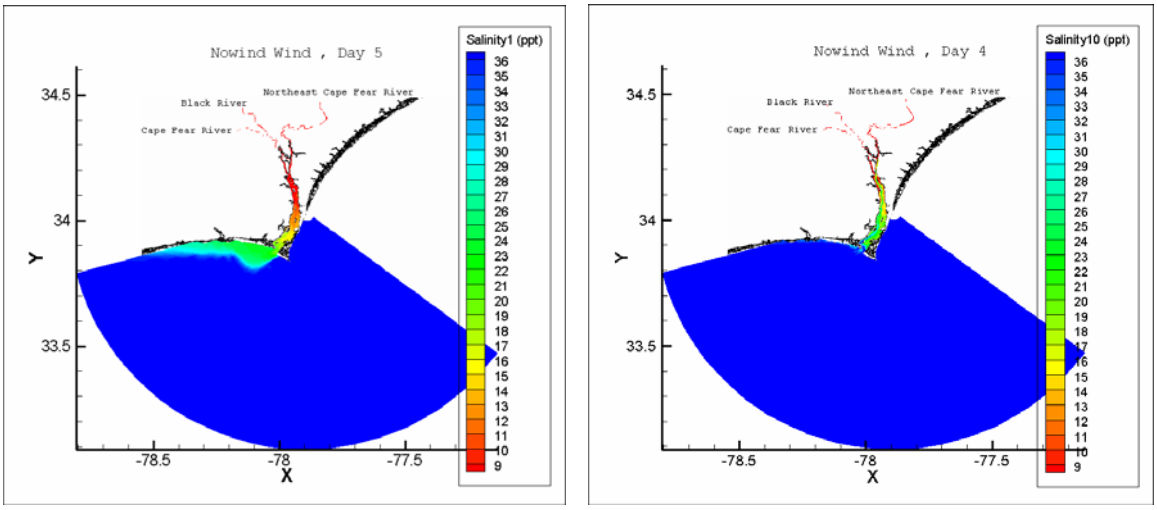


Figure 5. Simulation under the normal river discharge and Smolar-2 advection scheme

(a) Surface plume structure (b) Bottom plume structure

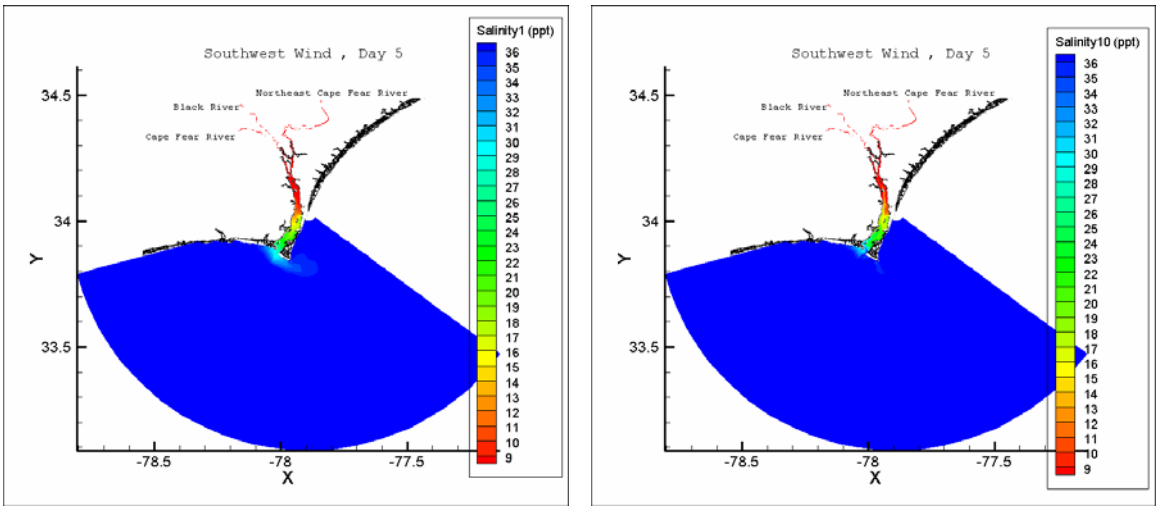


Figure 6. Simulation under the normal river discharge and upwind advection scheme

(a) Surface plume structure (b) Bottom plume structure

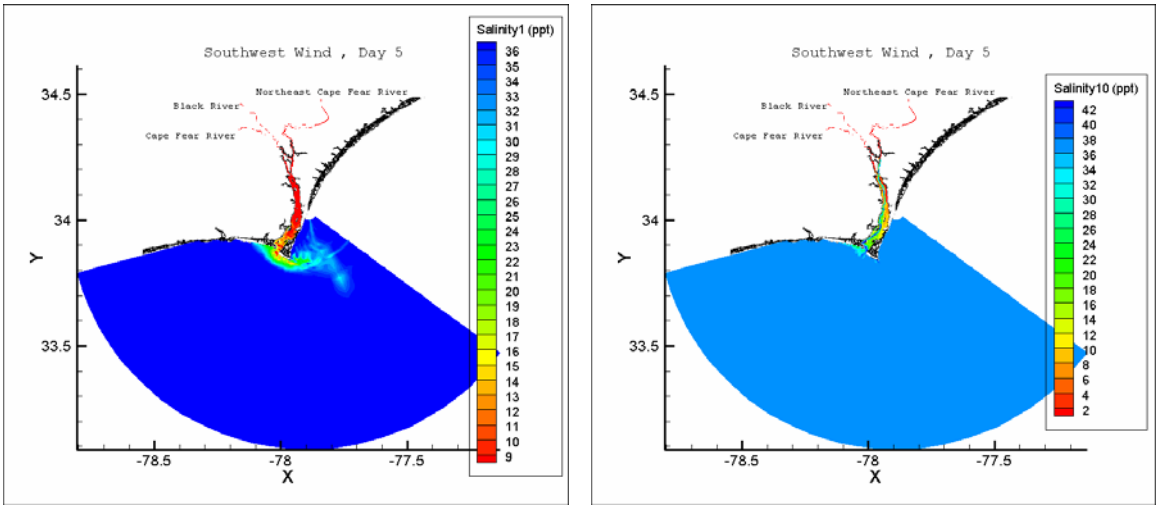


Figure 7. Simulation under the normal river discharge and central difference advection scheme

(a) Surface plume structure (b) Bottom plume structure

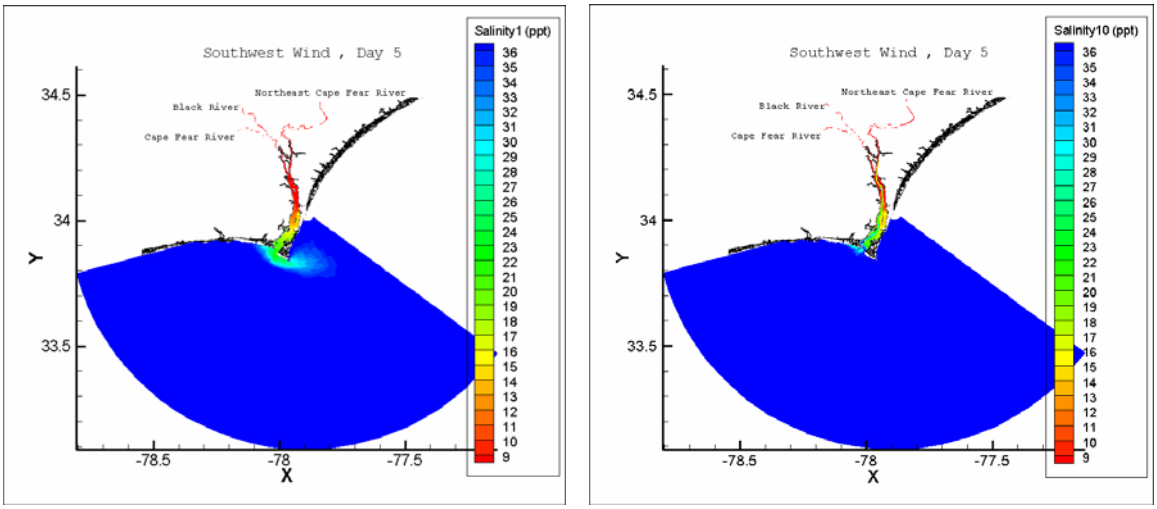


Figure 8. Simulation under the normal river discharge and Smolar-2 advection scheme

(a) Surface plume structure (b) Bottom plume structure

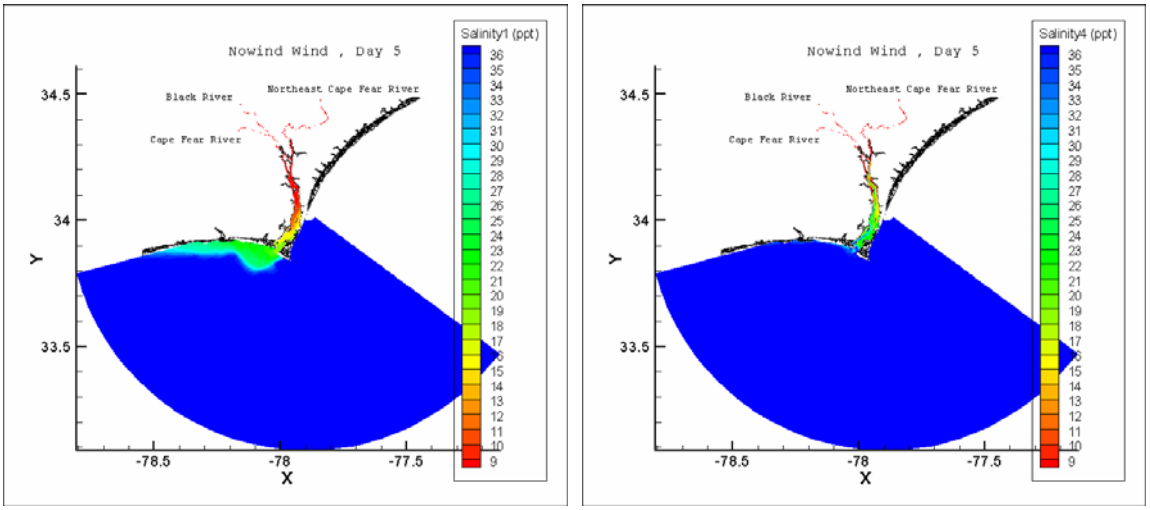


Figure 9. Simulation under 4 layer resolution and Smolar-2 advection scheme

(a) Surface plume structure (b) Bottom plume structure

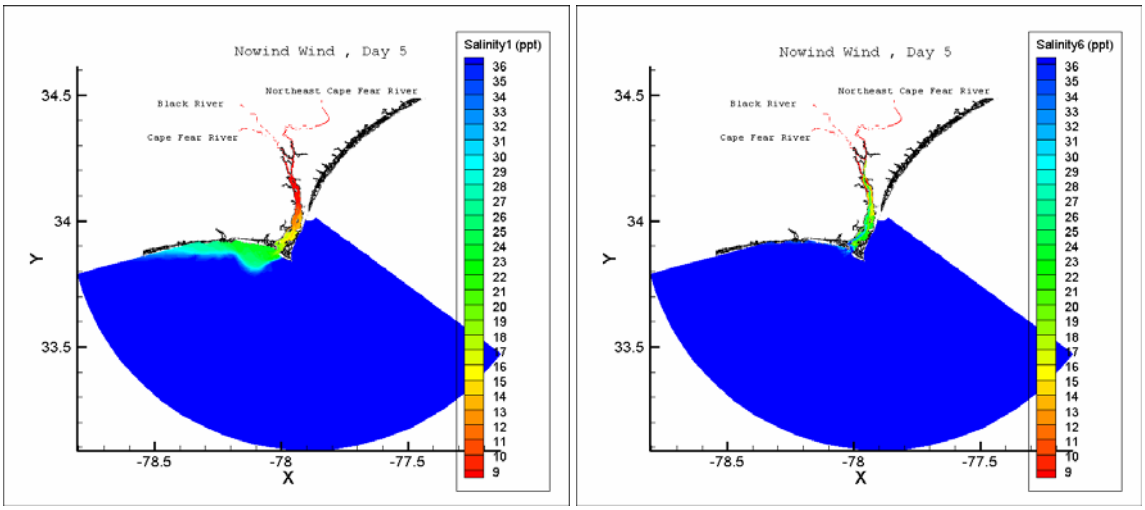


Figure 10. Simulation under 6 layer resolution and Smolar-2 advection scheme

(a) Surface plume structure (b) Bottom plume structure

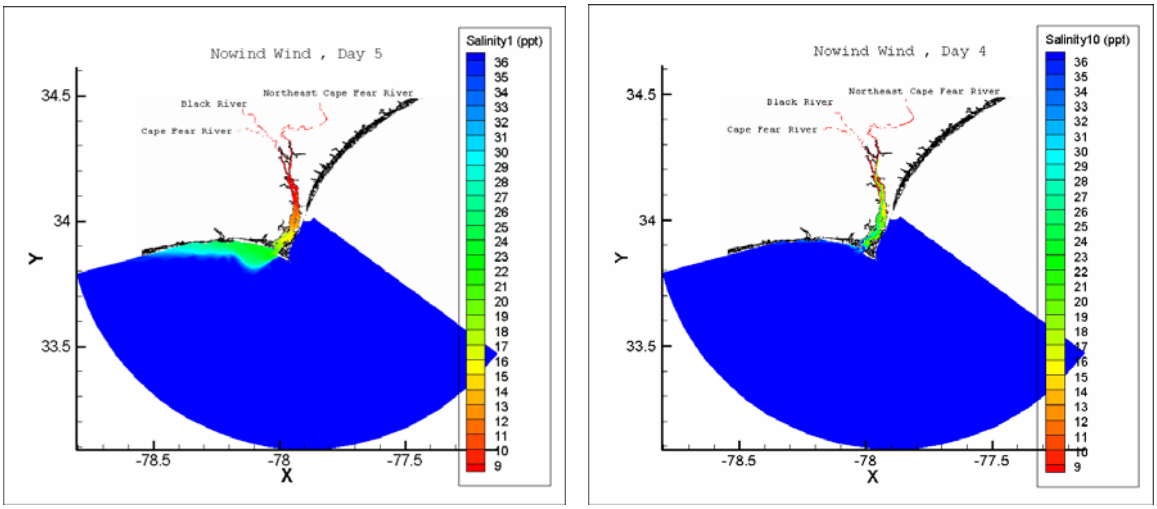


Figure 11. Simulation under 11 layer resolution and Smolar-2 advection scheme

(a) Surface plume structure (b) Bottom plume structure

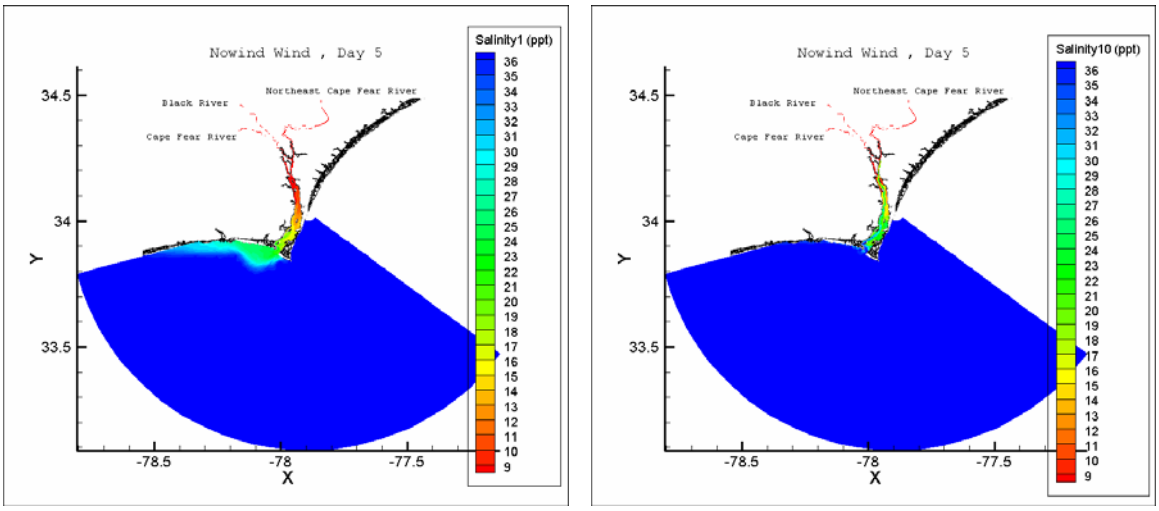


Figure 12. Simulation under 10 layer resolution and Smolar-2 advection scheme

(a) Surface plume structure (b) Bottom plume structure

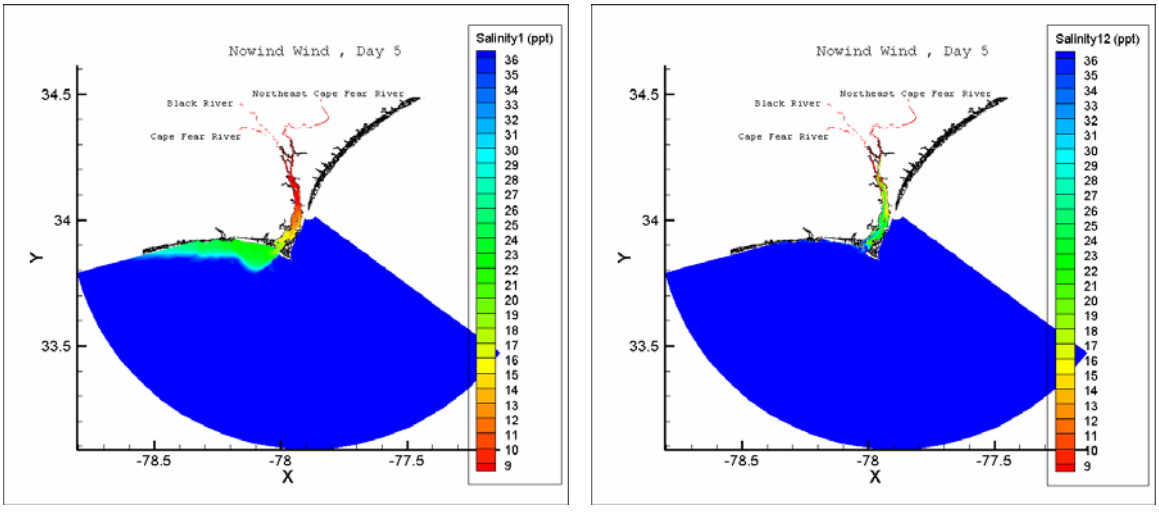


Figure 13. Simulation under 12 layer resolution and Smolar-2 advection scheme

(a) Simulation under the grid 2 (b) Simulation under the grid 1

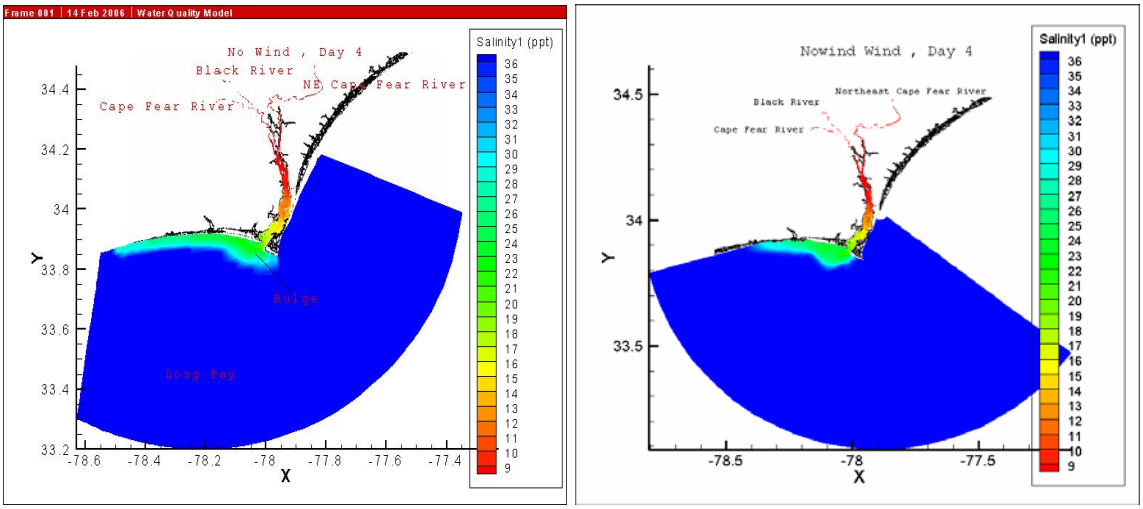


Figure 14. Simulation under 11 layer resolution and Smolar-2 advection scheme

# Chapter 5. A Numerical Study of Passive Tracer and Particle Trajectories in the Cape Fear River Estuary


## Abstract

In this study, the Environmental Fluid Dynamic Code (EFDC) is used to simulate the passive tracer distribution and path of the particle trajectories at the mouth of the Cape Fear River Estuary (CFRE) and adjacent ocean. The effects of the astronomical tide, river discharge and wind on the distribution were investigated. The simulations indicate that strong winds tend to influence the distribution of CFRE passive tracer and the path of the trajectories. Under high wind condition, the domains of the particle trajectories are much larger; the passive tracer was quickly diluted over a large area. Tidal currents do not play a key role in influencing the surface structure of the passive tracer whereas it plays an important role in the vertical distribution of the tracer plume. There are three existing types when we compared the plume structure, path of particle the trajectories, and the passive tracer structure and these different types will be discussed in this chapter.

# 1. Introduction

The Cape Fear River, a 200 mile river that flows through the heart of the North Carolina (NC) piedmont, has the largest watershed in NC. Originally known as the Waccamaw, the Cape Fear is the largest river basin in NC and the only one which flows directly into the ocean. The river begins near Greensboro and Winston-Salem as two rivers, the Deep River and the Haw River. These two rivers converge near Moncure to form the Cape Fear River. The Black River joins the Cape Fear 15 miles above Wilmington, and the Northeast Cape Fear River enters the system at Wilmington (Figure 1) . The Cape Fear River basin covers 9,000 square miles and encompasses streams in 29 of the state's 100 counties. The freshwater discharge from the Cape Fear River, the Northeast Cape Fear River, and the Black River converges in the Cape Fear Estuary and then flows into Long Bay. The average combined discharge from these rivers is about 221 $m^3/s$ (Dame et al., 2000), with a maximum of about 2000 $m^3/s$, which is larger than that of the Tar River, Neuse River and York River. The flowing fresh water carry loads of sediment, nutrients, and pollutants onto the Long Bay that affect the regional water quality and ecosystem (Mallin et al., 2005). Xia et al (2006) uses EFDC to simulate the salinity plume structure in this region. The path of particle trajectories and passive tracer structure in this region are also an interesting question. What are the difference and similarities between the tracer plumes and the particle trajectories? This question will be addressed in this Chapter.

In addition to the geographically determined factors, such as the influence of the Earth's rotation (Coriolis force) and the influence of the coastline and shelf slope for the CFRE, a number of oceanographic and meteorological variables, such as river discharge, wind effect

and tidal effect, also affect the dynamics and distribution of the passive tracer and the paths of particle trajectories. River discharge is a key factor affecting the CFRE plume, since it brings fresh water to the coast. Wind is also a key factor which plays a significant role in driving coastal dynamics. The astronomical tide is another important factor that influences these passive tracer structures and the paths of the particle trajectories.

The main objective of the paper is to simulate the path of particle trajectories and passive tracer distribution under the various hydrodynamic settings. The path of particle trajectories and passive tracer distribution was then compared to the salinity plume distribution. In this study, the Environmental Fluid Dynamic Code (EFDC) is used to simulate the path of particle trajectory and passive tracer structure of CFRE and investigate its sensitivity to wind and river discharge and tidal effect. Both of surface and vertical tracer structures were discussed in the paper. In section 2, the EFDC model is briefly described. Model Settings are presented in section 3, and results are discussed in section 4. The comparison of simulated salinity field with the observed salinity plume distribution is provided in section 5. The discussions are summarized in section 6.

## 2. Model description and configuration

The numerical model is based on a general purpose three-dimensional hydrodynamic model, EFDC (Hamrick, 1992). The physics of the EFDC model and many aspects of the computational scheme resemble the widely used Blumberg-Mellor model (Blumberg and Mellor, 1987). There are total 1895 grids in the relatively complex domain in the grid 1 (Figure 2a). The grid size varies from 100 meters to 10 km within the model domain.

The time step is 60 seconds which is in compliance with the Courant-Friedrich-Levy (CFL) criterion. The bathymetry is derived from the National Geophysical Data Center (NGDC) Coastal Relief Model Volume 02 (Figure 2b).

## 3. Model Settings

The initial salinity and temperature of the river and estuary were set up according to their respective values measured by the Lower Cape Fear River Program, while the continental shelf water was initially set up using recent, several year values obtained from the shipboard surveys conducted as part of the Coastal Ocean Research and Monitoring Program (CORMP). At the open boundary, the salinity was set as a constant (36.5 PSU) while the daily changes of the sea temperature was based on the observations collected as part of the CORMP routine sampling program. The passive dye was released at the mouth of CFRE with the concentration of 10 units. The particle was initially put at the surface layer at the entrance of the CFRE and the mouth of three rivers. At least a five-day spin-up was used in all experiments to allow for thermodynamic adjustment in the model.

## 4. Result

### 4.1 CFRE particle trajectory and passive tracer structure induced by normal river discharge

The base case simulation is a simulation only under the influence of river discharge, since topography and Coriolis force effects are the same in all simulations. As shown in Figures 3a, in the absence of other physical factors, such as wind and tidal effects, the passive tracer

shows an anti-cyclonic bulge structure off the mouth of the CFRE and a narrow coastal current which propagates downstream along the southern North Carolina coast. As shown in Figure 3b, the vertical passive tracer distribution shows a strong stratification due to fresher water discharge. The high concentration tracer was found at the bottom while low concentration was found at the surface since the fresher water induced stratification, and the bottom high concentration were influenced by the diffusion while the surface was influenced by both the diffusion and advection. The depth of the concentration changed with water depth. Under the normal fresher water effect, the low tracer concentration is only limited to part of the surface water. The tracer is constricted to the 2 or 3 meters in the surface layer at the mouth of CFRE. The paths of the particle trajectory are within the distribution of the passive trace. This passive tracer structure is very similar to the salinity plume simulation from Xia et al. (2006).

### 4.2 Response to normal river discharge and 5m/s wind speed under different wind directions

In the CFRE region, it is also important to include wind effects in CFRE plume modeling. We first consider how wind directions influence the passive tracer structure and path of particle trajectory.

As shown in Figure 4, the passive tracer structure is dramatically different under different wind directions with the normal river discharge and 5m/s wind speed. Under a northerly wind, the passive tracer stays away from the coast and flows toward the southwest. The tracer turns to the right and hugs the southern coast under an easterly wind, whereas the

tracer remains detached from the coast under a northeasterly wind. The tracer turns to the left towards north under a westerly wind. Easterly, southeasterly, and southerly winds will push the tracer along the coast to the west of the mouth of the CFRE. Westerly, southwesterly and northwesterly winds keep the tracer away from the coast. By comparing the tracer structure with and without wind effects, we find that under all the wind conditions the surface CFRE tracer size and structure are influenced by the effect of winds, and the wind distort the bulge due to surface mixing. Under some favorable winds, such as northerly wind, northwesterly wind, the passive tracer size is bigger than that with no wind effect. It is very clear that the paths of particle trajectory are totally within the corresponding passive tracer distribution from Figure 4.

As shown in Figure 3b and Figure 5, the vertical tracer structure under the wind-forced condition is different from that of no wind effect. Because of the wind induced mixing, the stratification is a little weaker than that in the no wind effect case. The surface tracer is lower under the influence of the wind effect compared to that of no wind effect case, while the deep water tracer value becomes a little lower due to the effect of wind mixing. The tracer depth could even reach 4 meter under some favorable winds, such as southwesterly wind. But the bottom structure is nearly the same under the various wind conditions. It is clear that the bottom structure was hardly influenced by the wind effect. Overall, the passive tracer structure does not make bottom contact under the 5m/s wind speed forcing. Compared to the no wind effect, the moderate wind effects will strengthen the surface tracer mixing while it has little influence on the tracer value near the bottom.

### 4.3 Response to different wind speeds under northeasterly and southwesterly winds

The northeasterly wind direction is approximately parallel to the major axis of the estuary and blows offshore, whereas the southwesterly wind case is the reverse. Northeasterly winds dominate this region in the fall while southwesterly winds dominate in spring (Pietrafesa et al., 1986). We will therefore select these two wind directions to study the sensitivity of the CFRE tracer structure and path of trajectories to different wind forcing.

As shown in Figure 6, the passive tracer size increased as the wind speed increased from 5m/s to 10m/s, 15m/s and then 20m/s under northeasterly winds due to enhanced wind forcing advection associated with increased wind speeds induced water speed. For the southwesterly wind, the wind direction is opposite to the flow direction of the estuary. The passive tracer size changed dramatically as the wind speed increased from 5m/s to 10m/s, 15m/s and then 20m/s from Figure 7, and it was highly diluted and nearly diminished with 20m/s. It is evident that the paths of particle trajectory are totally within the correspondingly passive tracer distribution under the various winds forcing from Figure 6 and Figure 7.

As shown in Figures 8 and 9, the vertical tracer distribution is more uniform as the wind speed and the subsequent vertical mixing increase. The stratification remains weak. The surface tracer value decreased as the wind speed increased from 5m/s to 10m/s, 15m/s and then 20m/s under either southwesterly or northeasterly winds. The bottom tracer value was slightly higher.

### 4.4 Sensitivity to river discharge under the influence of a southwesterly wind

Southwesterly wind is very common in the CFRE and adjacent ocean (Pietrafesa et al., 1986), we run the simulation with this wind to study the sensitivity of the CFRE tracer to river discharge. As the river discharge increased from zero to flood conditions, the size of passive tracer dramatically increased. The tracer plume under no river discharge condition is relatively small (Figure 10). The tracer size dramatically increased under relatively high river discharge or flood conditions.

As the river discharge increased from zero to flood conditions, the tracer was quickly diluted (Figure 11). The vertical distribution changed dramatically with increasing river discharge.

#### 4.5.1 Sensitivity to tidal effect under the normal river discharge and the influence of no wind

The surface tracer structures were plotted at both the high water level time and low water level time of the mouth (Figures 12a and 12b). The structures of the tracer plumes remain roughly unchanged over these two time periods. At the same time, the coastal Kelvin wave is much weaker compared to the non-tidal simulation (Figure 12a). So the tidal mixing plus the tidal current does not influence the surface tracer significantly.

Compared to the non-tidal effect, the tidal mixing plays a crucial role to the vertical passive tracer structure. Our non-tidal simulation shows that the passive tracer does not make bottom

contact under most of the conditions while the passive tracer is very easy to contact the bottom under the tidal influence. The stratification is weak under flood tide, so does the low tide. As seen from Figure 13, the passive tracer depth is much deeper compared to the non-tidal effect case.

### 4.5.2 Sensitivity to tidal effect under the normal river discharge and the influence of a southwesterly wind

Compared to the non-tidal effect case, the upshelf and downshelf intrusions are weak. As in the previous discussion of passive tracer under no wind effect and tidal influence, the passive tracer size is very similar under the tidal influence at both the low tide and high tide conditions (Figure 14).

From Figure 15, the distribution of the passive tracer is very similar to that under no wind effect. Compared to the weak or moderate wind cases, tidal mixing plays a crucial role in the passive tracer structure.

## 5. The comparison of the results to plume modeling

### 5.1 Type 1: CFRE plume induced by normal river discharge

The CFRE plume, passive tracer and particle trajectory were simulated only under the influence of the average river discharge value without wind effect and tidal influence. As shown in Figure 16a, in the absence of other physical factors, such as wind and tidal effects,

the plume shows an anti-cyclonic bulge structure off the mouth of the CFRE and a narrow coastal current which propagates downstream along the south of the North Carolina coast. The passive tracer also shows the same structure along the south of the North Carolina coast (Figure 17a). These two structures are very similar. The path of the trajectory is totally within the boundary of the passive tracer.

As shown in Figure 16b, the vertical salinity distribution shows a strong stratification due to fresher water discharge. The depth of the plume changed with the bathymetry. The isohaline is sparse at the deep water part while it is a little steeper in the shallow water. Under the normal fresher water effect, the low salinity water is only limited to part of the surface water. The plume is constricted to the 2 or 3 meters in the surface layer at the mouth of CFRE. As shown in Figure 17b, the vertical passive tracer distribution also shows a strong stratification due to fresher water discharge. The high concentration tracer was found at the bottom while low concentration was found at the surface. It is because fresher water induces stratification, and the bottom high concentration was mostly influenced by the diffusion other than advection while the surface was influenced by both the diffusion and advection. The river discharge dilutes the tracer concentration at the surface while it won't influence the bottom, so the high concentration exists in the left bottom (Figure 17b).

Under this type of the simulation, the size of the plume is very close the size of the passive tracer. The particles are totally within the domain of the plume or passive tracer. We defined this type of distribution as the type 1 distribution.

### 5.2 Type 2: CFRE plume induced by normal river discharge with 5m/s southwesterly wind

This type simulation was a simulation with 5m/s southwesterly wind and normal river discharge to study the comparison of the CFRE passive tracer and particle trajectories to the plume structure.

Southwesterly winds keep the plume away from the coast and move to the southwest part, passing the Diamond Shoal and could reach Onslow Bay (Figure 18a). The plume depth could even reach 4 meters under southwesterly wind, and the depth is a little deeper than that with no wind effect (Figure 18b). While southwesterly winds make the left part of the channel mix a little stronger and deeper compared to no wind effect. The passive tracer structure also shows a similar trend compared to the surface salinity structure while its domain is a little bigger (Figure 19a). Like the phenomena of the no wind effect passive tracer distribution, the bottom passive tracer distribution also has the high concentration (Figure 19b). This reason is very similar to that of no wind effect.

Under this type of the simulation, the size of the plume is a little smaller than that of the passive trace. The particles are within the domain of passive tracer while it is close to the boundary of the plume domain (Figure 19a).

### 5.3 Type 3: CFRE plume induced by normal river discharge with 20m/s southwesterly wind

Type 3 was a simulation with 20m/s southwesterly wind and normal river discharge under high wind forcing.

As shown in Figure 20b, the vertical plume salinity distribution is more uniform as the wind speed and the subsequent vertical mixing increase. The stratification remains weak. We nearly can't see the plume at the mouth. The plume will become deeper with decreasing stratification as wind stress increases due to increased vertical mixing.

From Figures 21b, the vertical tracer distribution is uniform under the high wind forgings and subsequent increasing vertical mixing. The domain of the passive tracer is much bigger under the strong wind forcing as saw from Figures 21a.

Under this type of the simulation, the size of the plume is much smaller than that of the passive tracer when we make comparison of Figure 20a and Figure 21a. The particles are within the domain of passive tracer while it is also beyond the boundary of the plume.

## 6. Summary and conclusions

In this study, the three-dimensional EFDC model is configured for the CFRE region to simulate the passive tracer distributions and the paths of the particle trajectories. The main conclusions are summarized below:

1) The CFRE passive tracer distribution is generally confined to the south-facing coastal shore line in upper Long Bay and propagates in the direction of Kelvin waves to form a long narrow trapped structure when river discharge is imposed without wind effects. This phenomenon is very similar to the salinity plume structure discussed in Xia et al (2006).
2) When the wind effect is added, the passive tracer structure is significantly different depending on wind directions. Even a moderate wind could fully reverse the buoyancy-

driven passive tracer structure in the CFRE under average river discharge conditions. With average river discharge, southwesterly, westerly, northwesterly, northerly and northeasterly winds all cause the passive tracer to depart from the coast to the south of CFRE. In contrast, under easterly, southeasterly, and southerly winds, the passive tracer structure becomes trapped along the coast under normal river discharge. This phenomenon is very similar to that of plume modeling results in Xia et al (2006). Under the high wind forcing, the domains of the particle trajectory are much larger; the passive tracer was quickly diluted and its size was much larger unlike the size of salinity plume which decreases with increasing wind forcing.

3) Tidal currents do not play a key role in influencing the passive tracer surface structure while it plays an important role in its vertical distribution.
4) Under the wind mixing and fresher water discharge, the passive tracer most likely will not contact with bottom. Under the tidal mixing, the passive tracer could easily make bottom contact under most cases while the passive tracer seldom contact bottom without the tidal effect in the simulation.
5) Overall, the paths of the particle trajectory are totally within the domain of passive tracer distribution. There are three existing types when we compared the plume, particle trajectory, passive tracer structure. The first type is that the size of the plume is very close the size of the passive tracer plume and the particles are totally within the domain of the plume or passive tracer plume; the second type is that the size of the plume is a little smaller than that of the passive tracer and the particles are within the domain of passive tracer while it is close to the boundary of the plume domain; the third type is that the size of the salinity plume is much smaller than that of the passive tracer plume and the

particles are within the domain of passive tracer while it is beyond the boundary of the plume.

## References


Blumberg, A.F., and Mellor, G.L. (1987). “A description of a three-dimensional coastal ocean circulation model, in Three-Dimensional Coastal Ocean Models.” *Editor:* N.S. Heaps, *Am. Geophys. Union*, 1-16.

Dame, R., Alber, M., Allen, D., Mallin, M., Montague, C., Lewitus, A., Chalmers, A., Gardner, R., Gilman, C., Kjerfve, B., Pinckney, J., Smith, N. (2000) “Estuaries of the South Atlantic Coast of North America: Their Geographical Signatures” *Estuaries* 23 793–819.

Hamrick, J.M. (1992). “A Three-Dimensional Environmental Fluid Dynamics Computer Code: Theoretical and Computational Aspects” *Special Report*, 317.*The College of William and Mary, Virginia Institute of Marine Science*, Williamsburg, Virginia. 63 PP.

Mallin, M.A., Cahoon, L.B., and Durako, M.J. (2005). “Contrasting food-web support bases for adjoining river-influenced and non-river influenced continental shelf ecosystems Estuarine.” *Coastal and Shelf Science*, 62, 55–62.

Pietrafesa, L.J., Janowitz, G.S., Chao, T.Y., Weisberg, R.H., Askari, F., and Noble, E. (1986). “The physical oceanography of the Pamlico Sound.” *UNC Sea Grant Publication UNC-WP-86-5*, Raleigh, N.C. 125PP.

Xia, M., Xie, L., Pitrefesa, L.J., (2006). “Cape Fear River Estuary Plume Modeling: Model Configuration and Sensitivity Experiments” *Proceedings of the Eighth International Conference on Estuarine and Coastal Modeling, Editors: Malcolm L. Spaulding*, 66-84.

## List of Figures

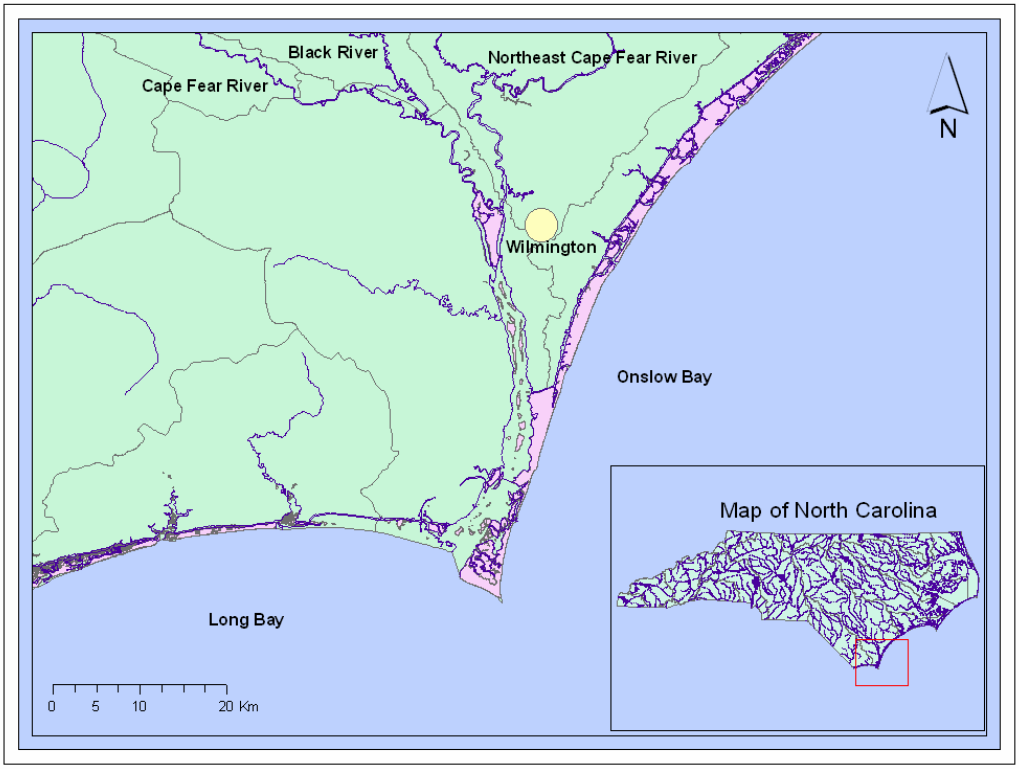


Figure 1. The location of the Cape Fear River Estuary

(a) The grid of the model domain (b) The bathymetry of the model domain

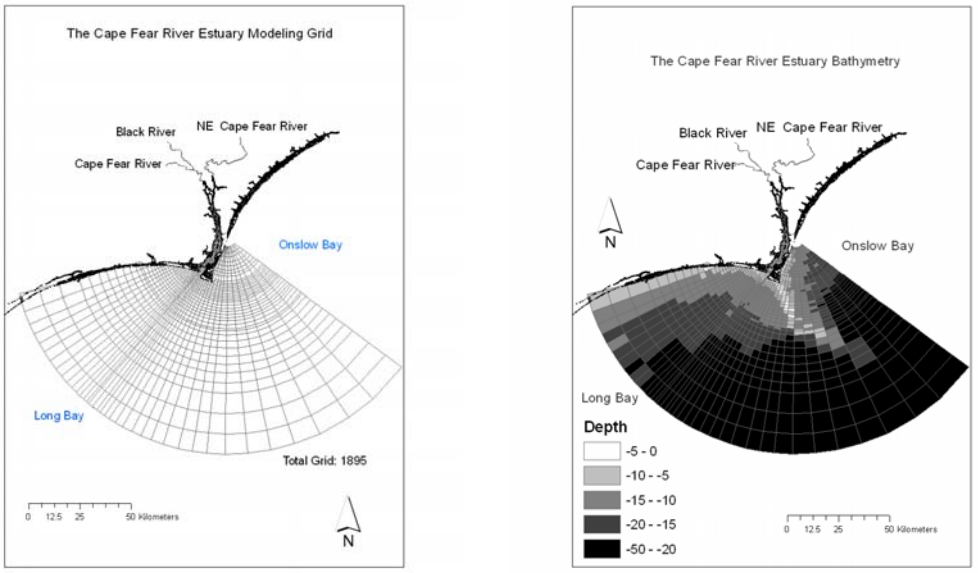


Figure 2. The grids and bathymetry in the CFRE modeling domain.

(a) The surface tracer structure after 5 days

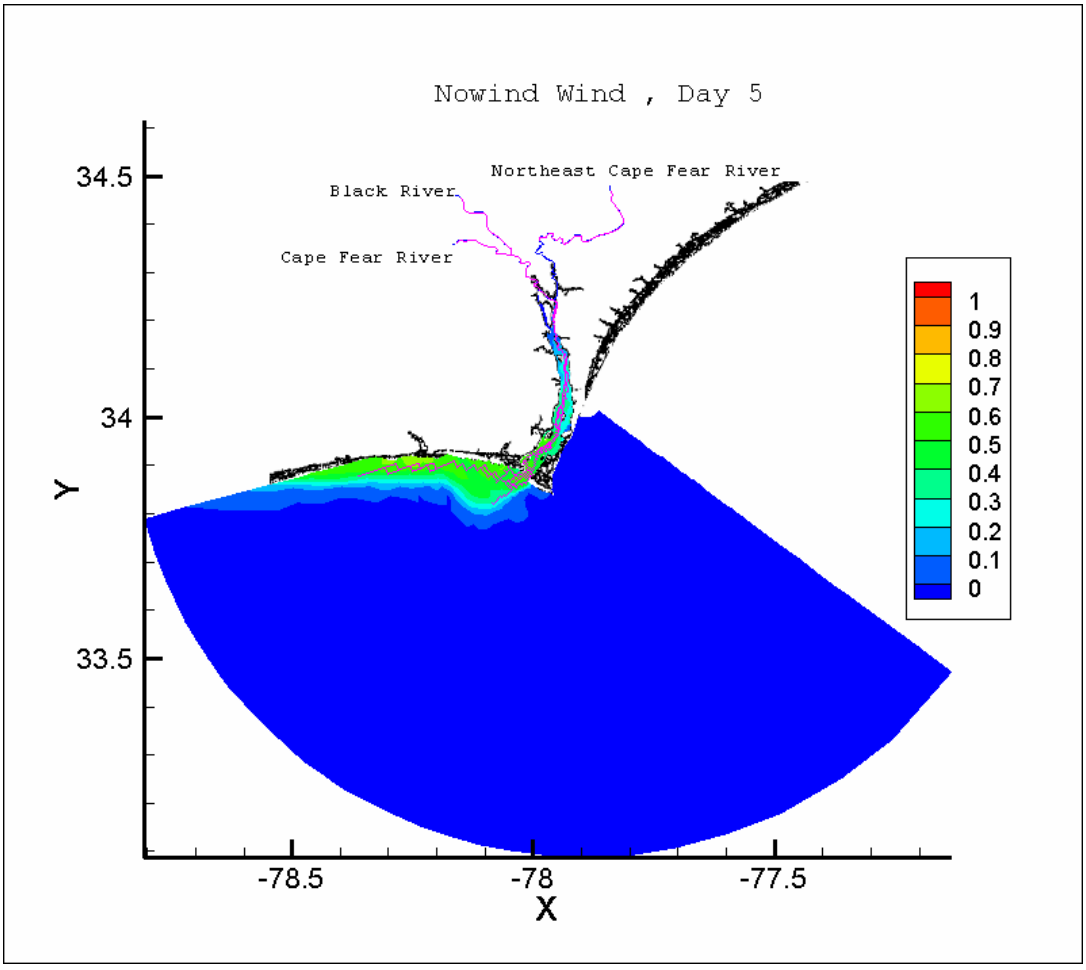


(b) The tracer vertical structure after 5 days

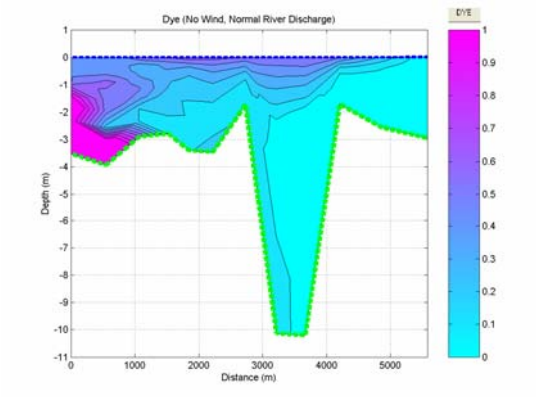


Figure 3. The sea traces fields forced by normal river discharge.

(a) Response to northerly winds

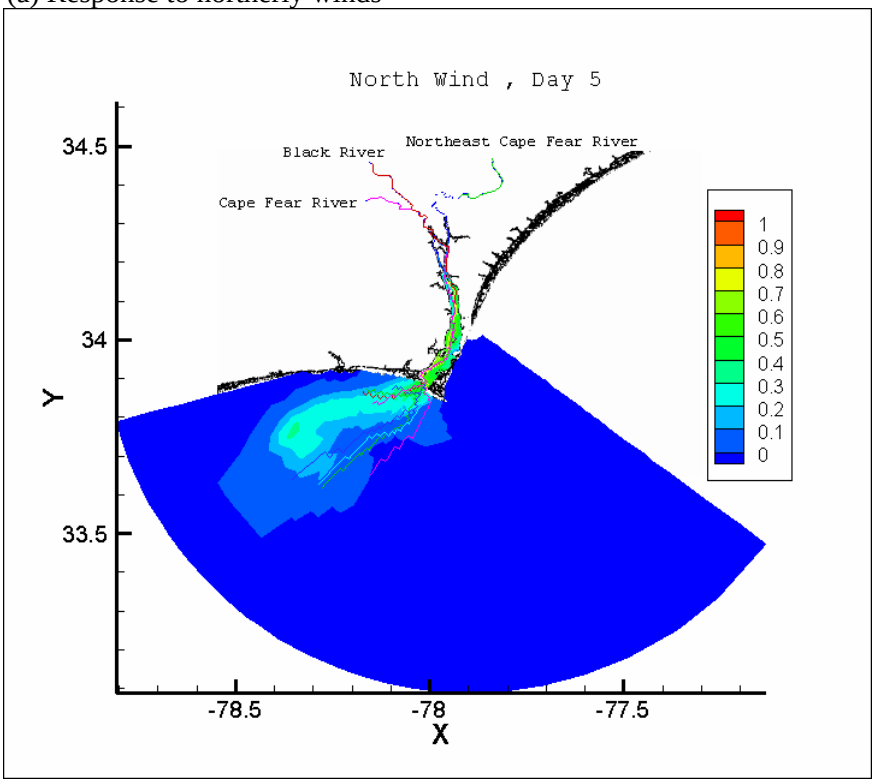


(b) Response to northeasterly winds

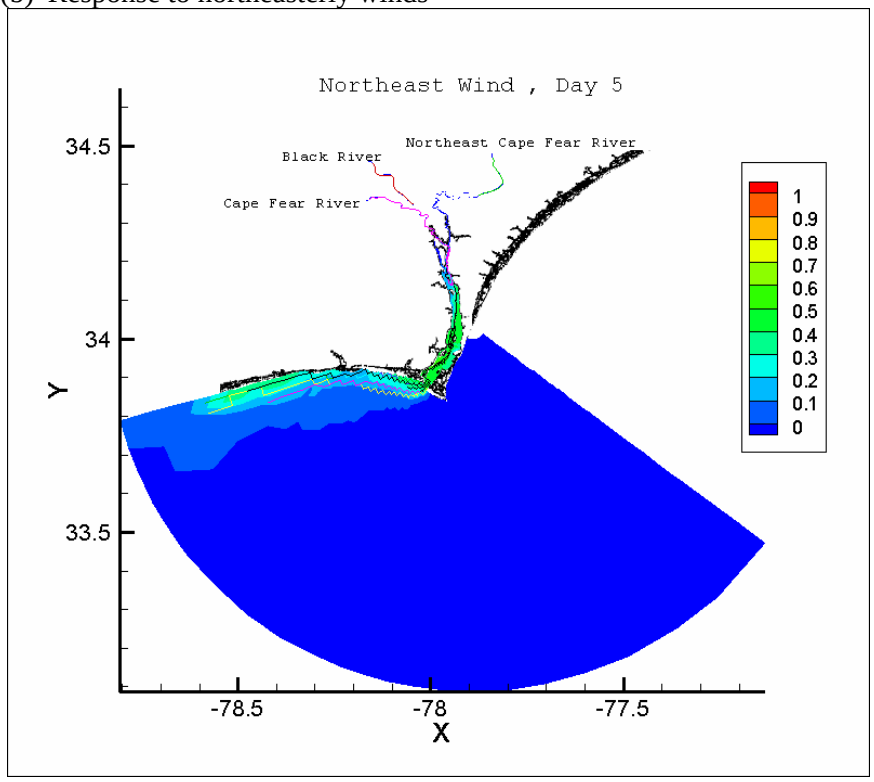

(c) Response to easterly winds:

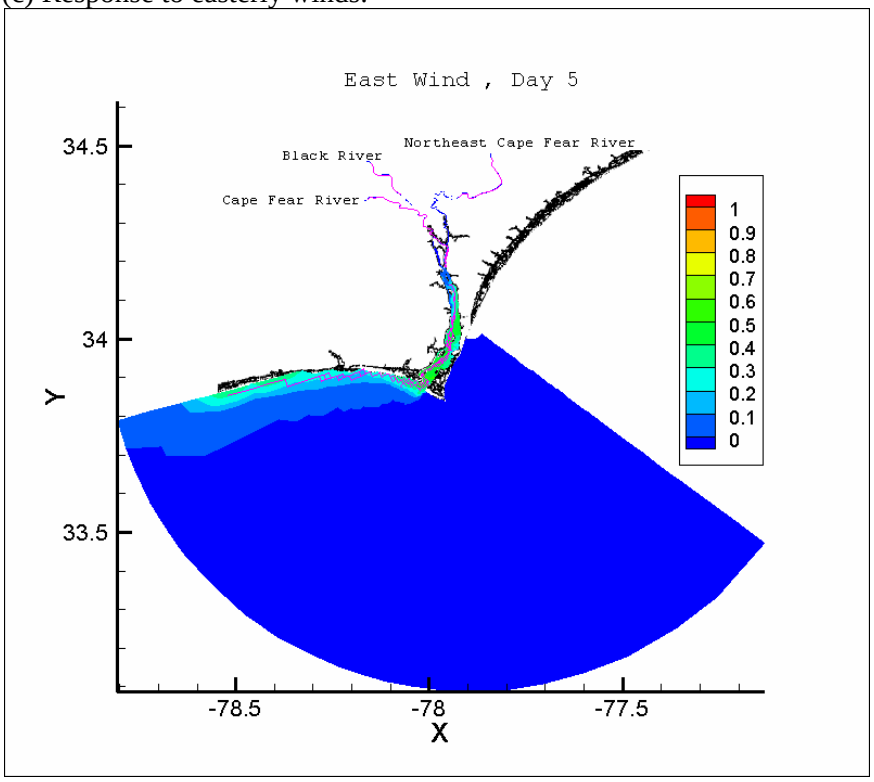


(d) Response to southeasterly winds

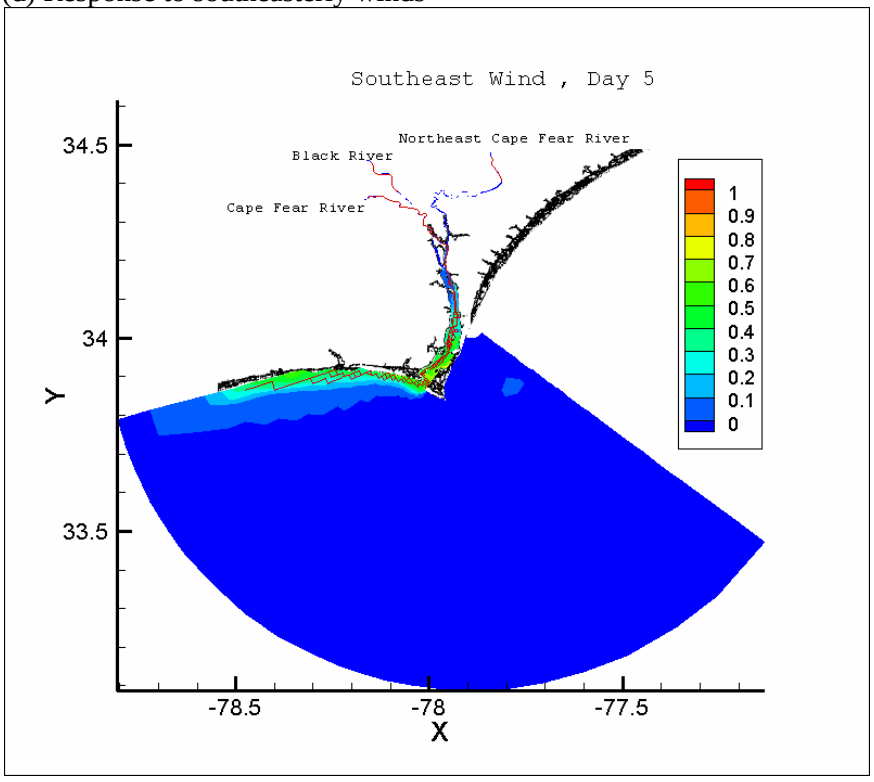

(e) Response to southerly winds

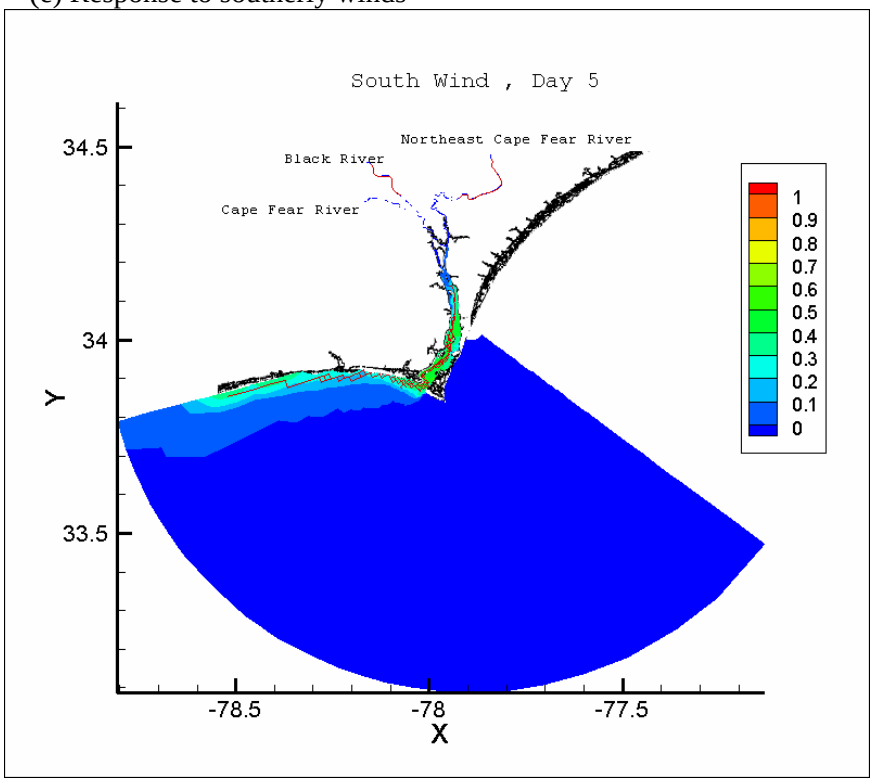


(f) Response to southwesterly winds

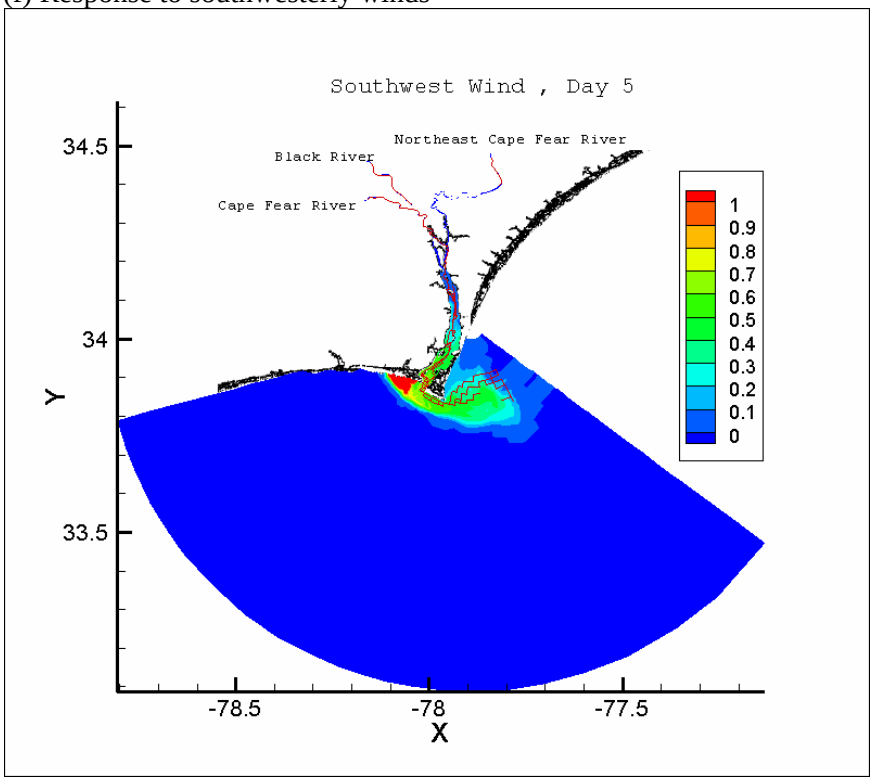

(g) Response to westerly winds

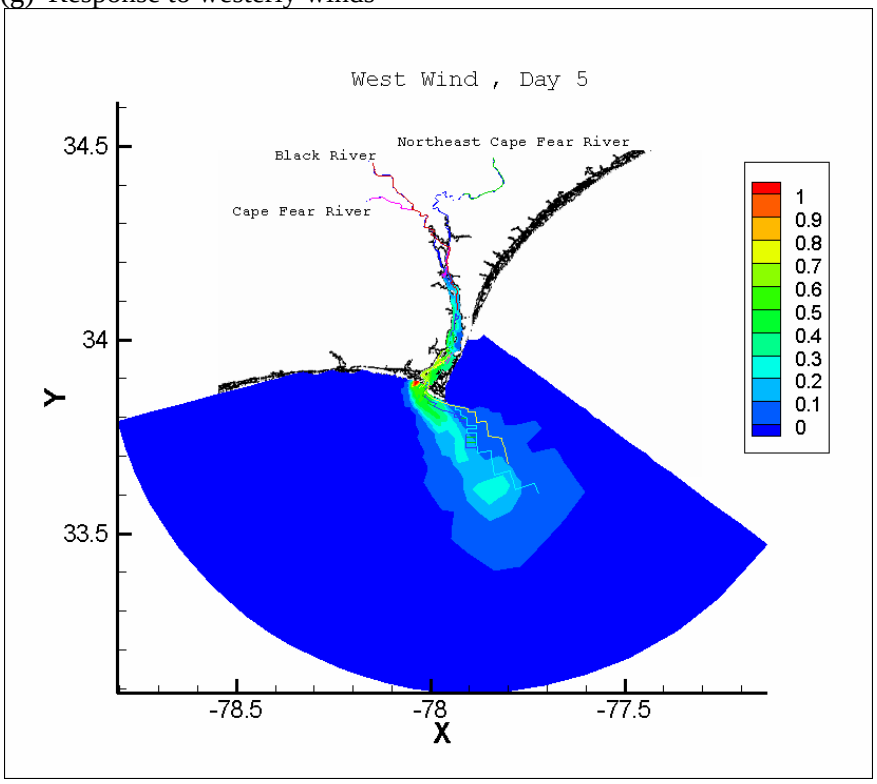


(h) Response to northwesterly winds

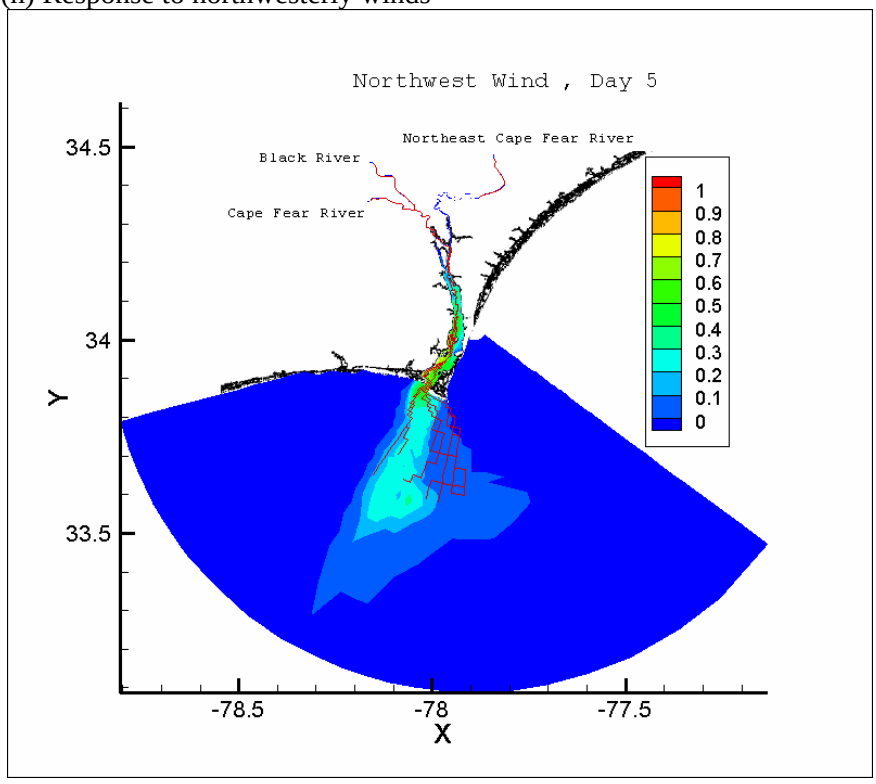


Figure 4. Sea surface traces fields forced by 5 m/s winds and normal discharge

(a) Response to the northerly wind

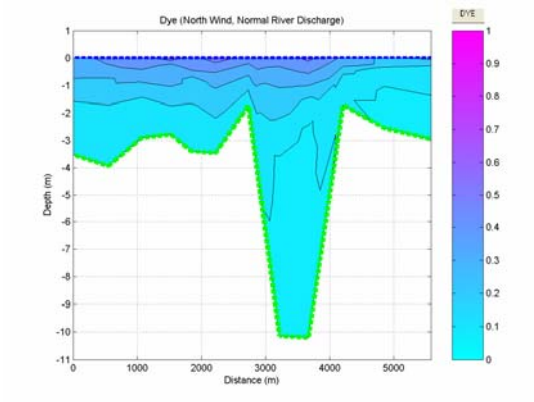


(b) Response to the northeasterly wind

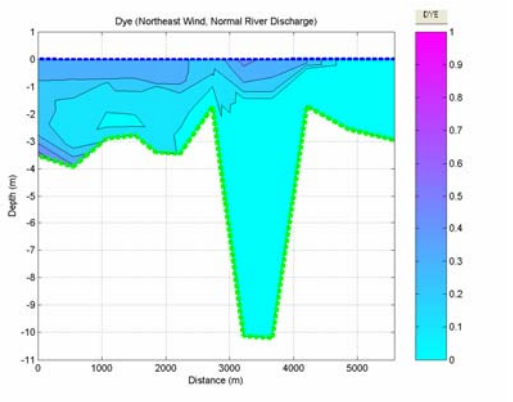


(c) Response to the easterly wind:

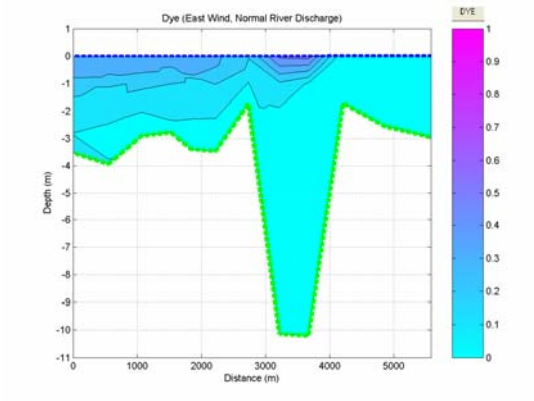


(d) Response to the southeasterly wind

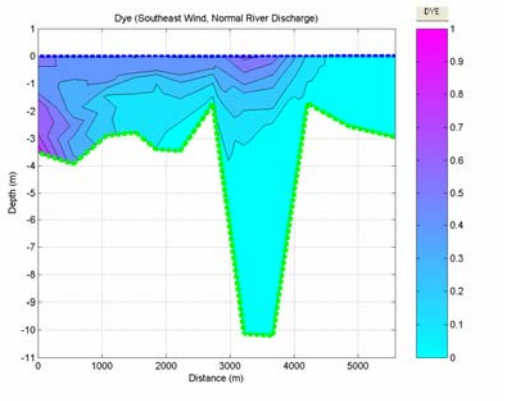


(e) Response to southerly wind

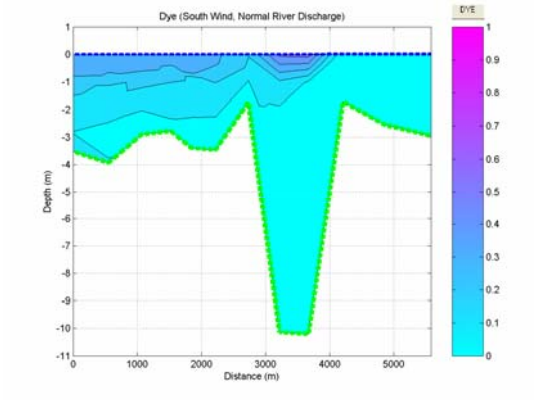


(f) Response to southwesterly wind

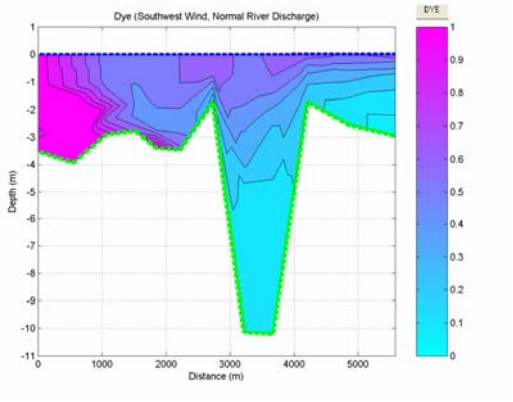

(g) Response to westerly wind (h) Response to northwesterly wind

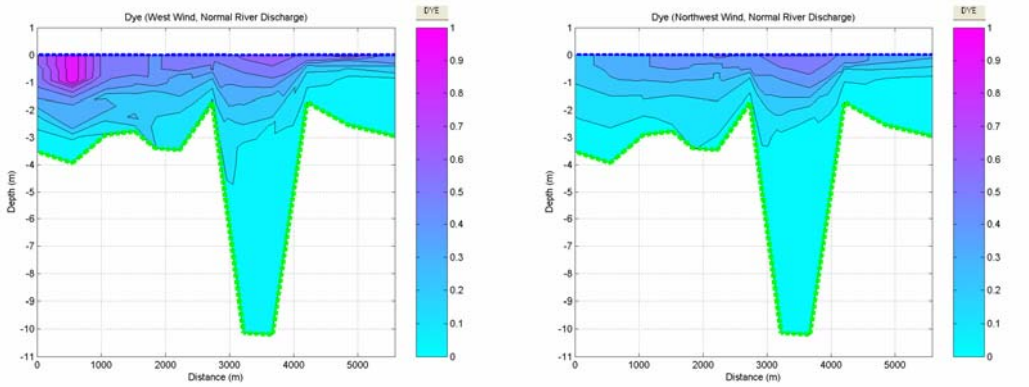


Figure 5. Vertical tracer fields forced by 5 m/s winds and normal discharge

(a) Response to 5 m/s wind speed

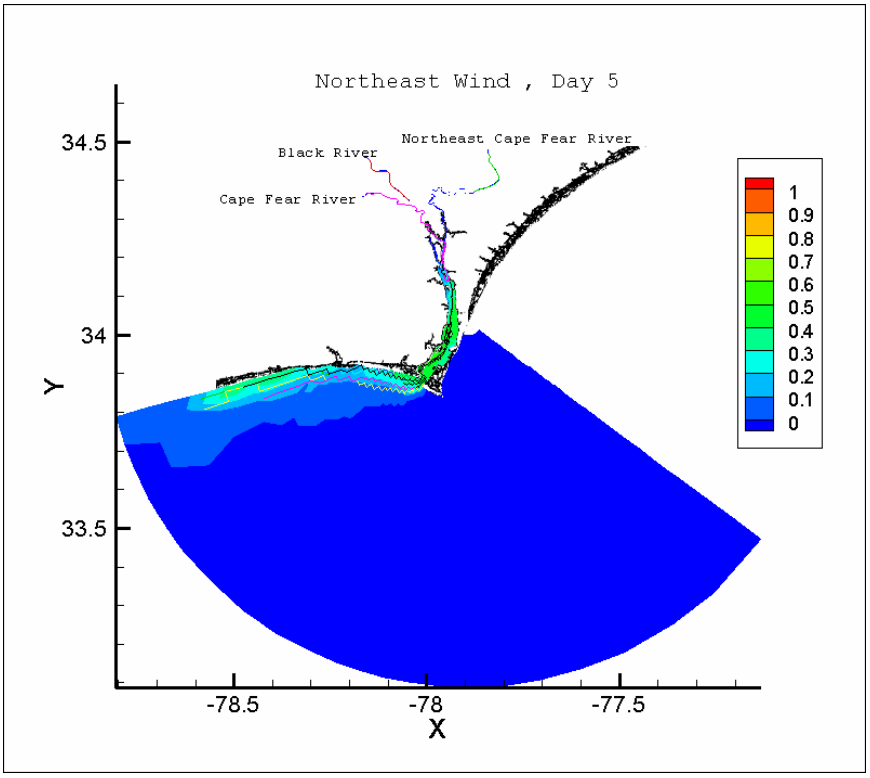


(b) Response to 10 m/s wind speed

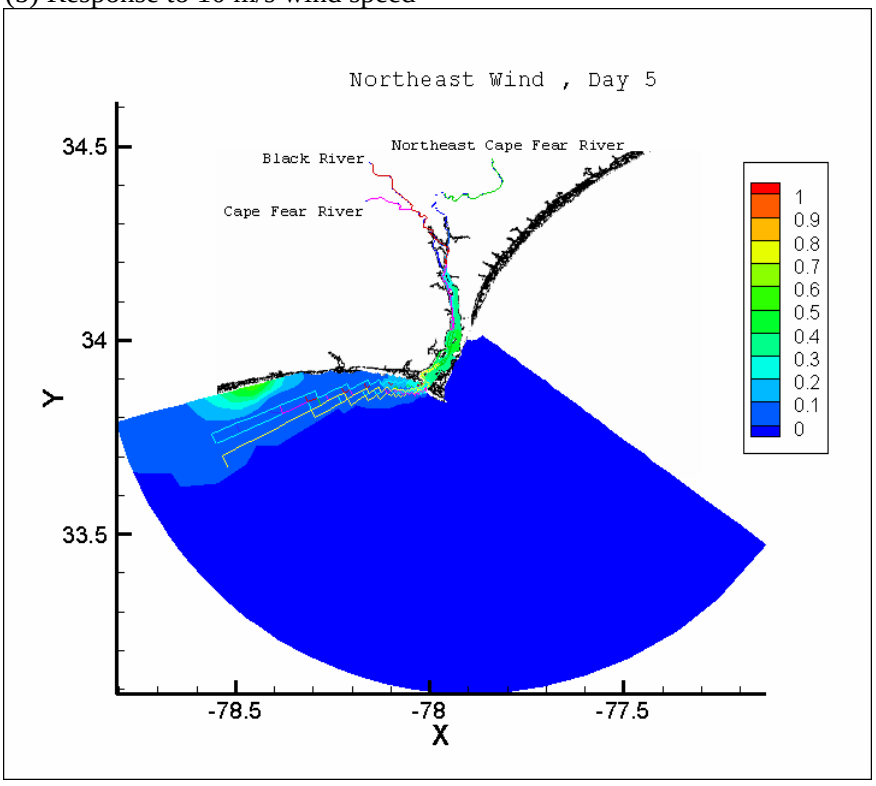

(c) Response to 15 m/s wind speed

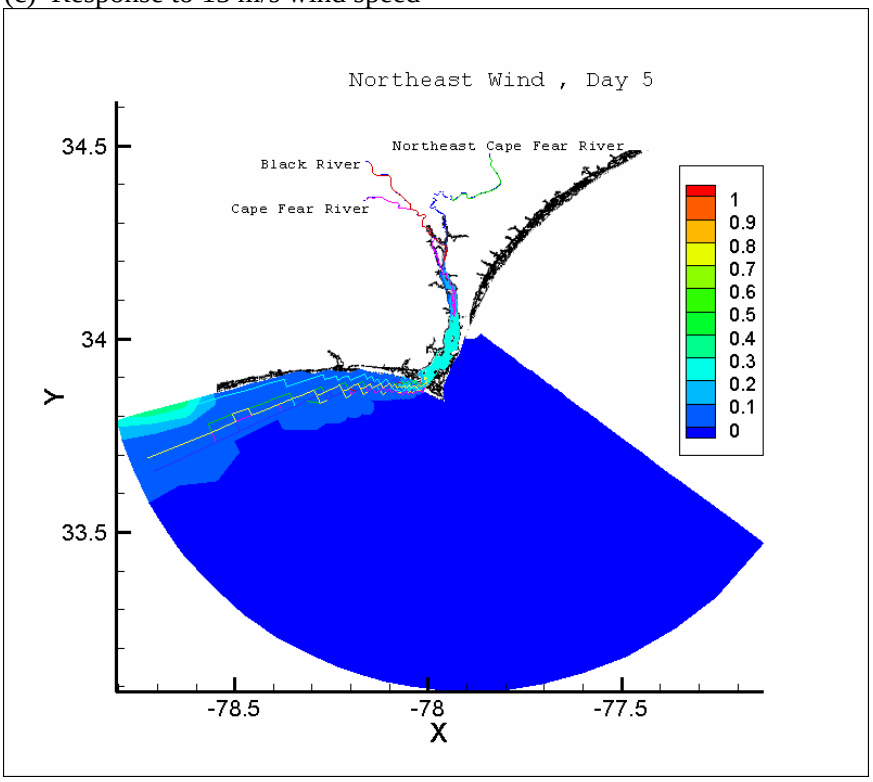


(d) Response to 20 m/s wind speed

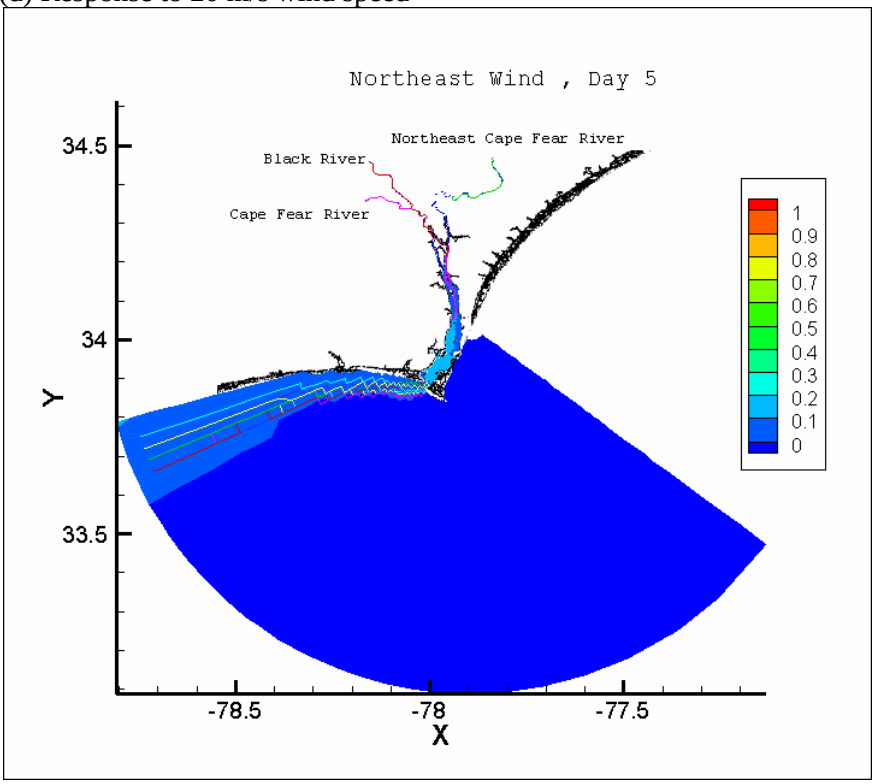


Figure 6. Sea surface traces fields under northeasterly winds and normal river discharge

(a) Response to 5 m/s wind speed

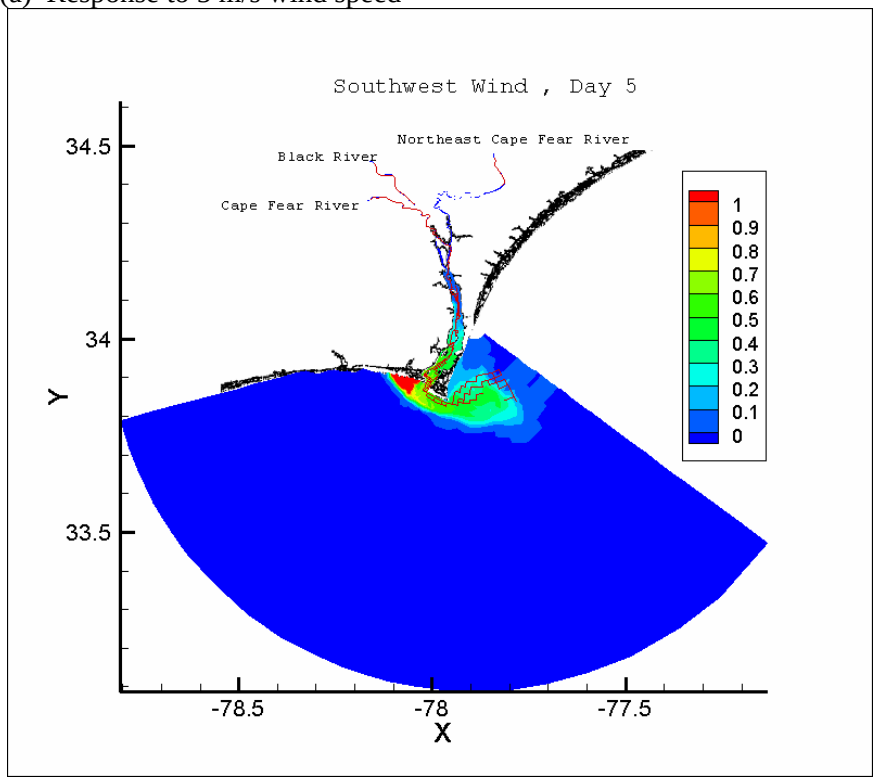


(b) Response to 10 m/s wind speed

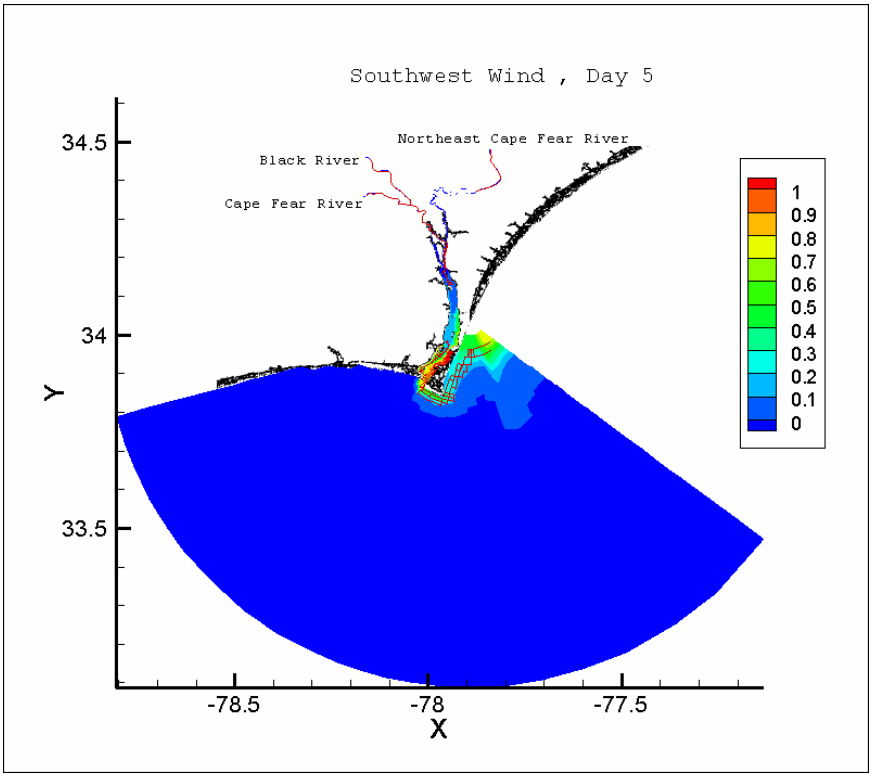

(c)Response to 15 m/s wind speed

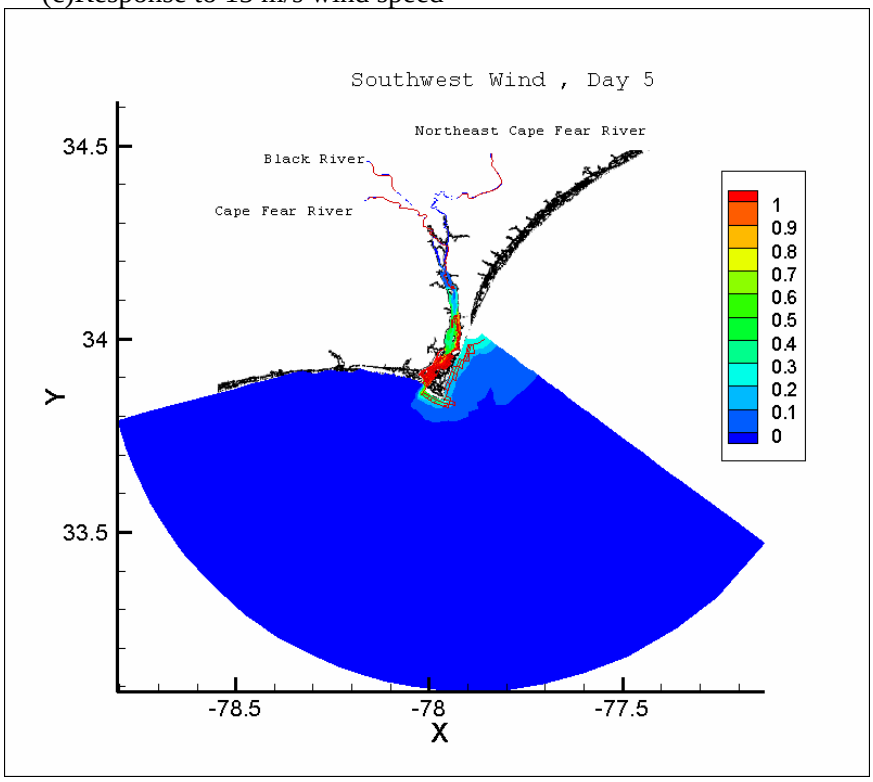


(d) Response to 20 m/s wind speed

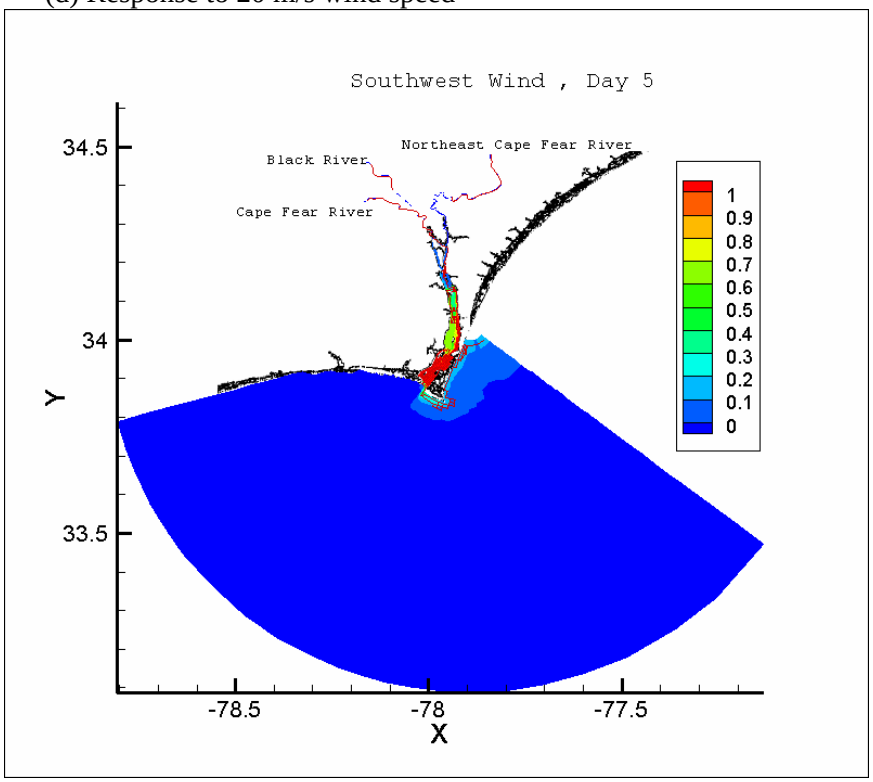


Figure 7. Tracer structure under southwesterly winds and normal river discharge

(a) Response to 5 m/s wind speed

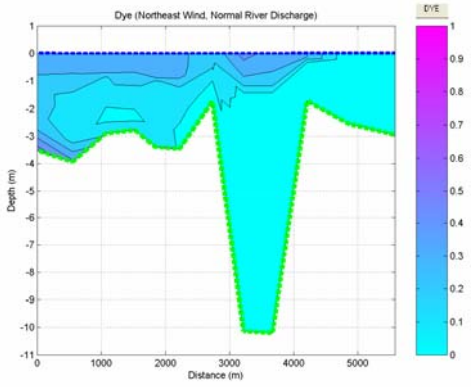


(b) Response to 10 m/s wind speed

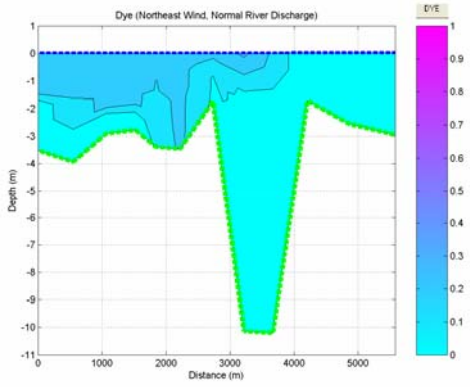


(c) Response to 15 m/s wind speed

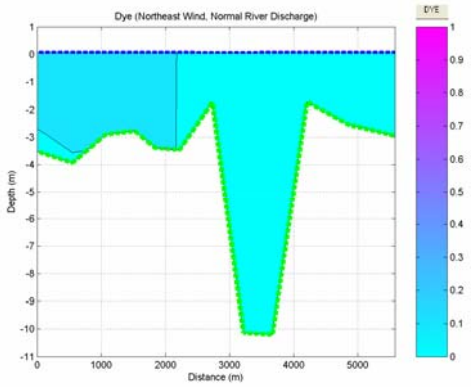


(d) Response to 20 m/s wind speed

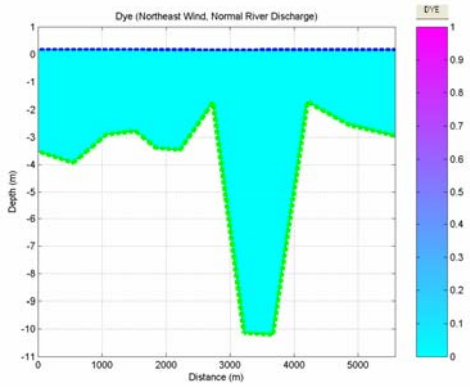


Figure 8. Tracer structure under northeasterly winds and normal river discharge

(a) Response to 5 m/s wind speed

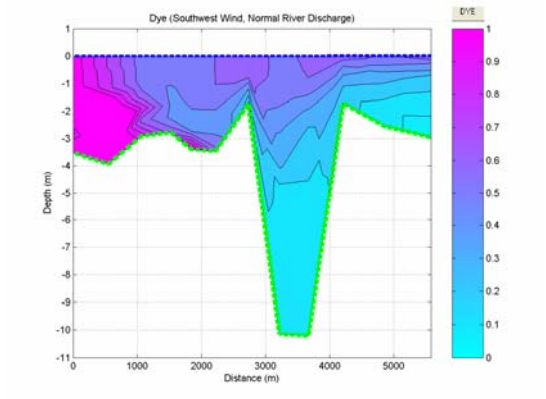


(b) Response to 10 m/s wind speed

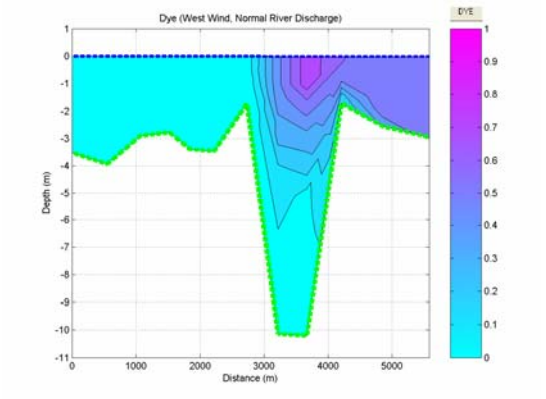


(c) Response to 15 m/s wind speed

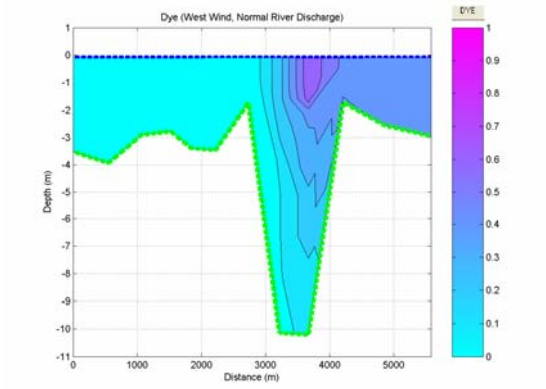


(d) Response to 20 m/s wind speed

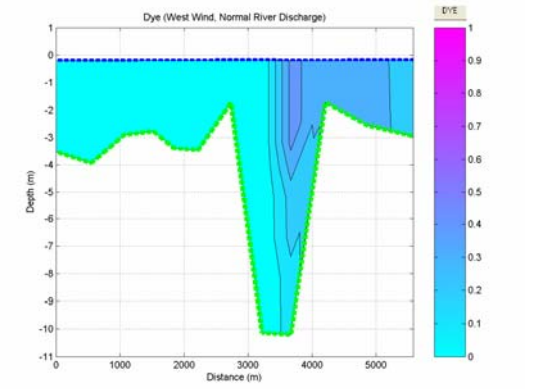


Figure 9. Tracer structure under southwesterly winds and normal river discharge

(a) Response to no river discharge

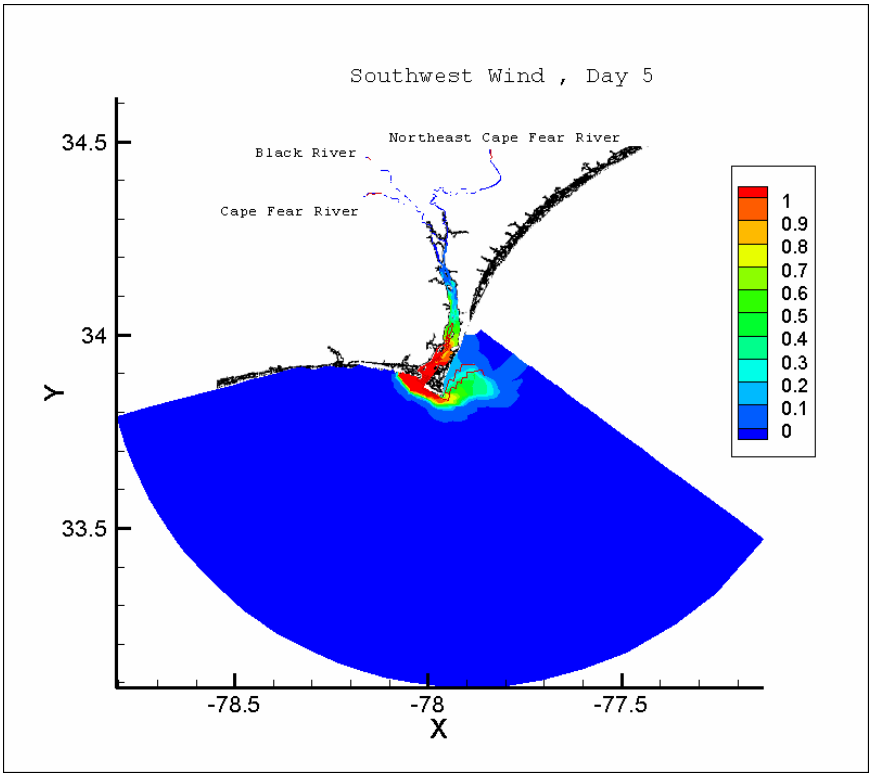


(b) Response to normal river discharge

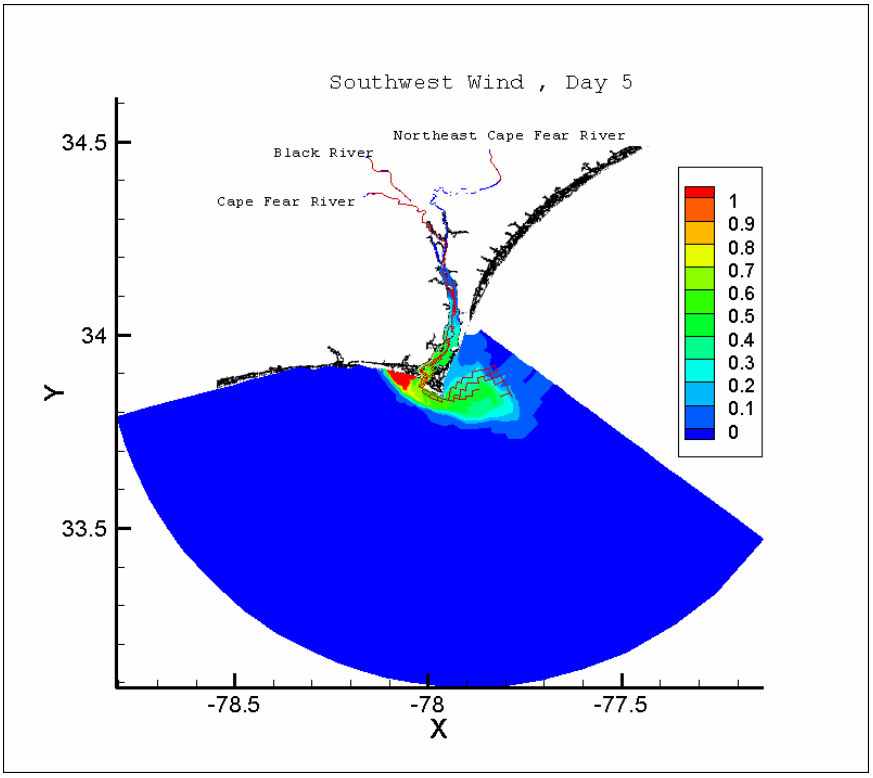

(c) Response to 1.5 times normal river discharge

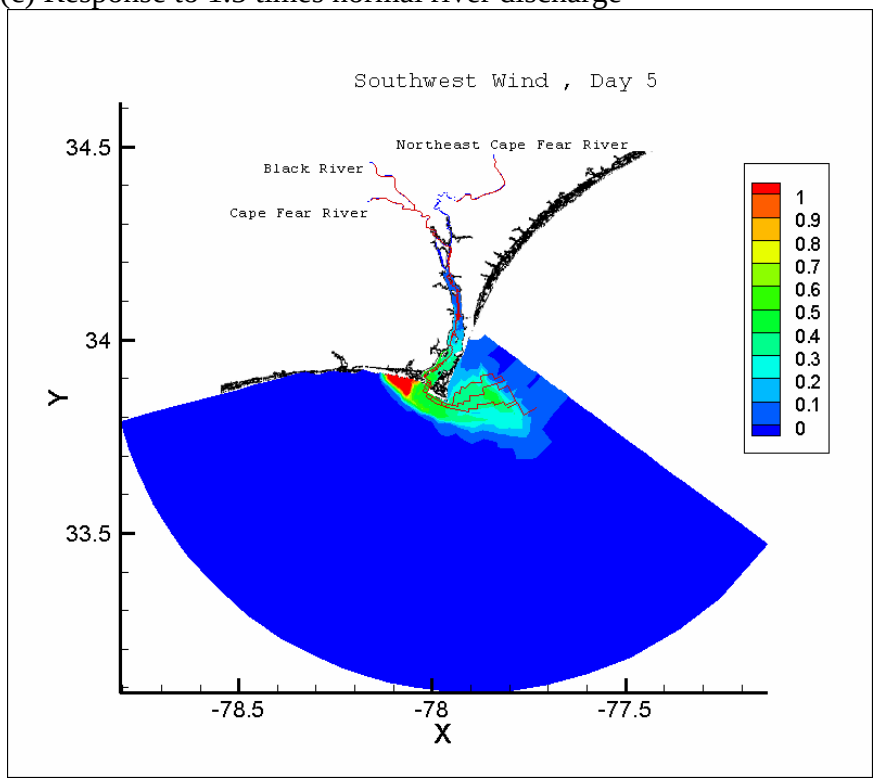


(d) Response to flood conditions

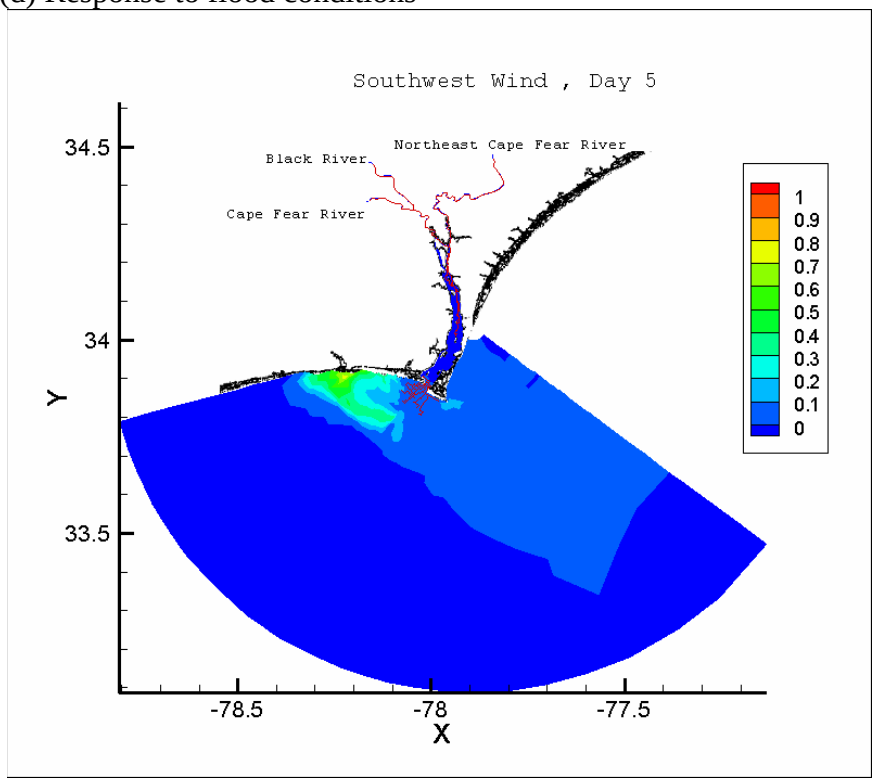


Figure 10. Tracer structure with southwesterly winds of 5m/s

(a) Response to no river discharge

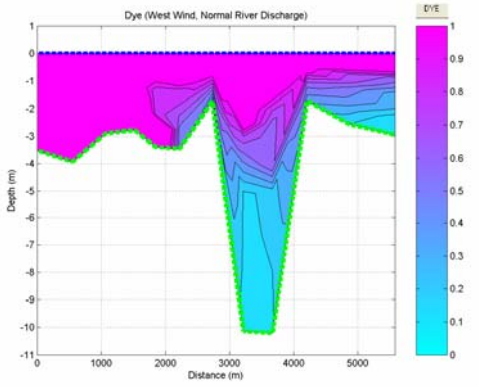


(b) Response to normal river discharge

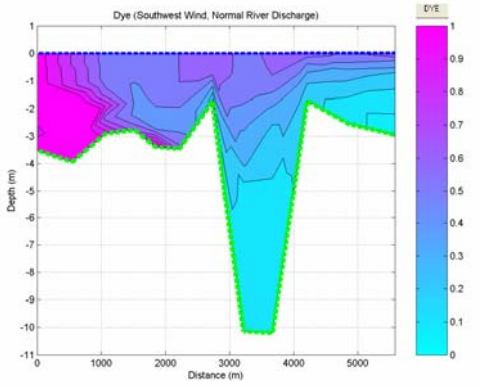


(c) Response to 1.5 times the normal river discharge

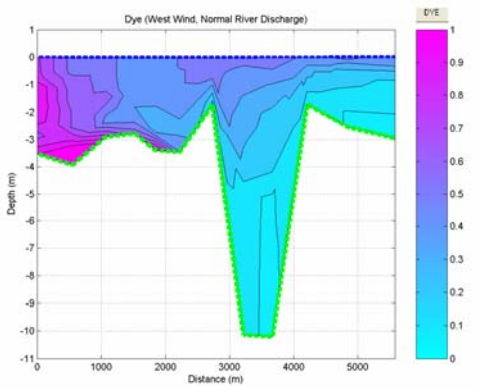


(d) Response to the flood condition

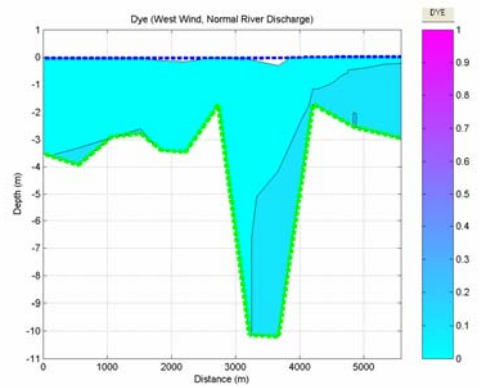


Figure 11. Tracer structure with southwesterly winds of 5m/s

(a) The structure at low tide

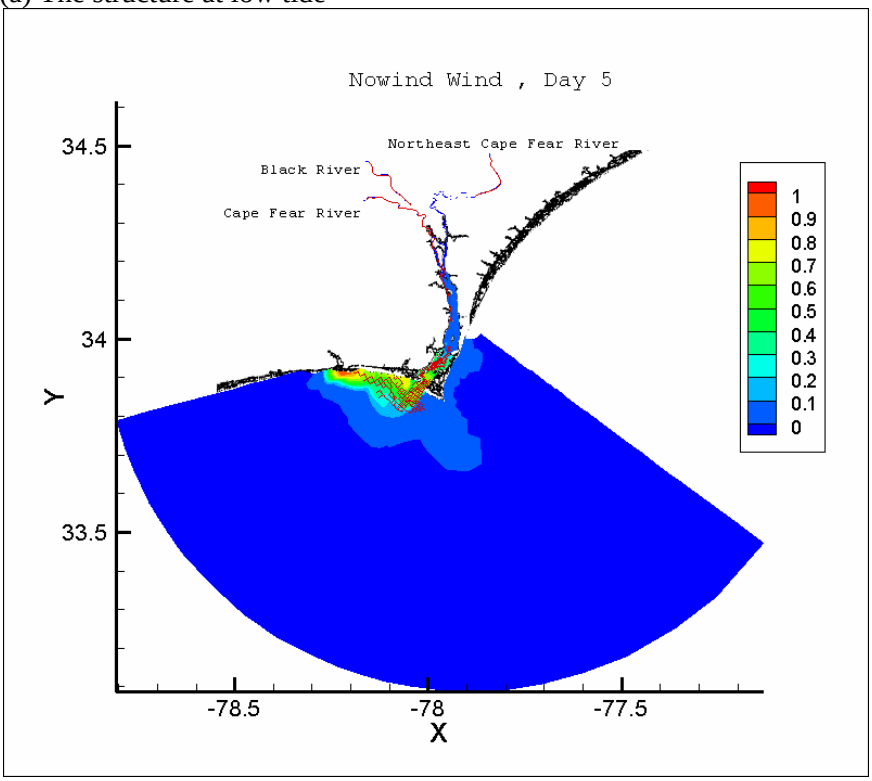


(b) The structure at high tide

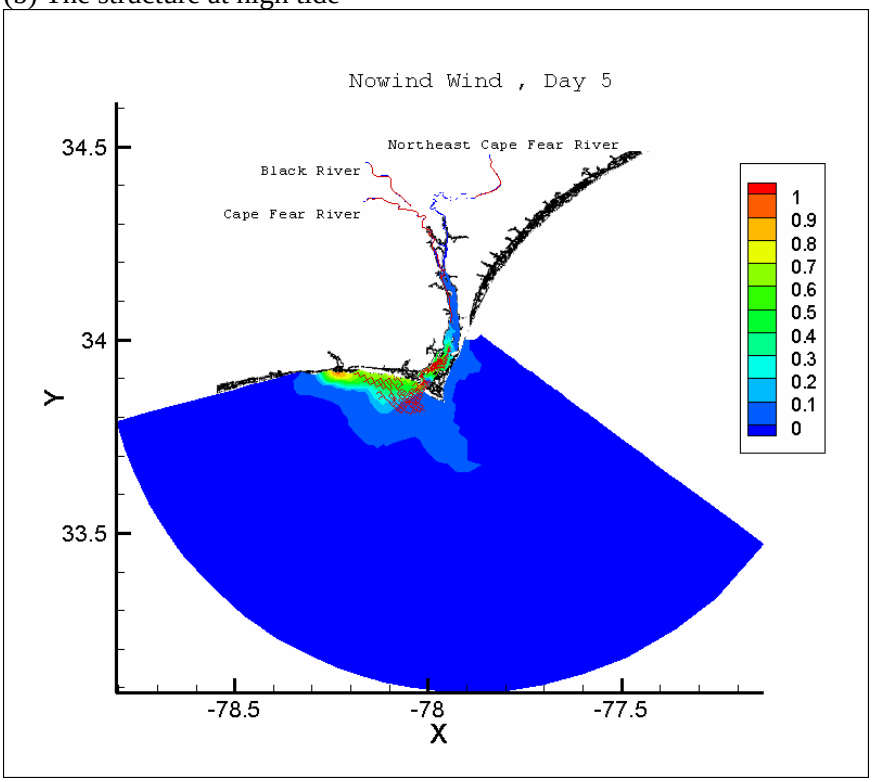


Figure 12. Tracer structure with no wind forcing and normal discharge

(a) Response to low tide condition

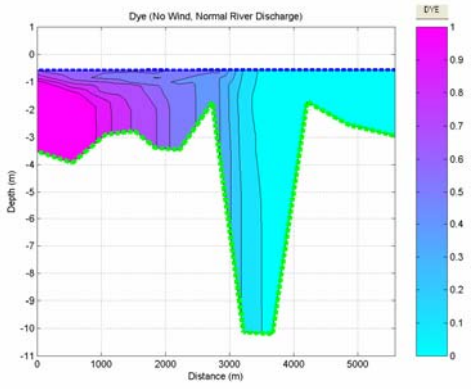


(b) Response to normal condition after low tide

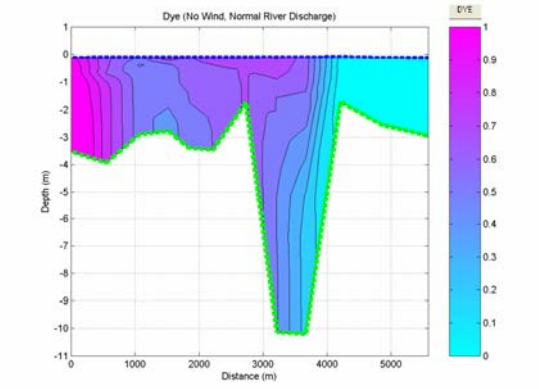


(c) Response to high tide condition

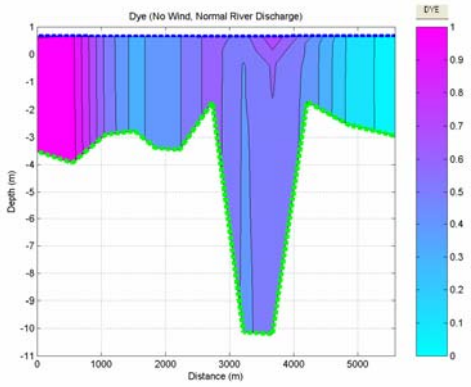


(d) Response to normal condition after high tide

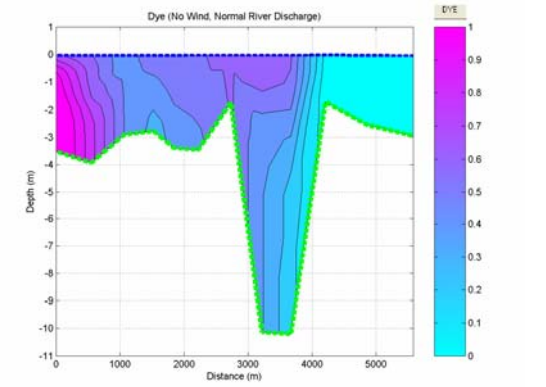


Figure 13. Tracer structure with no wind forcing and normal discharge

(a) The structure at low tide

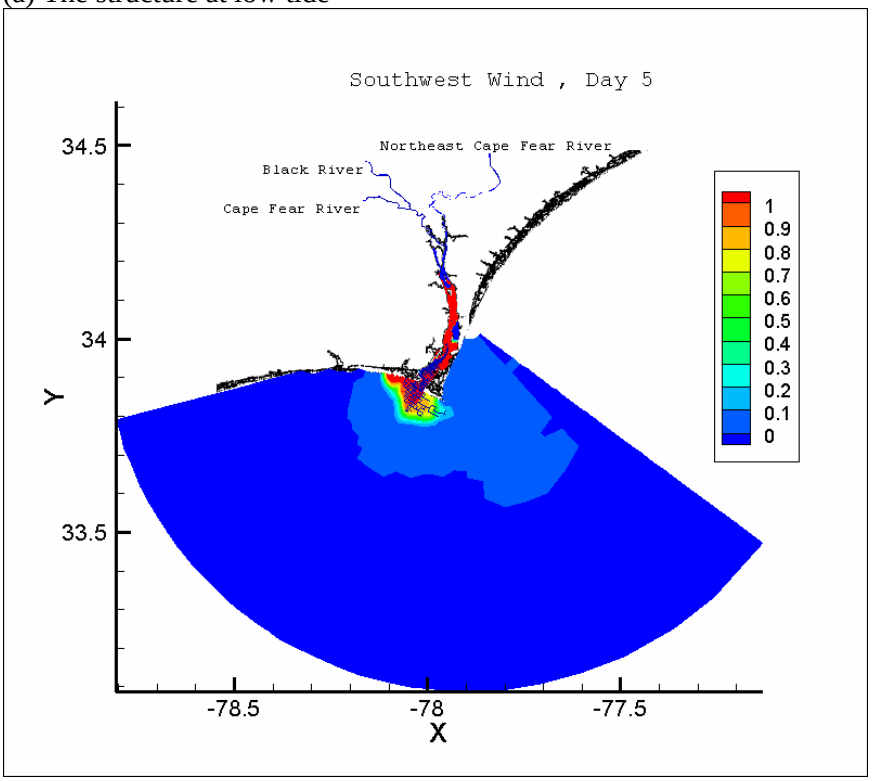


(b) The structure at high tide

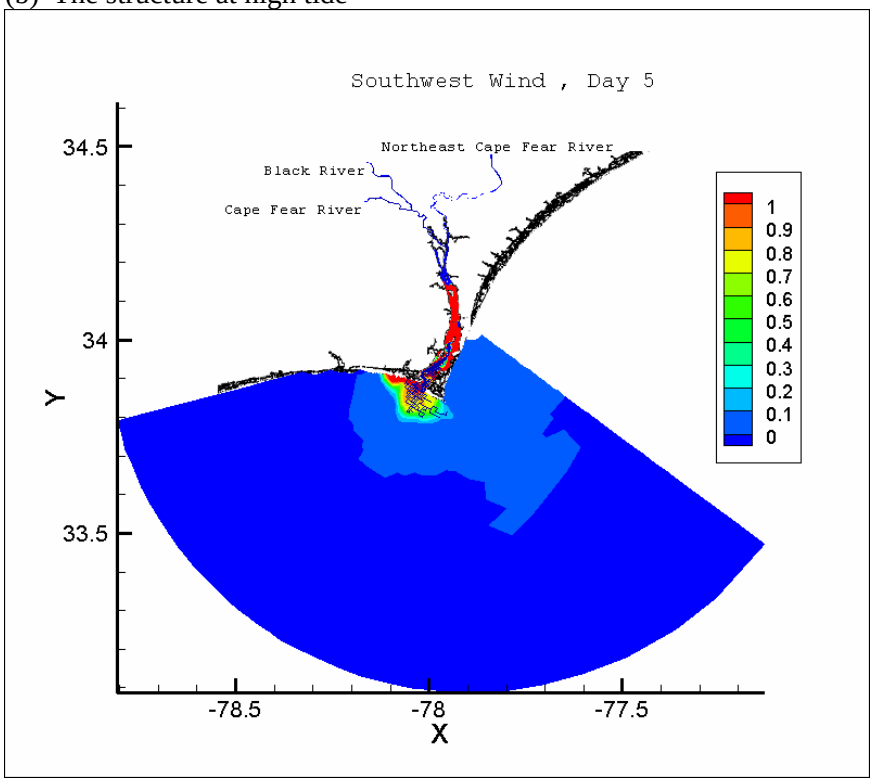


Figure 14. Tracer structure with southwest wind forcing and normal discharge

(a) Response to low tide condition

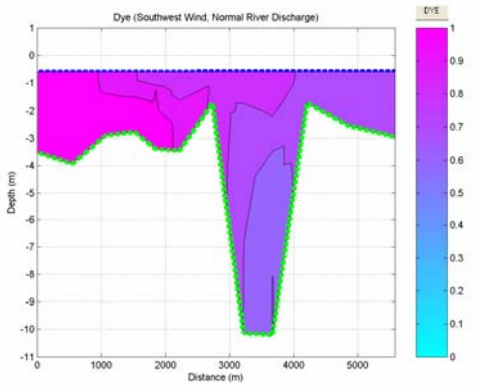


(b) Response to normal condition after low tide

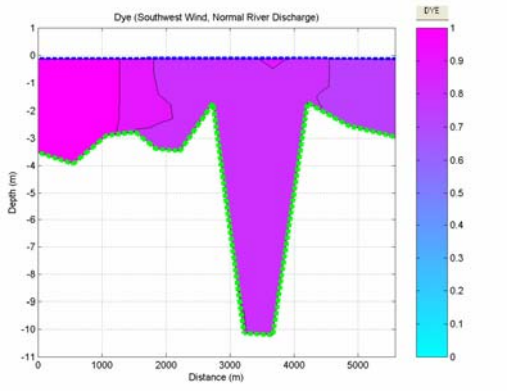


(c) Response to high tide condition

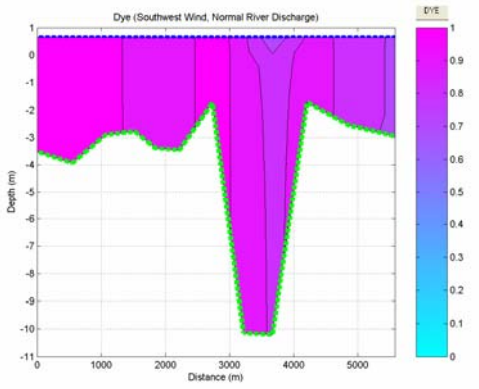


(d) Response to normal condition after high tide

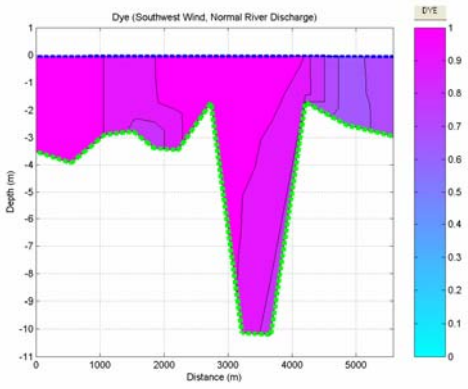


Figure 15. Tracer structure with southwest wind forcing and normal discharge

(a) The plume structure after 5 days

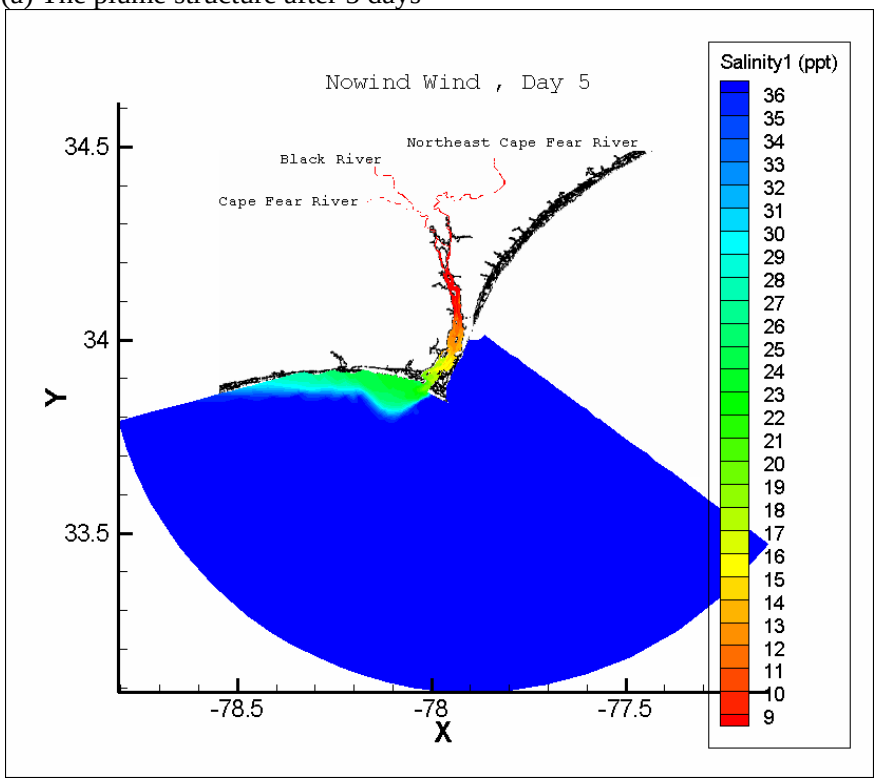


(b) The plume structure after 5 days

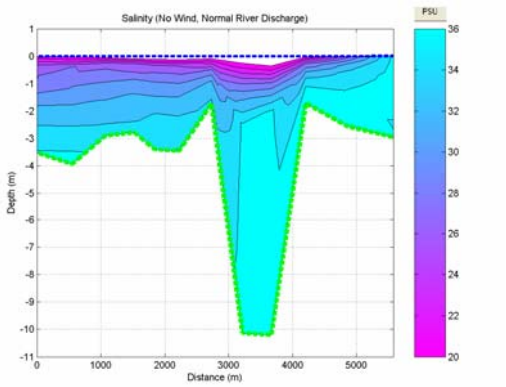


Figure 16. The Sea surface salinity fields forced by normal river discharge

(a) The structure after 5 days

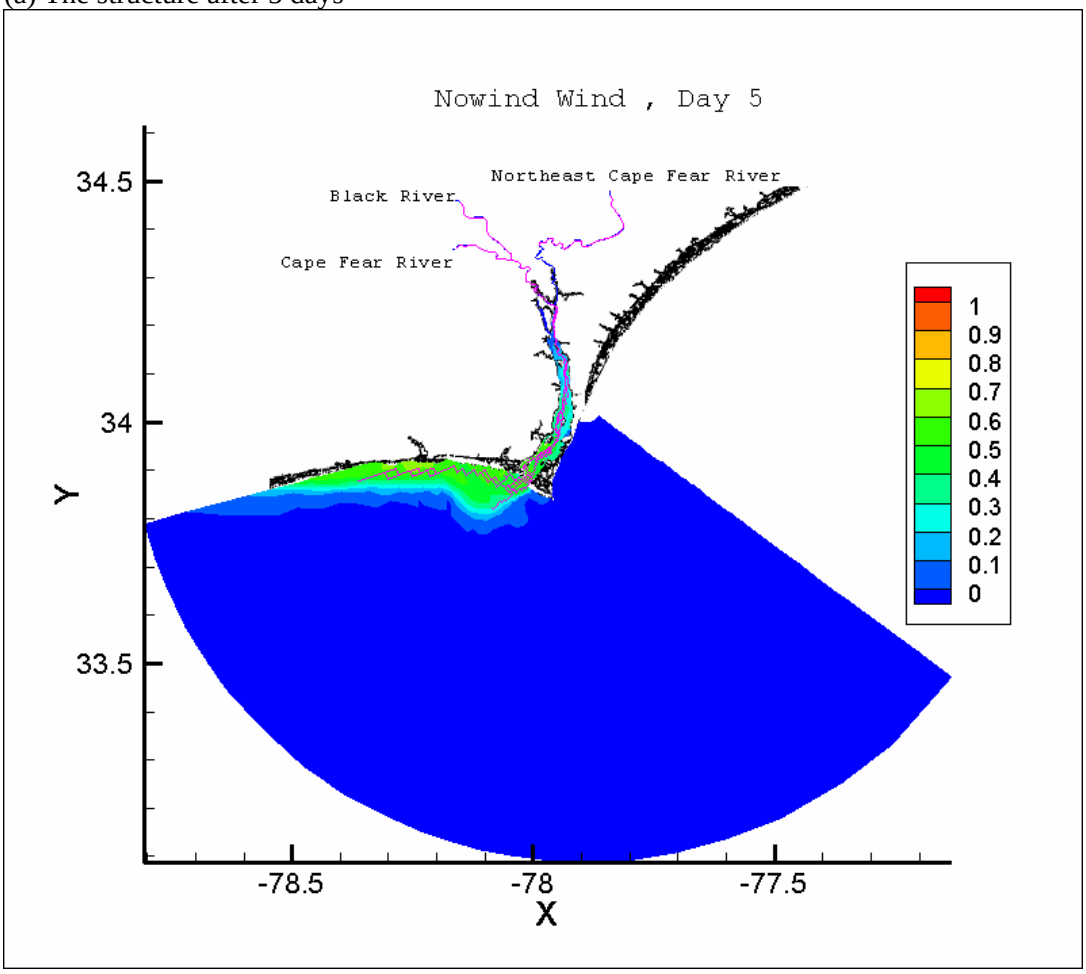


(b) The tracer structure after 5 days

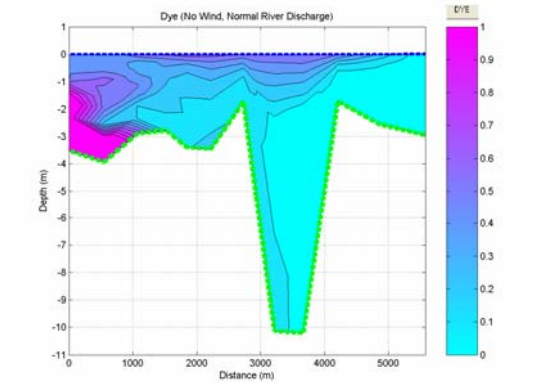


Figure 17. The sea surface tracer fields forced by normal river discharge

(a) Response to southwesterly winds

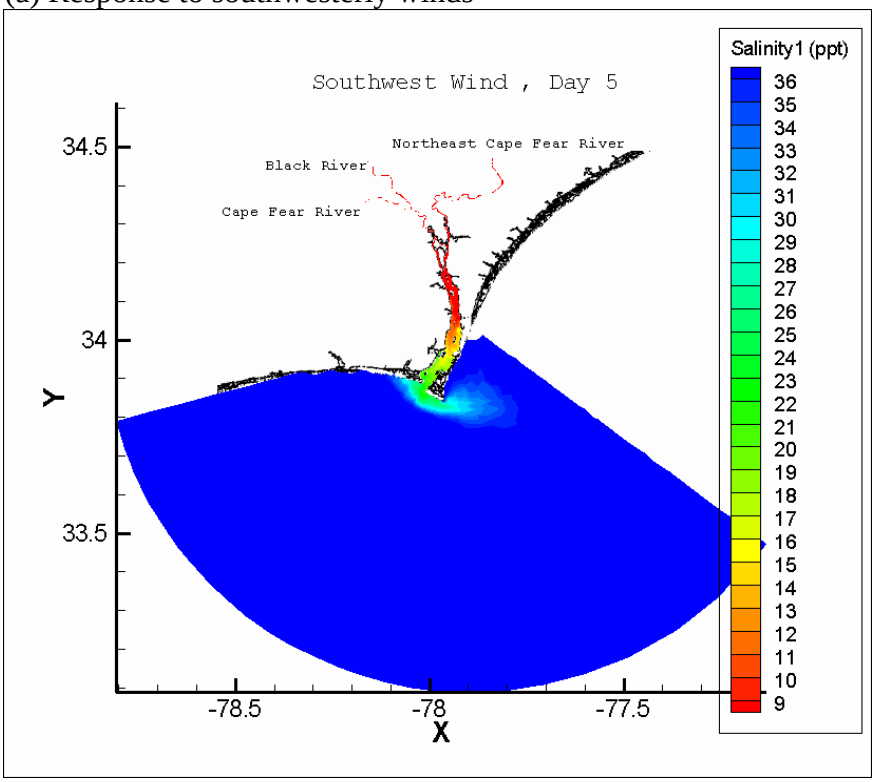


(b) Response to southwesterly wind

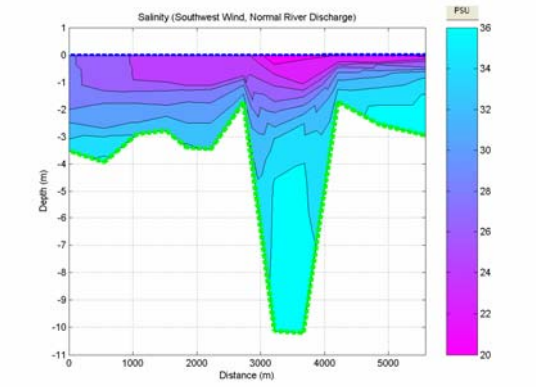


Figure 18. The Sea surface salinity fields forced by Southwest wind

(a)Response to southwesterly winds

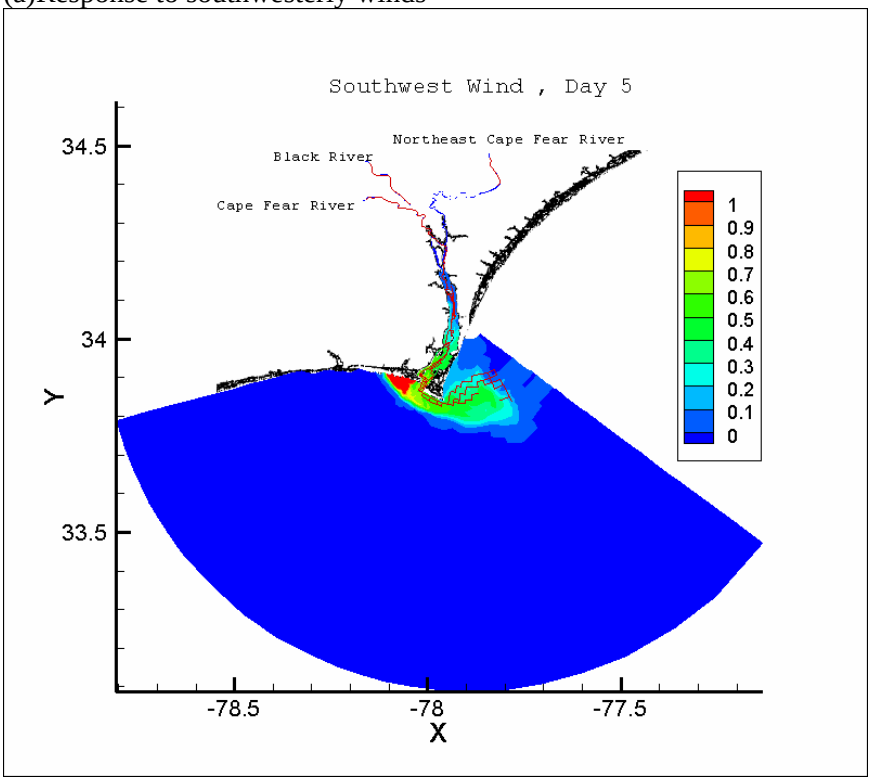


(b) Response to southwesterly wind

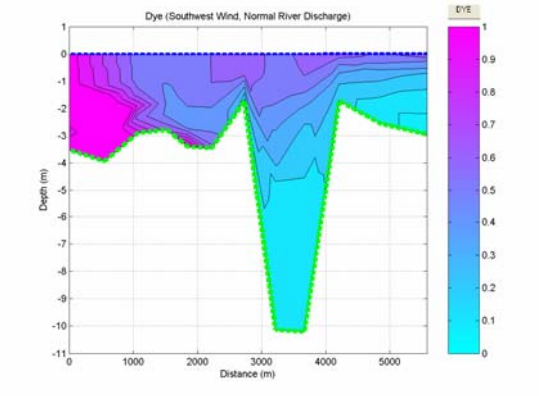


Figure 19. The sea surface traces fields forced by Southwest wind

(a)Response to 20 m/s wind speed

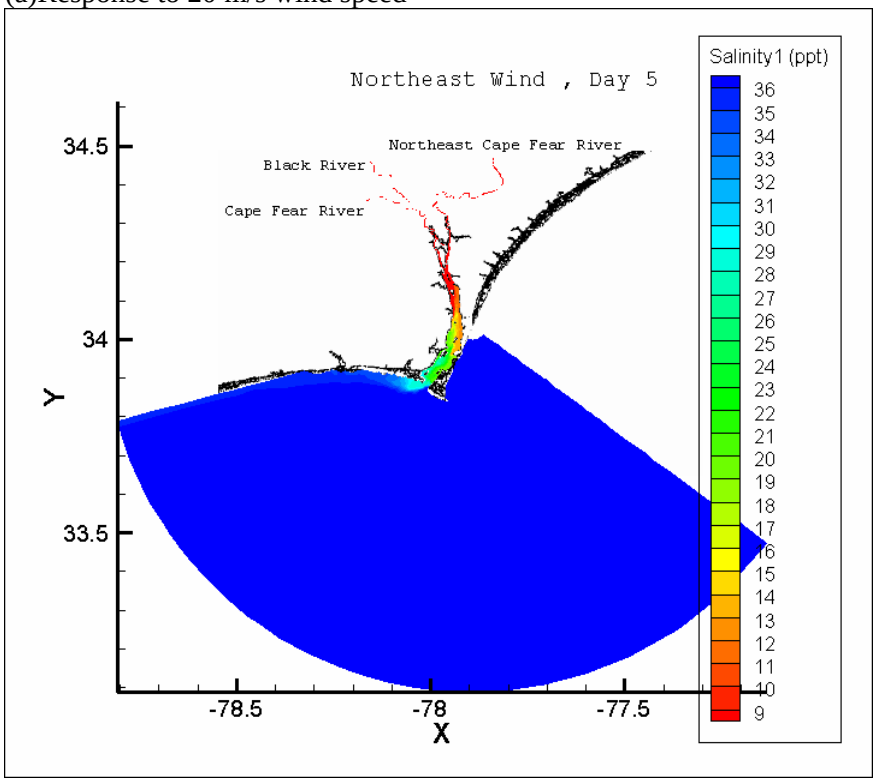


(b) Response to 20 m/s wind speed

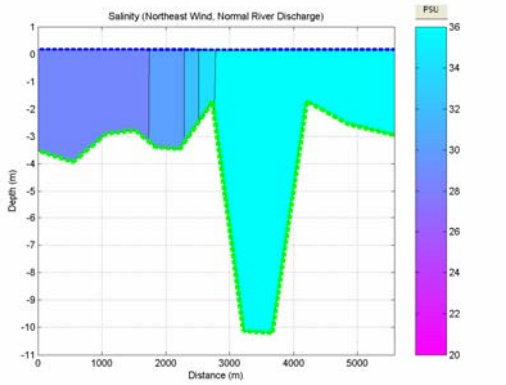


Figure 20. The Sea surface salinity fields forced by Northeast wind

(a) Response to 20 m/s wind speed

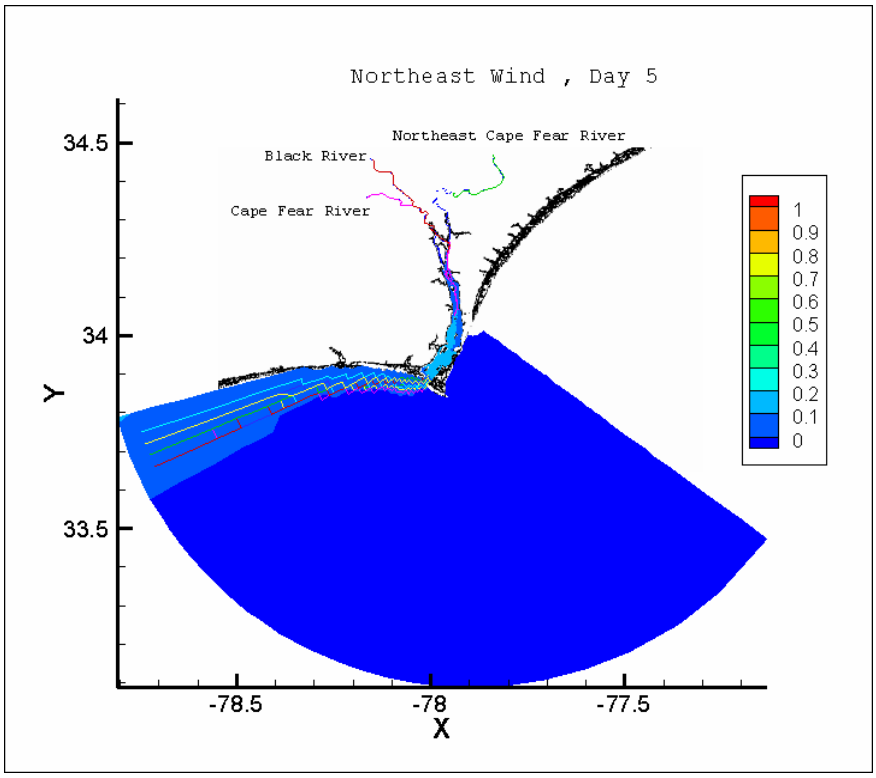


(b) Response to 20 m/s wind speed

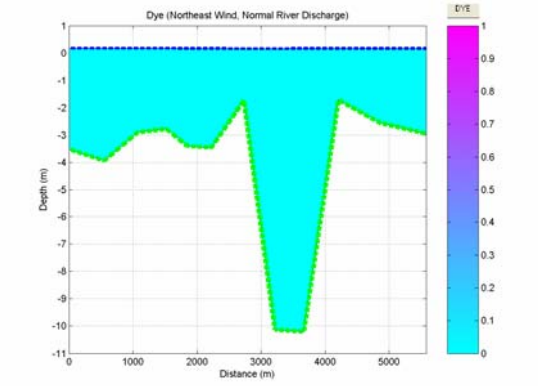


Figure 21. The sea surface traces fields forced by Northeast wind

# Chapter 6. Final Remarks

## 1. The response of storm surge distribution to the Hurricane track and intensity

From the discussion of chapter 2, we could see that hurricane-induced storm surge in the CFRE is very sensitive to hurricane tracks. When a hurricane's track passes to the west of the CFRE as in the case of Hurricane Charley, there is a greater likelihood of water being pushed into the entrance of Cape Fear Estuary to bring severe storm surge in the CFRE. When the hurricane track passes above or to the east of the CFRE as in Hurricanes Fran and Floyd, the chance is little water being pushed towards and into the entrance of the CFRE. The storm surge will be generated locally in the Onslow Bay. The maximum storm surge level in the CFRE and the adjacent ocean is very consistent with the hurricane intensity. The maximum storm surge level was highest for Hurricane Fran, then Hurricane Floyd and Bertha, and lowest for Hurricane Charley, which are corresponded very well to their respective intensities.

## 2. The influence of the best modeling setting to the plume simulation. Such as vertical resolution, horizontal resolution, advection scheme?

Advection schemes can have a significant effect either with or without wind forcing. Central differencing scheme should not be used in plume modeling since it produces unrealistic results. Upwind scheme can not simulate the plume structure well even under the wind forcing condition. Higher order advection schemes such as the Smolar-2 scheme can produce realistic plumes.

Vertical resolution is important to the upshelf intrusion. With the same surface thickness, the surface upshelf intrusion could be eliminated by increasing the number of layers. The surface plume structure is also controlled by the surface thickness. A sufficiently thin surface layer is required to capture the surface plume structure.

Horizontal grid is very important for the plume modeling. When the grid size is reduced to about a couple hundred meters, upshelf intrusion will be significantly reduced. Furthermore, the structure and the size of the plume are also very sensitive to the grids used.

## 3. The response of plume horizontal and vertical structure to the different wind forcing, river discharge effect, and tidal effect

The plume is generally confined to the south-facing coastal shore line in upper Long Bay and extends in the direction of Kelvin waves to form a long narrow trapped structure when river discharge is imposed without wind effects. The high river discharge induced plume could reach the shallow water bottom but not the deep water bottom. There is a very strong stratification in this case.

When the wind effect is added, the plume structure is significantly different depending on wind directions. Even a moderate wind could fully reverse the buoyancy-driven plume structure in the CFRE under average river discharge conditions. With average river discharge, southwesterly, westerly, northwesterly, northerly and northeasterly upwelling favorable winds all cause the plume to depart from the coast to the south of CFRE. In

contrast, under easterly, southeasterly, and southerly downwelling favorable winds, the plume becomes trapped along the coast under normal river discharge. Under the moderate or weak wind forcing and moderate fresher water discharge, the plume is unlikely to contact with bottom since the limitation of critical salinity depth. The different wind forcing will influence the vertical structure. The different wind direction could lead to the slightly different vertical plume structures. Strong wind could cause the plume to extend to the bottom water.

Astronomical tide is an important factor in influencing the plume horizontal structure. In addition, the plume was extended into the Long Bay during the ebb tide whereas the plume was reversed into the estuary during flood tide. Therefore, tidal currents play a key role in influencing the plume structure besides the vertical tidal mixing effect. Under the tidal mixing, the plume could make bottom contact under most cases while the plume seldom makes bottom contact without the tidal effect in the simulation. When compared to the weak or moderate wind effect, tidal mixing plays a crucial role in determining the vertical plume structure.

## 4. The influence of Frying Pan Shoals, between Long Bay and Onslow Bay to the storm surge circulation and plume distribution

From the discussion of chapter 2, we could conclude that the bottom topography plays an important role in the movement of storm-induced currents. It may cause dramatic difference in storm surge level between the right and left side of Frying Pan Shoals. The storm surge level in the Long Bay is much higher than that in the Onslow Bay during the passage of

Hurricane Charley, while the distribution of surge reverses during the passage of Hurricanes Fran, Floyd, and Bertha.

From the discussion of chapter 3, we could draw the conclusion that Frying Pan Shoals, between Long Bay and Onslow Bay, can affect the plume structure by inhibiting a plume from spreading from Long Bay to Onslow Bay. Under average river discharge conditions with northwesterly winds, the CFRE plume approximately follows the direction of Frying Pan Shoals. Even under flood conditions, the plume region was mostly limited to the Long Bay region. Under some favorable wind conditions, we could see some plume still could pass the Shoals and reach Onslow Bay.

## 5. The response of the passive trace horizontal and vertical structure and the path of particle trajectories to different wind forcing, river discharge effect, tidal effect.

When the wind effect is added, the passive tracer structure is significantly different depending on wind directions. Even a moderate wind could fully reverse the buoyancy-driven passive tracer structure in the CFRE under average river discharge conditions. With average river discharge, southwesterly, westerly, northwesterly, northerly and northeasterly winds all cause the passive tracer to depart from the coast to the south of CFRE. In contrast, under easterly, southeasterly, and southerly winds, the passive tracer structure becomes trapped along the coast under normal river discharge. This phenomenon is very similar to that of plume modeling results in Xia et al (2006). Under the high wind forcing, the domains of the particle trajectory are much larger; the passive tracer was quickly diluted and its size

was much larger unlike the size of salinity plume which decreases with increasing wind forcing.

Tidal currents do not play a key role in influencing the passive tracer surface structure while it plays an important role in its vertical distribution.

Under the wind mixing and fresher water discharge, the passive tracer most likely will not contact with bottom. Under the tidal mixing, the passive tracer could easily make bottom contact under most cases while the passive tracer seldom contact bottom without the tidal effect in the simulation.

## 6. Some differences and similarities between the salinity plumes, tracer plumes, and the particle trajectories.

Overall, the paths of the particle trajectory are totally within the domain of passive tracer distribution. There are three existing types when we compared the plume, particle trajectory, passive tracer structure. The first type is that the size of the plume is very close to the size of the passive tracer plume and the particles are totally within the domain of the plume or passive tracer plume; the second type is that the size of the plume is a little smaller than that of the passive tracer and the particles are within the domain of passive tracer while it is close to the boundary of the plume domain; the third type is that the size of the salinity plume is much smaller than that of the passive tracer plume and the particles are within the domain of passive tracer while it is beyond the boundary of the plume.